RECEIVED
LAWRENCE
RADIATION LABORATORY

NOV 20 1972

LIBRARY AND
DOCUMENTS SECTION

LBL-1256

BETA ASYMMETRY FROM ORIENTED MANGANESE 52

Sammy Tung-Chuen Hung
(Ph.D. thesis)

September 1972

AEC Contract No. W-7405-eng-48

For Reference

Not to be taken from this room

LBL-1256

DISCLAIMER

This document was prepared as an account of work sponsored by the United States Government. While this document is believed to contain correct information, neither the United States Government nor any agency thereof, nor the Regents of the University of California, nor any of their employees, makes any warranty, express or implied, or assumes any legal responsibility for the accuracy, completeness, or usefulness of any information, apparatus, product, or process disclosed, or represents that its use would not infringe privately owned rights. Reference herein to any specific commercial product, process, or service by its trade name, trademark, manufacturer, or otherwise, does not necessarily constitute or imply its endorsement, recommendation, or favoring by the United States Government or any agency thereof, or the Regents of the University of California. The views and opinions of authors expressed herein do not necessarily state or reflect those of the United States Government or any agency thereof or the Regents of the University of California.

TABLE OF CONTENTS

List of Figures----------v
Abstract----------vii
Introduction----------1
Chapter I, Beta Decay Theory----------4
Allowed Beta Decay----------6
Mixed Transition----------11
Chapter II, Time-Reversal Invariance----------12
Nuclear Orientation/Beta-Gamma
Correlation Technique----------13
Chapter III, Nuclear Orientation----------20
Thermometry----------25
Chapter IV, Low Temperature Particle Detectors----------28
Energy Resolution and Stability----------28
Low Temperature Operation----------30
Gamma-Rays Response----------34
Backscattering from the Detector----------35
Chapter V, Fundamental Difficulties and their
Solutions----------40
The Gamma Response of the Detector----------40
The Compton electrons----------42
Summary----------44
Chapter VI, The Apparatus----------47
The Liquid Helium Dewars System----------47
The Cryostat----------50
The Long Focusing Solenoid----------53
The Detector Chamber----------54
The Cooling Magnet----------56
The Salt Pill----------58
The Beta Detector----------61
The Gamma Detector----------61
The Electronics----------61

Chapter VII, The ^{52}Mn Beta Asymmetry Expt.----------65
Source Preparation----------65
Experimental Procedure----------67
Results----------68
Data Analysis----------70
Compton Electrons----------70
Pile-Up----------72
Scattering----------75
The Kurie Plot----------80
The Solid Angle Correction----------80
The Asymmetry Parameter----------82
Chapter VIII, The ^{60}Co Beta Asymmetry Expt.----------87
Chapter IX, Critique of the Experiment----------94
Comparison with other Expts.----------95
Time-Reversal Invariance----------99
References----------102
Appendix 1, Formulae for B_k, U_k and F_k----------104
Appendix 2, Pertinent Data Concerning ^{52}Mn----------106
Appendix 3, Gamma Response in Germanium Detectors--------107
Appendix 4, Some Useful Data Concerning the Dewars System----------108
Appendix 5, The Solid Angle Correction----------109
Acknowledgements----------112

LIST OF FIGURES

Fig. 1 Theoretical beta spectra of ^{52}Mn and ^{60}Co----------8

Fig. 2 Theoretical Kurie plot of ^{52}Mn beta spectrum----------10

Fig. 3 The "in-plane" and "out-of-plane" arrangements for the time-reversal invariance experiment----------16

Fig. 4 B_1, B_2 and B_4 terms of ^{52}Mn in Fe----------22

Fig. 5 The decay scheme of ^{60}Co----------24

Fig. 6 The decay scheme of ^{52}Mn----------26

Fig. 7 The use of anthracene scintillator for low temperature beta work----------29

Fig. 8 An arrangement to reduce the gamma response and the backscattering of the beta detector----------36

Fig. 9 The average range of electrons in germanium and silicon----------38

Fig. 10 The photoelectric cross-section of gamma rays in germanium----------41

Fig. 11 The experimental chamber----------43

Fig. 12 The experimental chamber without the long focusing solenoid----------45

Fig. 13 The beta spectrum of ^{52}Mn without the long solenoid----------46

Fig. 14 Schematic diagram of the dewars system-----48

Fig. 15 The cryostat----------51

Fig. 16 Schematic diagram of an indium seal--------52

Fig. 17 Schematic diagram of the detector chamber--55

Fig. 18 The cooling magnet----------57

Fig. 19 Schematic diagram of the salt pill assembly----------59
Fig. 20 Schematic diagram of the gamma detector-----62
Fig. 21 The electronic blocks diagram----------64
Fig. 22 The mounting of the source----------66
Fig. 23 The observed beta spectra of ^{52}Mn----------69
Fig. 24 The renormalized spectrum of ^{52}Mn----------77
Fig. 25 The Kurie plot of the ^{52}Mn spectrum--------79
Fig. 26 The solid angle correction of ^{52}Mn---------81
Fig. 27 Tabulation of the ^{52}Mn results----------84
Fig. 28 The asymmetry parameter of ^{52}Mn----------85
Fig. 29 The ^{52}Mn Fermi/Gamow-Teller mixing ratio vs the phase angle----------86
Fig. 30 The observed ^{60}Co beta spectra----------88
Fig. 31 The Kurie plot of the ^{60}Co spectrum-------89
Fig. 32 The solid angle correction of ^{60}Co--------90
Fig. 33 Tabulation of ^{60}Co results----------91
Fig. 34 The asymmetry parameter of ^{60}Co----------93
Fig. 35 A vs F/G-T mixing ratio of ^{52}Mn----------96
Fig. 36 The effect of magnetic field on the "in-plane" and "out-of-plane" measurements in a time-reversal expt.----------100
Fig. 37 The geometry for the solid angle correction calculation----------110

Beta Asymmetry from Oriented Manganese 52

By

Sammy Tung-Chuen Hung

Department of Chemistry

and

Lawrence Berkeley Laboratory

University of California

Berkeley, California 94720

September 1972

ABSTRACT

The nuclear orientation technique has been used to investigate the mixed allowed beta transition of ^{52}Mn. Nuclei of ^{52}Mn were polarized in an iron lattice utilizing the adiabetic demagnetization method to achieve low temperatures. The positrons emitted were detected with a high-purity germanium detector situated at the 1°K liquid helium bath. The angular distribution fits the correlation function

$$W(\theta) = 1 + (v/c)\, A\, (\langle m_z \rangle / I) \cos\theta$$

and the asymmetry parameter A was determined. The Fermi to Gamow-Teller mixing ratio can be calculated from the experimental value of A if time-reversal invariance is assumed. The value of the mixing ratio was found to be -14.5% . This value represents the largest negative interference term to date on the ^{52}Mn mixed transition, although a comparable but positive interference term has been reported on the same nuclide. A large interference term implies that ^{52}Mn is a favorable candidate for further investigation on the time-reversal invariance property. However, many other serious experimental difficulties should be taken into consideration, and they are discussed in this report. To further test the accuracy of the system, the beta asymmetry of ^{60}Co was also measured. The value of A was found to be -0.971, which agrees well with the theoretical prediction of -1.00 .

INTRODUCTION

The nuclear orientation technique is a well-established method for determining certain nuclear properties such as the multipolarity of electromagnetic radiations, nuclear spin and matrix elements. Nuclei can be oriented (either polarized or aligned) in a magnetic field if they are cooled to a temperature such that their Zeeman splitting is comparable to the thermal energy kT . The radiations from these oriented nuclei exhibit a dependency on the field axis due to the conservation law of angular momentum. In general, the angular distribution function can be written as:

$$W(\theta) = 1 + \sum_{k \text{ odd}} A_k Q_k U_k B_k P_k(\cos\theta) + \sum_{k \text{ even}} A_k Q_k U_k B_k P_k(\cos\theta)$$

(see Chpt. 3)

The k odd terms are normally discarded based on the argument that parity is violated. However, the discovery of parity violation in weak interactions[1] suggests that beta particles not only exhibit an angular dependency on the field axis, they are also sensitive to the nuclear polarization direction as well. By measuring the k odd terms, in fact, parity violating forces can be uncovered.

The doubt about the time reversal symmetry (T) in weak and electromagnetic interactions has been expressed many times in the past fifteen years. The first experiment on time reversal invariance by Ambler et al[2] did not reveal any significant violation in the weak interaction. The latter discovery of CP violation in K_2 decay[3] stimulated further interest in the question of possible time reversal symmetry violation in both weak and electromagnetic interactions.

However, experiments to date have yet uncovered any conclusive evidence of time reversal violation. The recent accurate experiment by Commins et al[4] in fact found T violation to be less than 10^{-3} for the ^{19}Ne decay.

In order to obtain accurate results from a time reversal invariance experiment, it is desirable to choose a nuclide which undergoes a mixed allowed beta transition with a large Fermi to Gamow-Teller mixing ratio. The magnitude of the Fermi to Gamow-Teller mixing ratio (F/G-T) can be determined from either beta-gamma circularly polarized angular correlation studies, or beta asymmetry experiments from polarized nuclei. Therefore the present work can best be viewed as a first step toward the more definitive test of time reversal invariance using the nuclear orientation technique.

The nuclide ^{52}Mn is chosen because of two reasons: firstly, a detectable Fermi to Gamow-Teller interference term (about 5 %) has been found; more importantly, the results from many different studies in the past on the magnitude of Fermi to Gamow-Teller mixing ratio of ^{52}Mn are too widely different to be conclusive. An accurate determination of the F/G-T ratio is highly desirable not only because it helps to determine the desirability of ^{52}Mn as a candidate for the time reversal invariance experiment (a small F/G-T term would render it less attractive) , but also because the accuracy of the final time reversal invariance data is directly related to the accuracy of the knowledge of the F/G-T ratio.[2] (See Chapter 2)

Recent improvements of nuclear orientation techniques and the advent of reliable low temperature beta detectors compelled the completion of this work. ^{52}Mn was oriented in a ferromagnetic host at low temperature using the adiabetic demagnetization method,

and the asymmetric emission of positrons with respect to the direction of the polarizing magnetic field was detected with a high purity germanium detector held at $1^{o}K$. In addition, in order to check for the possible systematic error of the entire system, beta asymmetry from polarized ^{60}Co was also observed under equivalent conditions. ^{60}Co undergoes a pure Gamow-Teller transition, and its decay scheme is well known, therefore its theoretical beta asymmetry can be calculated. The agreement between experimental and theoretical results of ^{60}Co beta asymmetry boasts the degree of confidence in the ^{52}Mn result.

CHAPTER I

Beta Decay Theory

Beta decay theory has been presented in detail in numerous publications.[5-9] To avoid redundancy, beta transition theory will be described here only to provide a continuity to the allowed beta transition theory.

Beta Interaction Theory

The beta interaction energy density may be viewed as the coupling between the nucleonic transition current and the leptonic transition current:

Eq.1-1 $$h_\beta = 8^{\frac{1}{2}} g J_\alpha(pn) J_\alpha(e\nu) + c.c.$$

The leptonic transition current is written as:

Eq.1-2 $$J_\alpha(e\nu) = \varphi_e^+ \beta \gamma_\alpha \varphi$$

where $\varphi = \frac{1}{2}(1+\gamma_5)\Psi$ is a left-handed projection from the actual state of the fermion Ψ; γ_α and $\beta=\gamma_4$ are the usual γ matrices. The present knowledge of beta decay indicates that the nucleonic transition current can be written as:

Eq.1-3 $$J_\alpha(pn) = \frac{1}{2}(C_V J_\alpha^V - C_A J_\alpha^A)$$

where J_α^V is the vector current;

J_α^A is the pseudo-vector current;

C_V and C_A are the corresponding coupling constants.

The significance of Eq.1-3 is that only vector and pseudo-vector interactions are responsible for beta decay. The scalar (S),

pseudo-scalar (P) and tensor (T) interactions vanish from the picture altogether.

Without going into detail, the beta interaction operator may be derived from Eq.1-1 as:

$$\text{Eq.1-4} \qquad H_\beta = 2^{\frac{1}{2}} g \sum_j \left[(C_V - C_A \gamma_5^j)\, \beta^j \gamma_\alpha^j\, \tau_+^j \right] \left[J_\alpha (e\nu) \right]_{\underline{r}_j} + \text{h.c.}$$

where $\tau_+ = \frac{1}{2}(\tau_1 + i\,\tau_2)$ is a raising operator of the isospin τ . The leptonic transition current has to be evaluated at its proper location within the nucleus $\underline{r}_j$ and summed over all the transitioning nucleons j .

There are two major approximations made for the allowed beta transitions.

1) The beta particle's energy is of the order of electron rest mass mc^2 . The deBroglie wavelength is:

$$\lambda = h/p \sim h/mc \sim 10^{-11} \text{ cm}$$

The nuclear radius is, however, much smaller (about 10^{-13} cm). Therefore as a good approximation, the leptonic transition currents may be evaluated at $\underline{r}_j = 0$.

2) Since the nucleon mass is large compared to the energy involved in beta decay, non-relativistic approximations may be applied to Eq.1-4 . All the terms involving γ_5 and $\underline{\alpha} = i\beta\underline{\gamma}$ are therefore dropped because they are all proportional to v/c .

Eq.1-4 now simplifies to:

$$\text{Eq.1-5} \qquad H_\beta \text{ (allowed)} = 2^{\frac{1}{2}} g \sum_j \left[C_V - C_A(i\sigma) \right] \tau_+^j \left[J(e\nu) \right]_{\underline{r}_j = 0}$$

The beta transition matrix elements $\langle f | H_\beta | i \rangle$ are then proportional to $C_V \langle i | f \rangle$ and $C_A \langle f | \underline{\sigma} | i \rangle$.

The matrix element $\int 1$ carries no angular momentum, and is called the Fermi matrix element. It gives rise to the singlet radiation which is isotropic in nature with respect to the nuclear spin.

The matrix element $\int \underline{\sigma}$ is called the Gamow-Teller matrix element, and it carries one unit of angular momentum. Eq.1-5 thus provides for the following selection rules for allowed beta transition.

<u>Allowed Beta Decay</u>

The selection rules for allowed beta decay are:

Fermi : $\Delta \underline{I} = 0$ ($I_i = I_f$); no parity change.

Gamow-Teller: $\Delta \underline{I} = 1$ ($I_i = I_f$, or $I_i = I_f \pm 1$; no $0 \rightarrow 0$) ; no parity change.

Because the total energy available has to be shared between the beta particle and the neutrino, the energy spectrum of beta decay is a continuum. The sharing of the energy is assumed to be statistical, i.e. the transition probability is proportional to the density of states of the beta particle and the neutrino, and a "statistical" spectrum may be derived theoretically. The result is:

Eq.1-6 $\frac{dN}{dE} \sim (N/f_o)\ E\ (E_o - E)^2\ (E^2 - 1)^{\frac{1}{2}}$

where f_o is a normalization integral;

N is the number of beta particles within the energy interval E and $E + dE$;

E_o is the end point energy;

all the energies are expressed in units of 511 kev , the rest mass energy of electron, plus the rest mass energy as well (which is unity) .

In addition to the statistical sharing of the available energy, Coulombic force due to the positive charge of the nucleus also plays a role in the spectral shape. For positron emitters, the positrons are pushed out of the nuclei by the Coulombic force. Consequently all the positrons gain in energy, and very few positrons remain at the low energy end of the spectrum. For negatron emitters, the Coulombic attraction reduces the kinetic energy of the negatrons, and some of the negatrons may even get trapped within the nuclei. The result is a high count rate at the low energy portion of the spectrum.

When the Coulombic effect is also taken into account, the spectral shape can be written as:

Eq.1-7 $\frac{dN}{dE} \sim pE\ (E_o - E)^2\ F(Z,E)\ /\ f(Z,E_o)$

Here p is the momentum of the beta particle, and is given by:

Eq.1-8 $p = \beta E$

Eq.1-9 $\beta = v/c = \sqrt{E^2 - 1}\ /\ E$

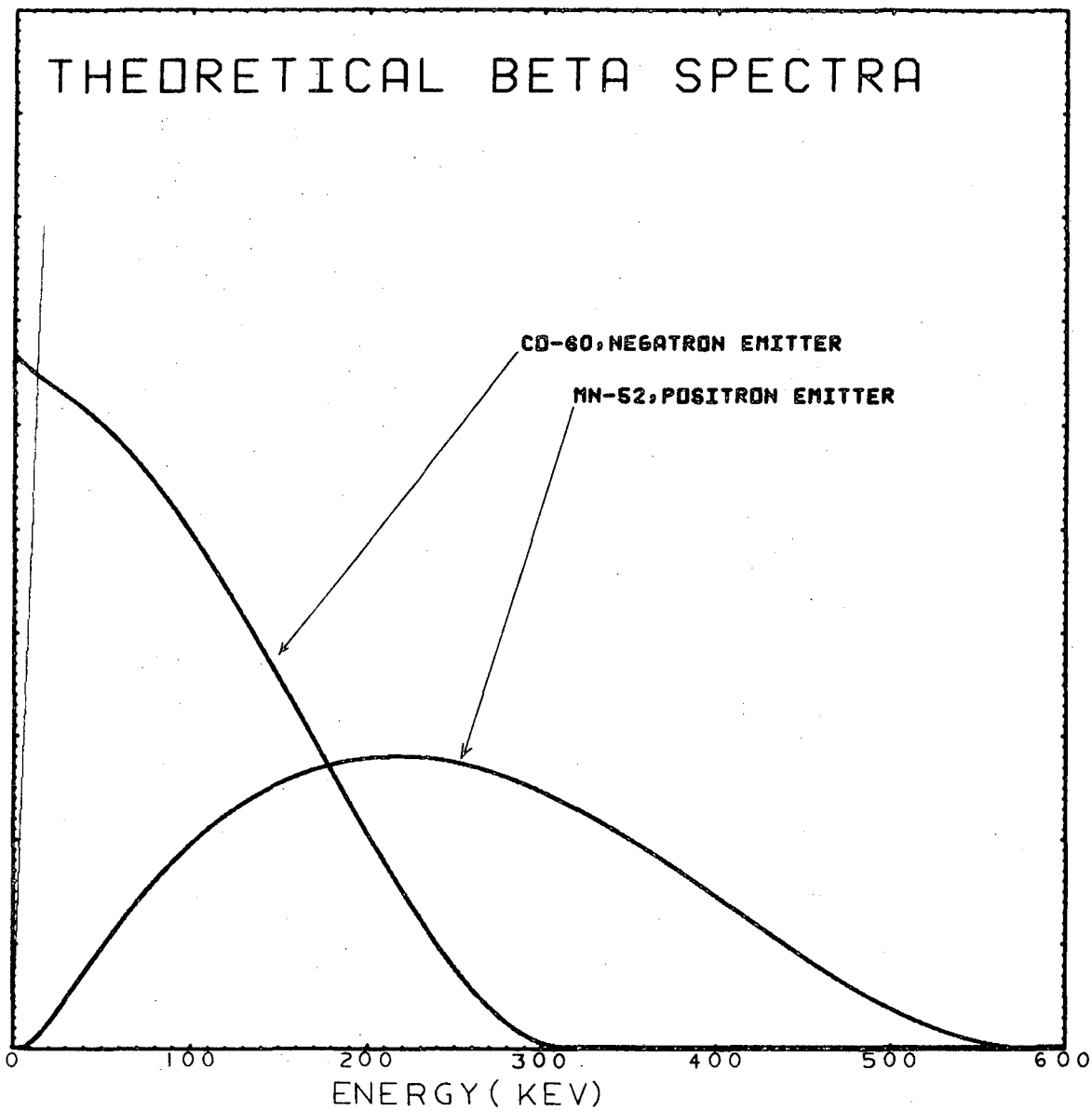

XBL 727-1272

Fig. 1. Theoretical beta spectra of ^{52}Mn and ^{60}Co .

$f(Z,E_o)$ is a normalization integral ; it is a function of the nuclear charge Z and the end point energy E_o .

$F(Z,E)$ is given by:

Eq.1-10 $$F(Z,E) = \frac{\gamma}{e^{\gamma} - 1}$$ for positrons;

Eq.1-11 $$F(Z,E) = \frac{\gamma}{1 - e^{\gamma}}$$ for negatrons;

Eq.1-12 $$\gamma = \frac{2\pi Z \alpha}{\beta}$$

where $\alpha = 1/137$, the fine structure constant.

The theoretical spectra of ^{52}Mn (a positron emitter) and ^{60}Co (a negatron emitter) are given in Fig. 1 .

An investigation of Eq.1-7 indicates that the plot of $\sqrt{\frac{N}{pE\ F(Z,E)}}$ vs. E should yield a straight line with a negative slope and an X-intercept at $E = E_o$. This is the so-called Kurie plot. A Kurie plot is very instructive for the understanding of an experimental beta spectrum. (Fig. 2)

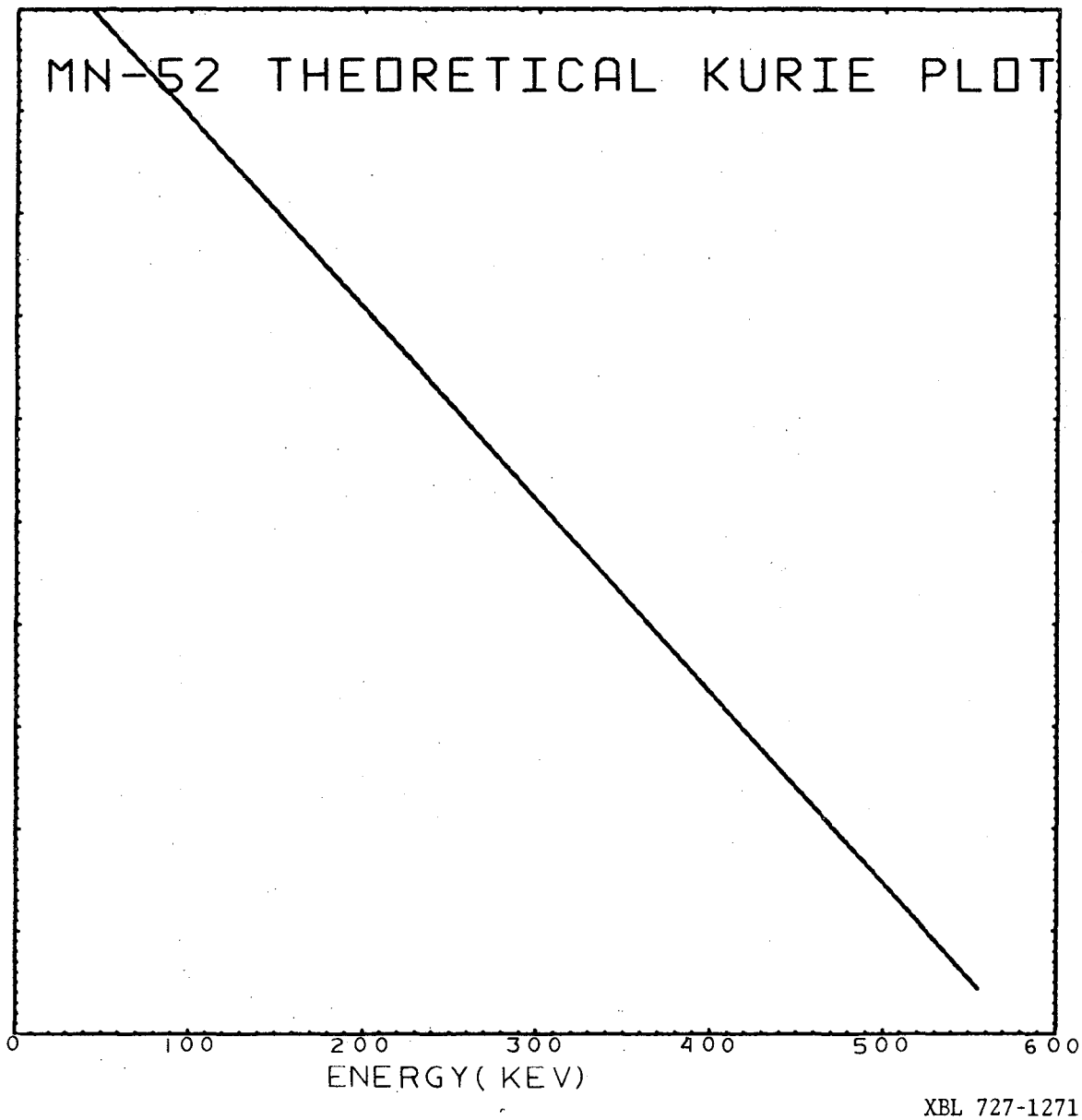

Fig. 2. Theoretical Kurie plot of ^{52}Mn beta spectrum.

Mixed Transition

Interference between the Fermi and Gamow-Teller matrix elements may occur in a mixed trnsition. An allowed I (β) I transition may come about through either pure Fermi or Gamow-Teller interactions. But very often both interactions contribute to the decay. Experimental evidences to date[5] seem to indicate that the triplet radiation predominates over the singlet radiation.*** However, even though the magnitude of $C_V M_F$ ** may be small, the interference term $C_V M_F C_A^* M_{GT}^*$ may still contribute significantly to the over all interaction picture. The beta asymmetry with respect to the nuclear spin direction is highly sensitive to the magnitude of the interference term, whereas the time reversal symmetry is sensitive to both the magnitude and the phase of the coupling of the Fermi and Gamow-Teller matrix elements.(See Chapter 2 and 3)

** From now on, $C_V M_F$ stands for the Fermi matrix element and its coupling constant; $C_A M_{GT}$ stands for the Gamow-Teller matrix element and its coupling constant.

*** This can be explained by the " Isospin Selection Rule" which will be discussed in Chapter IX .

CHAPTER II

Time Reversal Invariance

This chapter on time reversal invariance is included only because this work was done with the possibility of a future T invariance experiment in mind.

Time reversal symmetry may be understood from a non-relativistic point of view, although it is strictly a symmetry that arises from relativistic wave mechanics.

Consider the Schrodinger equation:

$$\text{Eq.2-1} \qquad H\Psi(t) = -i\frac{h}{2\pi}\frac{d\Psi(t)}{dt}$$

If we let $t \longrightarrow -t$ in Eq.2-1 , we obtain:

$$\text{Eq.2-2} \qquad H\Psi(-t) = +i\frac{h}{2\pi}\frac{d\Psi(-t)}{dt}$$

Here we are assuming a time independent Hamiltonian. Eq.2-1 and Eq.2-2 actually describe two different sets of physical laws, unless the following is true:

$$\text{Eq.2-3} \qquad H = H^*$$

We can show the condition as stated in Eq.2-3 is true by taking the complex conjugate of Eq.2-2 :

$$\text{Eq.2-4} \qquad H^*\Psi^*(-t) = -i\frac{h}{2\pi}\frac{d\Psi^*(-t)}{dt}$$

Eq.2-4 and Eq.2-1 are equivalent with the following transformation properties:

As $t \longrightarrow -t$,

$\Psi(t) \longrightarrow \Psi^*(-t)$,

<u>provided</u> that $H \longrightarrow H^*$ (i.e. H must be real).

Thus, if the Hamiltonian H is real, time reversal symmetry is invariant in the sense that the time forward state $\Psi(t)$ and the time reversed state $\Psi^*(-t)$ both satisfy the same Schrodinger equation.

If the Hamiltonian H consists of two types of interactions, such as the case of mixed allowed beta transition:

Eq.2-5 $$H = C_V H_F - C_A H_{GT}$$

The implication of Eq.2-3 is as followed:

Eq.2-6 $$C_V H_F - C_A H_{GT} = C_V^* H_F^* - C_A^* H_{GT}^*$$

If both $C_V H_F$ and $C_A H_{GT}$ are of the same phase, then by an appropriate choice of phase, both terms can be made real. However, if $C_V H_F$ and $C_A H_{GT}$ differ in phase, then only one term can be made real, and the other term must remain complex. The conclusion is that if time reversal is a symmetry at all, the relative phase between the Fermi and Gamow-Teller matrix elements must be either zero or 180 degree. The amount of time reversal violating forces is therefore proportional to the quantity $\mathrm{Im}\left[C_V M_F C_A^* M_{GT}^* \right]$.

Nuclear Orientation/Beta-Gamma Correlation Technique

This work on the beta asymmetry experiment only provides information on the ratio $|C_V||M_F|/|C_A||M_{GT}|\, e^{-i\theta}$, where θ is the relative phase between $C_V M_F$ and $C_A M_{GT}$. The absolute magnitude of the F/G-T mixing ratio can be determined only if the value of θ

is assumed. To measure the phase angle θ as well, coincidence measurement between the beta radiation and the following gamma cascade may be taken after the nuclei have been polarized.

For the allowed transition $J\ (\beta)\ J\ (\gamma)\ J'$, where J and J' are the nuclear spins, the correlation function is :[10,11,12,13]

$$\text{Eq. 2-7} \qquad W(\underline{p},\underline{k},\underline{J}) = \sum_{\nu} \Bigg\{ B_{2\nu}\left[A\left(1-\frac{\nu(2\nu+1)}{J(J+1)}\right)+B\right]\left[P_{2\nu}(\underline{J}\cdot\underline{k})\right]$$

$$-\left(\frac{v}{c}\right) B_{2\nu-1}\left(\frac{(2J+2\nu+1)(2J-2\nu+1)}{4J(J+1)(4\nu-1)(4\nu+1)}\right)^{\frac{1}{2}}\left[2\nu\left(J(J+1)\right)^{-\frac{1}{2}}C-D\right]$$

$$\left[\underline{p}\cdot\underline{k}\ P_{2\nu}'(\underline{J}\cdot\underline{k})-\underline{p}\cdot\underline{J}\ P_{2\nu-1}'(\underline{J}\cdot\underline{k})\right]$$

$$-\left(\frac{v}{c}\right) B_{2\nu+1}\left(\frac{(J+\nu+1)(J-\nu)}{J(J+1)(4\nu+1)(4\nu+3)}\right)^{\frac{1}{2}}\left[(2\nu+1)\left(J(J+1)\right)^{-\frac{1}{2}}C+D\right]$$

$$\left[\underline{p}\cdot\underline{k}\ P_{2\nu}'(\underline{J}\cdot\underline{k})-\underline{p}\cdot\underline{J}\ P_{2\nu+1}'(\underline{J}\cdot\underline{k})\right]$$

$$-\left(\frac{v}{c}\right) B_{2\nu}\left[\left(4J(J+1)\right)^{-\frac{1}{2}}E\right]\left[\underline{J}\cdot\underline{p}X\underline{k}\ P_{2\nu}'(\underline{J}\cdot\underline{k})\right] \Bigg\} F_{2\nu}(LJ'J)$$

Here $\underline{p}$ is the direction of the beta emission;

$\underline{k}$ is the direction of the following gamma;

$\underline{J}$ is the nuclear spin direction;

L is the multipolarity of the gamma ray.

The sum on ν is from zero to the lesser of J, J' and L. For ^{52}Mn, the multipolarity of the $6+(\gamma)4+$ 744 kev gamma line is 2 .

Therefore the highest term to be contended with is $F_4(246)$.
The functions $P_{2\nu}(\cos\theta)$ are the usual Legendre polynomials.
The function $F_{2\nu}(LJ'J)$ is the well known angular correlation function.[14]
The coefficients A,B,C,D,E cotain information on the Fermi and Gamow-Teller mixing ratio:

$$A = |C_A|^2 |M_{GT}|^2$$

$$B = |C_V|^2 |M_F|^2$$

$$C = \pm\, |C_A|^2 |M_{GT}|^2 \qquad \text{for} \quad \beta^{\pm}$$

$$D = -\left[C_V M_F C_A^* M_{GT}^* + C_V^* M_F^* C_A M_{GT} \right] = -2\left[|C_V|\,|M_F|\,|C_A|\,|M_{GT}| \right]\cos\theta$$

$$E = i\left[C_V M_F C_A^* M_{GT}^* - C_V^* M_F^* C_A M_{GT} \right] = 2\left[|C_V|\,|M_F|\,|C_A|\,|M_{GT}| \right]\sin\theta$$

where θ is the phase between the Fermi and Gamow-Teller terms.

Eq.2-7 can be greatly simplified if we use an arrangement as shown in Fig. 3 . In such an arrangement, the beta detector and the polarization axis are perpendicular to each other. The gamma detector is so placed that the plane defined by the gamma detector and the nuclear spin axis, and the plane defined by the beta detector and the nuclear spin axis are mutually perpendicular. This is what may be called the "out-of-plane" measurement. In an "out-of-plane" measurement, all the terms involving $\underline{p}\cdot\underline{k}$ and $\underline{p}\cdot\underline{k}$ vanish, and Eq.2-7 reduces to:

$$\text{Eq.2-8} \qquad W(\underline{p},\underline{k},\underline{J}) = \sum_{\nu}\Bigg[B_{2\nu}\left(A\left[1 - \frac{\nu(2\nu+1)}{J(J+1)}\right] + B \right) P_{2\nu}(\underline{J}\cdot\underline{k})$$

$$- \left(\frac{v}{c}\right) B_{2\nu}\left(\left[4J(J+1)\right]^{-\frac{1}{2}} E \right) \underline{J}\cdot\underline{p} \times \underline{k} \;\; P_{2\nu}'(\underline{J}\cdot\underline{k}) \Bigg] F_{2\nu}(LJ'J)$$

Fig. 3. The "in-plane" and "out-of-plane" arrangements for the time-reversal invariance experiment. An angle of 45° between the γ detector and the polarization axis H provides the greatest sensitivity. If the time-reversal symmetry is invariant, there should be no change in count rate when the polarizing field H is reversed in direction in the "out-of-plane" arrangement.

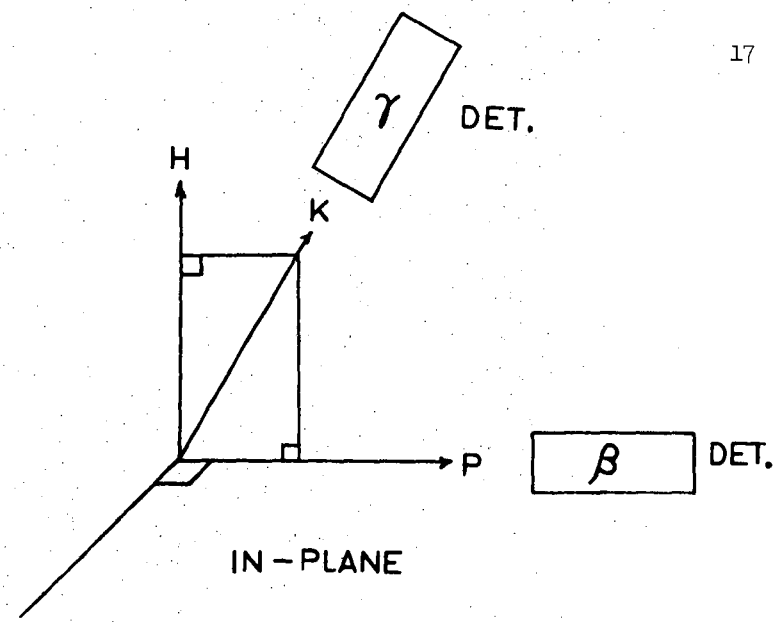

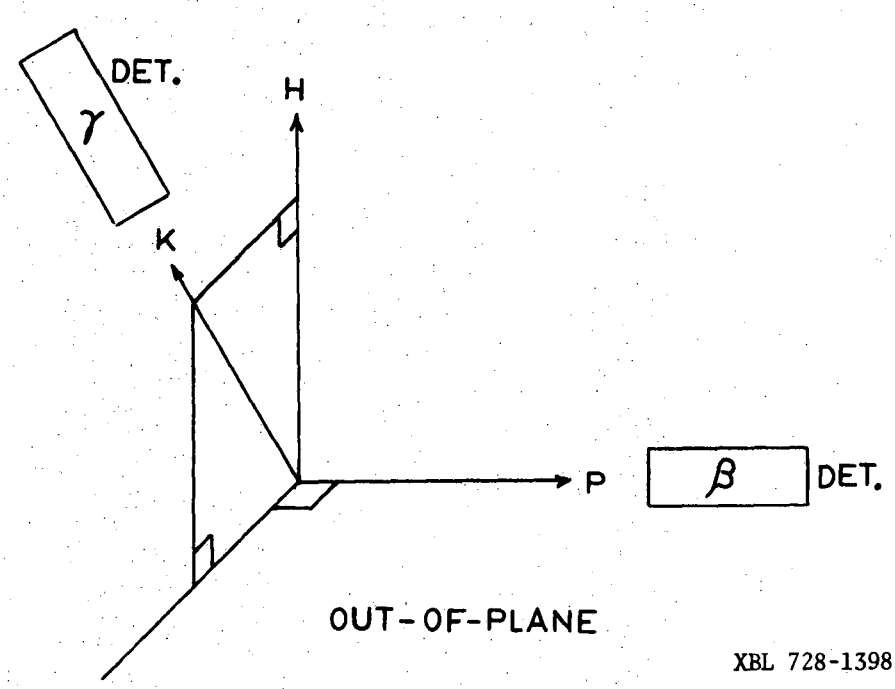

XBL 728-1398

Fig. 3.

It should be pointed out that the $P'_{2\nu}(\underline{J}\ \underline{k})$ terms are odd with respect to $\underline{J}$, whereas the $P_{2\nu}(\underline{J}\ \underline{k})$ terms are even with respect to $\underline{J}$. Therefore the difference in count rates between forward polarizing field direction and backward polarizing field direction measurements can be given by:

$$\text{Eq. 2-9} \quad \left[W(\underline{p},\underline{k},\underline{J}) - W(\underline{p},\underline{k},-\underline{J})\right]/2$$

$$= \left(\frac{v}{c}\right) \sum_{\nu} \left[B_{2\nu} \left(4J(J+1)\right)^{-\frac{1}{2}} \quad \underline{J}\cdot\underline{p} \times \underline{k} \quad P'_{2\nu}(\underline{J}\ \underline{k}) \quad \frac{E}{A+B} \right] F_{2\nu}(LJ'J)$$

where the correlation functions $W(\underline{p},\underline{k},\underline{J})$ and $W(\underline{p},\underline{k},-\underline{J})$ have been normalized to unity when the source is warm. The factor $\frac{E}{A+B}$ is simply:

$$\text{Eq. 2-10} \quad \frac{E}{A+B} = \frac{2\ |C_V|\,|M_F|\,|C_A|\,|M_{GT}|\ \sin\theta}{|C_V|^2|M_F|^2 + |C_A|^2|M_{GT}|^2}$$

$$= \frac{2\ a\ \sin\theta}{1 + a^2}$$

where a is the absolute magnitude of the F/G-T ratio. When $\theta = 0$ or π, the factor $E/(A+B)$ vanishes, and there should be no difference in the forward field and backward field measurements. In theory, the degree of time reversal violation is proportional to the effect $W(\underline{p},\underline{k},\underline{J}) - W(\underline{p},\underline{k},-\underline{J})$. In practice, however, the analysis of the experimental results may be a lot more involved. There may be some "in-plane" contribution to the over all effect $W(\underline{p},\underline{k},\underline{J}) - W(\underline{p},\underline{k},-\underline{J})$.

In an "in-plane" measurement, the gamma detector, beta detector and the nuclear spin axis all lie in the same plane.(Fig. 3) This causes the terms involving $\underline{J}\cdot\underline{p} \times \underline{k}$ to vanish from Eq.2-7 . In addition, the beta detector is placed perpendicular to the nuclear spin axis as in the case of "out-of-plane" measurement, and this arrangement causes the $\underline{p}\cdot\underline{J}$ terms to disappear also. A careful examination of the Eq.2-7 indicates that the "in-plane" arrangement basically measures the quantity $a \cos\theta / (1+a^2)$. In fact, the quantity $W(\underline{p},\underline{k},\underline{J}) - W(\underline{p},\underline{k},-\underline{J})$ is maximum in an "in-plane" measurement if time reversal is invariant. The fact that $W(p,k,J) - W(p,k,-J)$ is non-zero in the "in-plane" arrangement complicates the data analysis of the "out-of-plane" experiment. A slight deviation in the geometric arrangement of the detectors with respect to the polarizing field may cause some contribution from the "in-plane" effect. In short, Eq.2-7 should be used to correct for a geometric effect, which is judged to be the most serious source of experimental error in the future time reversal experiment.

It should be pointed out that both "in-plane" β-γ coincidence experiment and the beta asymmetry experiment measure the same quantity $a \cos\theta /(1+a^2)$. However, the beta asymmetry experiment is judged to provide more accurate result. The knowledge of the term $a \cos\theta/(1+a^2)$ (from beta asymmetry) and the term $a \sin\theta/(1+a^2)$ (from Eq.2-10) enables one to compute the magnitude of θ .

CHAPTER III

Nuclear Orientation

Nuclear orientation theory has been well described in many review papers[15]. The angular distribution of radiation with respect to the nuclear spin direction is a natural cosequence of the conservation law of angular momentum. In order for a particle to be emitted preferentially in a certain direction, the magnetic sub-states of the nuclei must be preferentially populated. When the Zeeman splitting of an isotope is comparable to the thermal energy*, the Boltzmann distribution law dictates that the lower states be significantly more populated than the upper states**. The adiabetic demagnetization technique is capable of bringing the nuclei down to a temperature of 5×10^{-3} ^{o}K. The thermal energy kT is then about 10^{-18} ergs. ^{52}Mn, ^{60}Co and many other nuclei have magnetic moments of about 10^{-24} ergs/gauss***. A field of about 10^{5} G is therefore necessary to achieve a reasonable degree of orientation. One hundred kilogauss is just about the technological limit of the present high field superconducting magnets. Although the so-called "brute-force" technique may be used for isotopes with large magnetic moments, the degree of orientation in general is rather small.

---

* We assume here the condition of thermal equilibrium.

** From a statistical mechanical point of view, the ensemble of the nuclei are so dilute in the lattice that both the Bose-Einstein and the Fermi-Dirac statistics become unimportant.

*** Nuclear magneton $\mu_N = 5.05 \times 10^{-24}$ ergs/gauss.

Advantage may be taken of the large hyperfine field when certain isotopes are implanted into a ferromagnetic lattice. The hyperfine field of ^{52}Mn in Fe is -226.97 KG [16], and is anti-parallel to the external polarizing field direction. The B_1, B_2 and B_4 terms of ^{52}Mn as a function of temperature are plotted in Fig. 4. As can be seen from the graph, the degree of orientation is quite large for temperature less than 10^{-2} ^{o}K.

The angular distribution function for gamma radiation can be given as:

Eq.3-1 $$W(\theta) = 1 + U_2B_2F_2Q_2P_2(\cos\theta) + U_4B_4F_4Q_4P_4(\cos\theta) + \ldots \;;$$

Since most of the gamma photons are of the multipolarity of 2, the series normally terminates at the $P_4(\cos\theta)$ term. The B_k terms are the statistical tensors which describe the degree of orientation. The B_k terms contain the temperature dependency. The Q_k terms are the solid angle correction factors which take into account the effect due to solid angle subtended by the detector. The F_k terms are the well known angular correlation functions, and they contain information about the angular momentum of the system. The U_k terms are the reorientation parameters. They take into consideration the reorientation due to previous unobserved radiation. A set of formulae for the B_k, U_k and F_k are given in Appendix 1.

The correlation function for an allowed beta transition is:

Eq.3-2 $$W(\theta) = 1 + \left(\frac{v}{c}\right) A_{\pm} \frac{\langle m_z \rangle}{I} \cos\theta$$

where $A_{\pm}$ is the asymmetry parameter of $\beta^{\pm}$;

$\langle m_z \rangle$ is the average z-component of the ensemble of nuclei with spin I. The polarization term $\frac{\langle m_z \rangle}{I}$ is

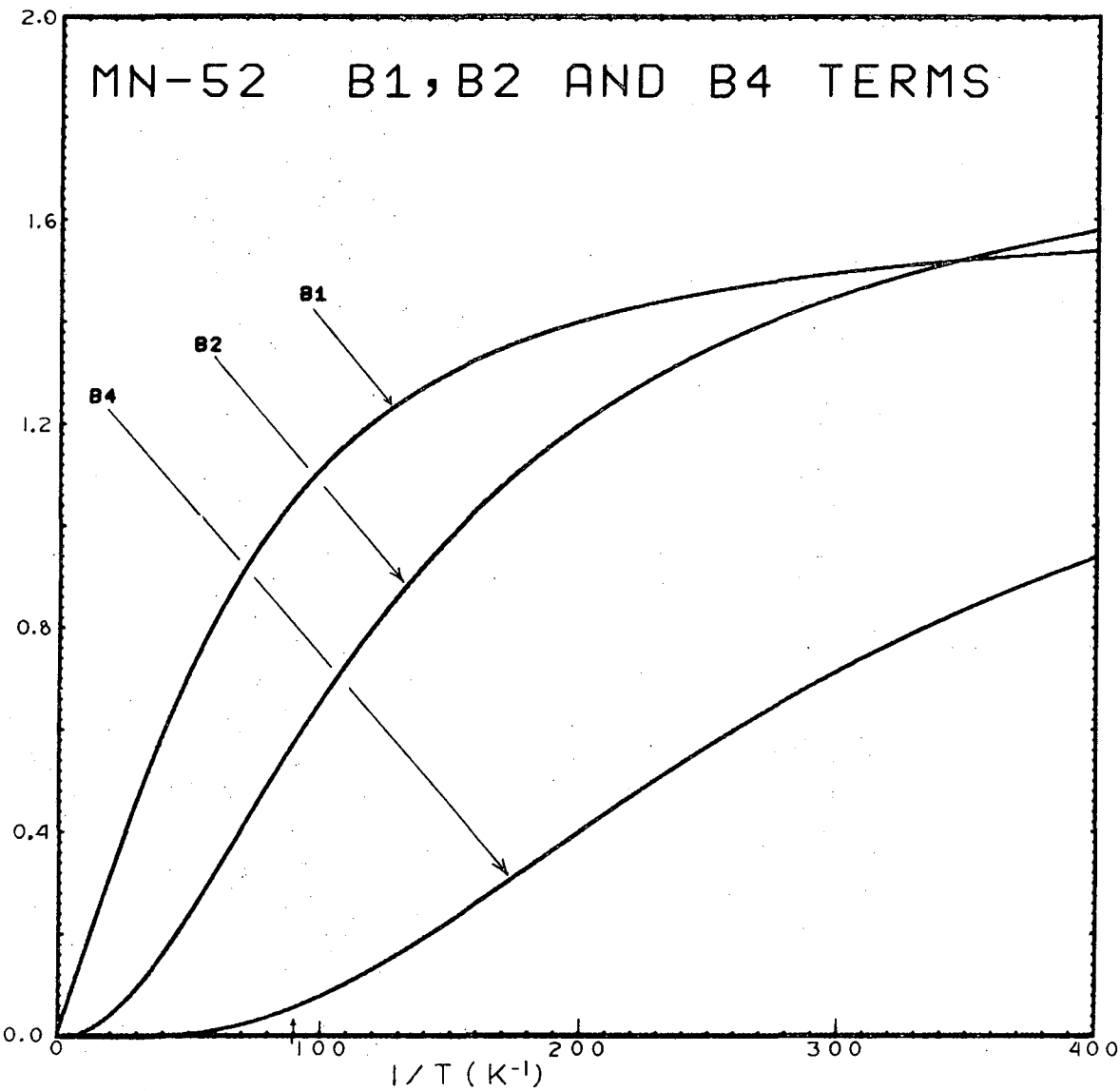

XBL 727-1278

Fig. 4. B_1 , B_2 and B_4 terms as functions of the temperature of ^{52}Mn.

related to the statistical tensor B_1 as:

$$\text{Eq.3-3} \qquad B_1 = \sqrt{3I/(I+1)}\ \frac{\langle m_z \rangle}{I} .$$

For a mixed allowed transition such as ^{52}Mn , $A_\pm$ is given by the equation: [17]

$$\text{Eq.3-4} \qquad A_\pm = \frac{\pm \frac{1}{I+1} |C_A|^2 |M_{GT}|^2 - 2\sqrt{\frac{I}{I+1}}\ (C_V C_A^* M_F M_{GT}^*)}{|C_V|^2 |M_F|^2 + |C_A|^2 |M_{GT}|^2}$$

Let $a = |C_V||M_F|/|C_A||M_{GT}|$

and $C_V M_F = C_A M_{GT}\ a\, e^{i\theta}$, then Eq.3-4 becomes:

$$\text{Eq.3-5} \qquad A_\pm = \frac{\pm \frac{1}{I+1} - 2\sqrt{\frac{I}{I+1}}\ a \cos\theta}{1 + a^2}$$

For pure Gamow-Teller transition, such as ^{60}Co , then:

$$\text{Eq.3-6} \qquad A_\pm = \pm \lambda \qquad \text{where } \lambda = 1 \text{ for } I_f = I_i - 1 ;$$

$$\lambda = - I_i/(I_i+1) \quad \text{for } I_f = I_i + 1 .$$

The spin sequence for ^{60}Co is $5+(\beta)4+(\gamma)2+(\gamma)0+$, therefore it has a theoretical asymmetry of -1 . Comparison can thus be made between the theoretical value of A and the value determined experimentally from this work.

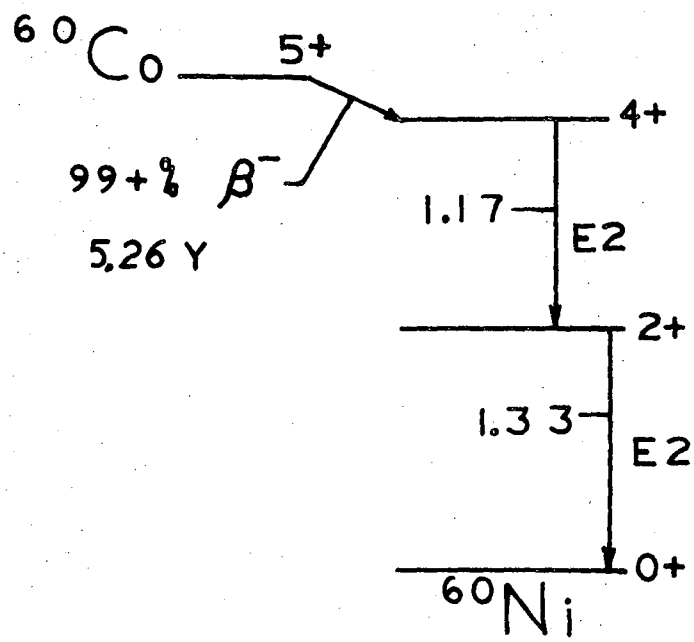

XBL 728-1397

Fig. 5. The decay scheme of ^{60}Co .

Thermometry

In order to calculate the parameter A , the degree of polarization of the isotope must be known. This requires a knowledge of the final temperature achieved. For the case of the ^{60}Co beta asymmetry experiment, ^{60}Co thermometry is well known,[18] and the determination of the temperature can be done by observing the anisotropy of either the 1.17 or the 1.33 Mev gamma lines as a function of temperature T . The decay scheme of ^{60}Co is presented in Fig.5 .

The decay scheme for ^{52}Mn is slightly more complicated. (See Fig. 6) 89% of ^{52}Mn undergoes a 6+(β)6+ transition, and in order to calculate the U_k coefficients (k = 2, 4) , we assume the transition is a pure Gamow-Teller transition. This is justified on the basis that we expect the Fermi contribution to be small, and it can be further justified from the experimental result of this work. The coefficients $U_2(661)$ and $U_4(661)$ can thus be calculated. (See Appendix 1) A maximum error of 5% is expected on the temperature scale determined from the gamma anisotropy of ^{52}Mn.

Only the 744 kev line should be used in the ^{52}Mn thermometry. First of all, although the gamma cascades of ^{52}Mn are "stretched" , the 935 kev and 1.434 Mev lines are also fed by the other 11% ^{52}Mn which do not go through the 6+(β)6+ transition. Of the 11% ^{52}Mn, 3% of which undergo transitions which are not well known at the present time. Secondly, the response of the gamma detector to the 1.434 Mev line is low. The 1.434 line is further complicated by the presence of the 1.37 line from ^{56}Co which exist as an impurity in the source.

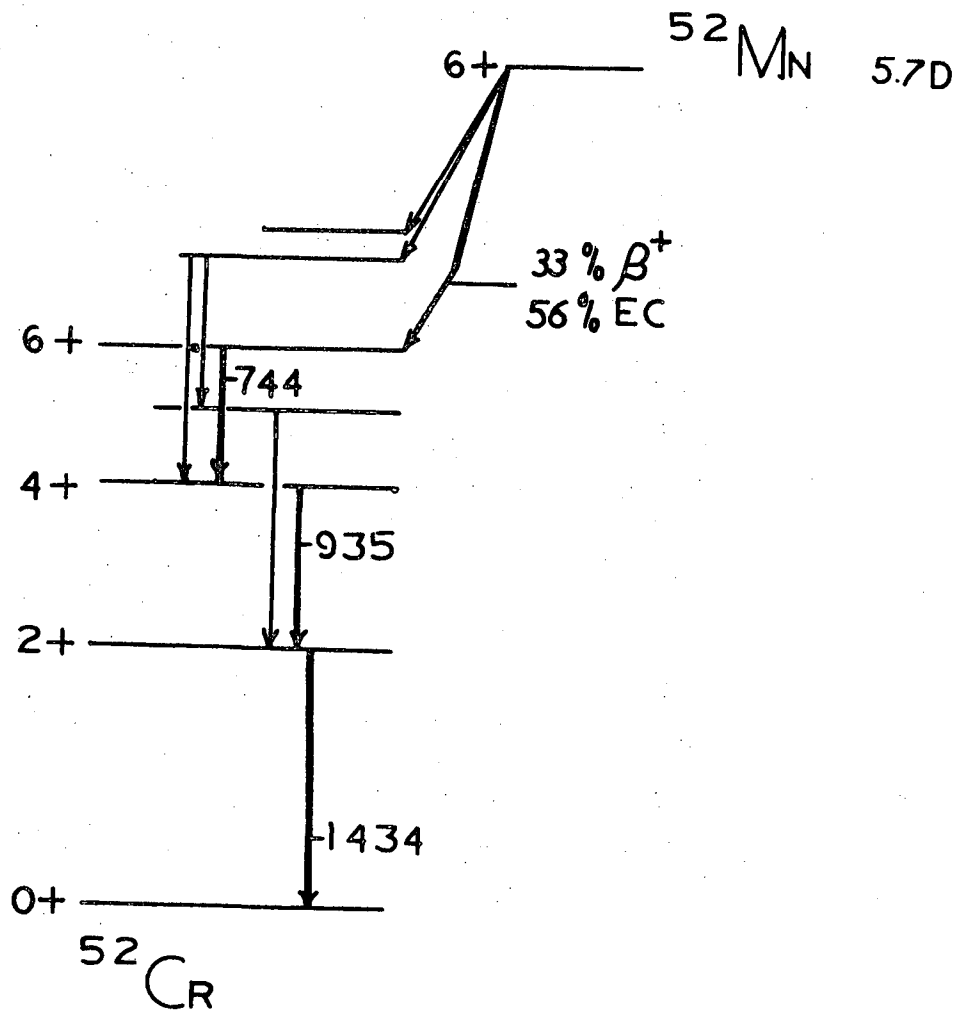

XBL 728-1396

Fig. 6. The decay scheme of ^{52}Mn .

It should be pointed out that a 5% error in the temperature determination would result only in a 1% error in the determination of the polarization (B_1 term) of the isotope in the 10^{-2} °K region. This is an insignificant error compared to other more serious sources of errors which will be discussed later. A list of pertinent data on ^{52}Mn is given in Appendix 2 .

CHAPTER IV

Low Temperature Particle Detectors

An ideal beta detector for the beta asymmetry measurement should have the following properties:

1) Good stability, linearity and energy resolution.
2) Functional down to $1^{o}K$.
3) Minimal gamma ray response.
4) Minimal backscattering of the beta particles from the detector.
5) Ability to distinguish beta particles from other high energy electrons.
6) Ease of operation.

Energy Resolution and Stability

A good detector should have good stability, linearity, energy resolution and reliability - even down to low temperature. Scintillator counters normally have high efficiency, but the energy resolution is sacrificed. Since they utilize the photo-multiplier (PM) tubes to amplify the signals, these counters cannot tolerate moderate magnetic fields unless the PM tubes can be placed far from the scintilators. But in so doing further degradation in energy resolution is introduced due to the photo loss in the connecting light pipes.

Special problems are created when scintillator counters are used as particle detectors at low temperature. First of all, since the scintillator crystals have to be within the cryostat whereas the PM tubes cannot, scintillations have to be conducted to the exterior with light pipes. The energy resolution is therefore worsened in addition to special mechanical and vacuum problems. The very first experiment on parity violation by Ambler *et al*[19] in fact utilized an anthracene scintillator for their beta asymmetry measurement. (Fig. 7)

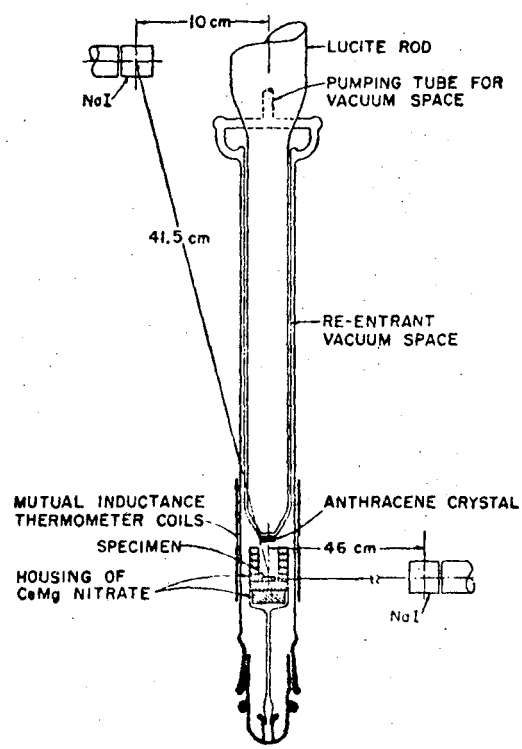

XBL 728-1414

Fig. 7. The use of an anthracene scintillator for low temperature beta work (taken from Ref. 19).

Solid state detectors have found increasing acceptances in the field of perticle detectors. They have good energy resolution and linearity; they are magnetic field independent as well as relatively insensitive to high voltage power supply fluctuation. Their shortcoming lies perhaps in their narrow temperature range of operation. They normally have to be kept at LN temperature because the leakage current is too large at room temperature.

Low Temperature Operation

Detectors functional down to $1^{o}K$ are highly desirable. Since the nuclei very often are cooled down to milli-degrees, a "hot" detector may present a source of sizable radiation heat leak.* It is of course important to keep the nuclei as cold as possible for as long as possible. A "hot" detector may require using a mechanism which can continuously absorb the heat influx into the system. The He^3-He^4 refrigeration technique may be useful for this purpose, but the adiabetic demagnetization technique using chrome alum ($CrK(SO_4)_2 \cdot 12H_2O$) may also serve the purpose. Chrome alum has a much larger heat capacity than CMN ($Ce_2Mg_3(NO_3)_{12} \cdot 24H_2O$), but it too, like the He^3-He^4 refrigerator, would have difficulty in cooling the nuclei down to below 15 ^{o}mK ($1/T = 70$).

---

* Radiation energy is given as σT^4 , where $\sigma \sim 10^{-5}$ ergs/sec/cm^2 . If $T = 40\ ^{o}K$, then radiation heat leak is $\sim 10^{-5} \times (40)^4$ ~ 10 ergs/sec/cm^2 , which is one order of magnitude higher than the capability of CMN.

Surface barrier detectors have found their usage in the area of low temperature particle detection.[20] It is not uncommon to find surface barrier detectors capable of working below 1 ^{o}K. Their shortcoming lies in their unreliability. Not only do many crystals have to be tried before one emerges as a functional detector, but the functional one may also behave differently from experiment to experiment.

A surface barrier detector consists basically of a block of silicon or germanium crystal. Electrodes are attached to the front and back surfaces by the deposition of thin films of gold. For reasons still unknown, perhaps due to the impurity or the oxidation of the surface layers before the deposition of the electrodes, an electric barrier junction exists between the bulk material and the front electrode. The high resistance of the barrier produces an intense electric field across the junction when a high voltage is applied at the electrodes. The region within which the intense electric field exists is termed the "depletion zone". Within the depletion zone, ionizations due to radiation are quickly swept away by the electric field to produce electric pulses. If the depletion depth is greater than the average stopping range of the particles, the detector is called an E detector. An E detector is very useful since the pulse height produced from an ionizing radiation is proportional to the energy of the particle.

Alpha particles and fission fragments have very short range in silicon or germanium, therefore surface barrier detectors can behave as E detectors for alpha and fission fragment spectroscopy. On the other hand, beta particles have relatively long range in silicon or germanium* - certainly longer than the barrier depth -

---

* About 1.3 mm/Mev in Ge or 2.4 mm/Mev in Si .

therefore better alternatives have to be found. Nevertheless, surface barrier detectors can still serve as transmission (dE/dx) detectors for beta spectroscopy. The energy response of the dE/dx detectors would have to be known, and this requires energy calibration with various mono-energetic sources.[21] Normally the beta spectrum after the so-called unfolding process deviates greatly from the anticipated spectral shape.

A semi-conductor behaves like a perfect diode. If reversed biased voltage is applied, a depletion zone is developed with the depletion depth D given by [22]

$$\text{Eq.4-1} \qquad D = \frac{K\,(V + V_0)^{\frac{1}{2}}}{2\pi N}$$

where K is the dielectric constant of the material;
N is the net density of electrically active centers in the doped region;
V_0 is the built-in potential under equilibrium conditions;*
V is the applied voltage.

The important features of Eq.4-1 is that

$D \sim V^{\frac{1}{2}}$ and

$D \sim 1/N$.

The depletion depth can be increased by applying a high bias voltage. There is a limit to the high voltage, however, above which avalanche breakdown of the detector would occur.**

---

* ~ 0.3 volt for germanium, and 0.7 volt for silicon.

** About 250 KV/cm

The depletion depth can also be increased by decreasing the amount of doping. However, there is again a physical limitation due to the failure of humans' ability to create high purity crystal. Purity of one part in 10^8 is readily available for germanium, but such a level of impurity is not acceptable even when cooled to the liquid nitrogen (LN) temperature of 77^oK .

The number of impurity charge carriers (N) can be electrically compensated by drifting lithium into the semi-conductor under the infuence of an electric field at high temperature.[23] Such lithium drifted germanium detectors have found wide spread usage in gamma spectroscopy. In the area of low temperature beta studies, pioneering work has been done by Bill Brewer,[24] in which lithium drifted beta detectors were used at a temperature of 17^oK . Heaters and thermometers had to be provided since the detector chambers were situated right in the 1^oK liquid helium (LHe) bath, but the heat leak did not present itself as a great problem. The shortcoming of the lithium drifted detectors lies in their instability at room temperature. When the detector has to be warmed up periodically with the cryostat as in the present work, detector deterioration may become a major concern. Lithium drifted silicon detectors are much more stable at room temperature, but the most successful ones fail to operate beyond the lower limit of about 40^oK .[25]

Charge trapping is the most serious problem for detectors operating at low temperature. Traps exist in the material due to the impurity centers or crystal imperfections. Traps provide intermediate pathways through which recombination or generation processes can take place, but they are of no serious concern to cryogenic experimenters. More serious are the traps which exhibit selectivity for holes or electrons. Trapped carriers are not easily re-excited at low temperature, and localized storage of charge may occur.

This is called polarization, and the collection of carriers is inhibited in the detector due to the intense localized electric field. In essence, the amount of trapping centers determines the low temperature limit of a detector.

Trapping centers cannot be compensated by lithium drifting. However, recent development in the area of high purity germanium technology produced a break-through. Now, high purity germanium detectors can be made with impurity level of one part in 10^{11} or better, and some of these detectors have been demonstrated to function properly down to $6^{o}K$.[25]

The detector used for this work is a high purity germanium detector with the depletion depth slightly greater than 1/2 mm thick. It has worked consistently well at a temperature below $1.2^{o}K$, but it tends to polarize after a period of about twelve hours. It also exhibit the phenomenon of radiation damage, as it deteriorates faster when the count rate is increased. A forward voltage of 1 - 2 volts may be applied to sweep out the trapped charges after each counting period.

Gamma-rays Response

A perfect particle detector is one which can discriminate against any gamma background. In favorable cases where the end-point energy of the beta particles is greater than all the gamma energies, this is not an important criterion. Although the gamma rays are going to contribute significantly to the beta spectrum at the low energy side, beta asymmetry can still be determined from the high energy side of the beta spectrum.[24]

Unfortunately, practically all mixed allowed beta transitions are accompanied by gamma rays of higher energies. The 744 kev, 935 kev and 1.43 Mev lines of ^{52}Mn were detected on top of the

beta spectrum when the detectors reported in Ref. 24 were used*. Other means must therefore be employed to reduce the gamma response to a minimum. One possible technique utilizes an arrangement as illustrated in Figure 8 .[26] A transmission detector is placed in front of a thick E detector. Since the thin dE/dx detector is relatively transparent to the gamma rays, coincident counts between the transmission detector pulses and the full E detector pulses should reveal a beta spectrum relatively free of gamma background.** This arrangement is abandoned, however, for technical reasons which will be discussed later.

For positron emitters, an additional technique may be applied. Positrons may be stopped completely in a medium, and the annihilation photons may be detected in coincidence with external gamma detectors. Besides the problem of low efficiency, this method is unable to detect the beta particles as a function of their energy, therefore the (v/c) dependence of the beta asymmetry is lost .

Back-scattering from the Detector

It has been estimated[24] that around 30% of all electrons would be back-scattered from the surface of the detector. The partial deposition of energy of these back-scattered beta particles results in a large count rate at the lower energy portion of the beta spectrum. In order to have a good beta spectrum, means must be provided to eliminate the counting of these back-scattered electrons. The arrangement as illustrated in Figure 8 is capable of doing just that with an appropriate choice of the window on the transmission detector pulses. The arrangement was abandoned in this work for the following reasons:

---

* Depletion depth of 1.5 mm .

** Other effects such as Compton electrons can interfere severely with the beta spectrum.

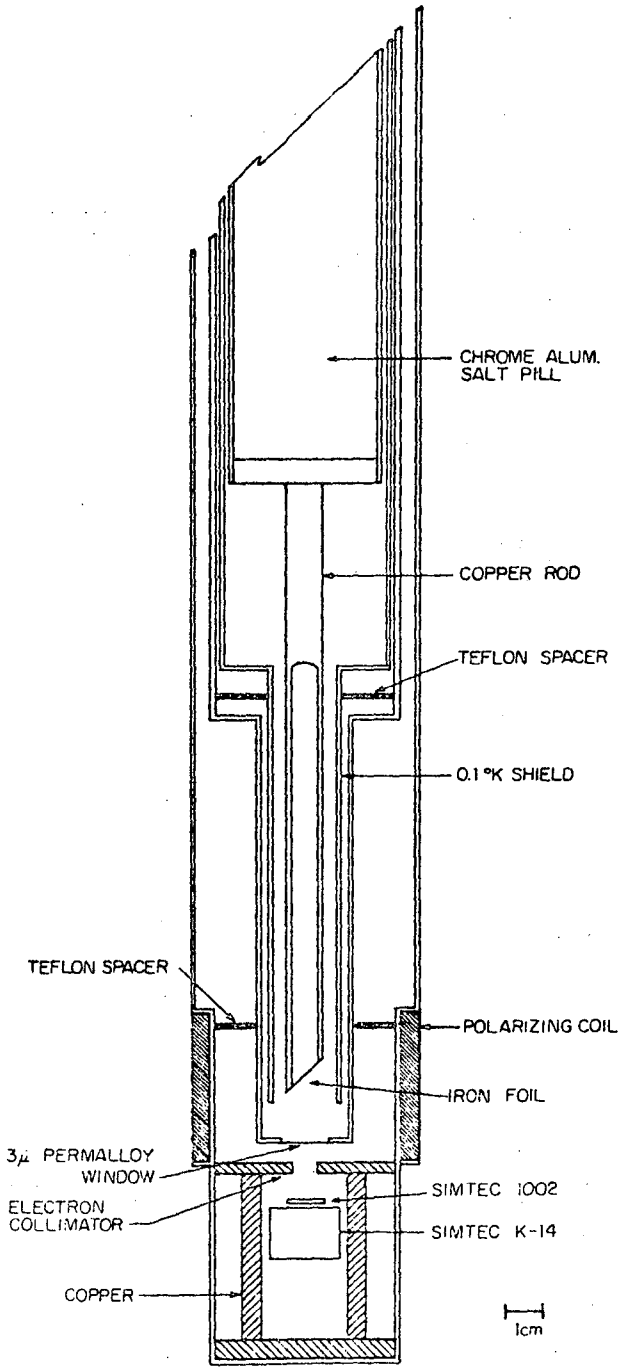

XBL 728-1401

Fig. 8. An arrangement specifically to reduce the gamma response and the backscattering of the beta detector. (Taken from Ref. 26)

1) A low temperature transmission detector is not available at the present moment. A layer of lithium has to be drifted into the high purity germanium crystal to form the n- contact. This layer should not be made too thin* if the detector is to be functional. The use of a silicon transmission detector operating at $77^{o}K$ was judged to be unwise for this work because, as mentioned previously, a "hot" detector prohibits the achievement of low temperature of the source, and therefore reduces the degree of orientation of the nuclei.

2) The most serious problem with low temperature beta spectroscopy arises from the interference of the Compton electrons. For nuclear orientation experiments, the chambers in which the beta particles are in flight are invariably small. For unfavorable cases such as ^{52}Mn , a large amount of Compton electrons are produced from the interactions of the numerous gamma rays with the cryostat walls, copper fins and the detector chambers' walls. The arrangement of Fig. 8 cannot fare better in this significant area than any other detector.

---

* About 100 microns.

Fig. 9. The average range of electrons in germanium and silicon as functions of the electron kinetic energy.

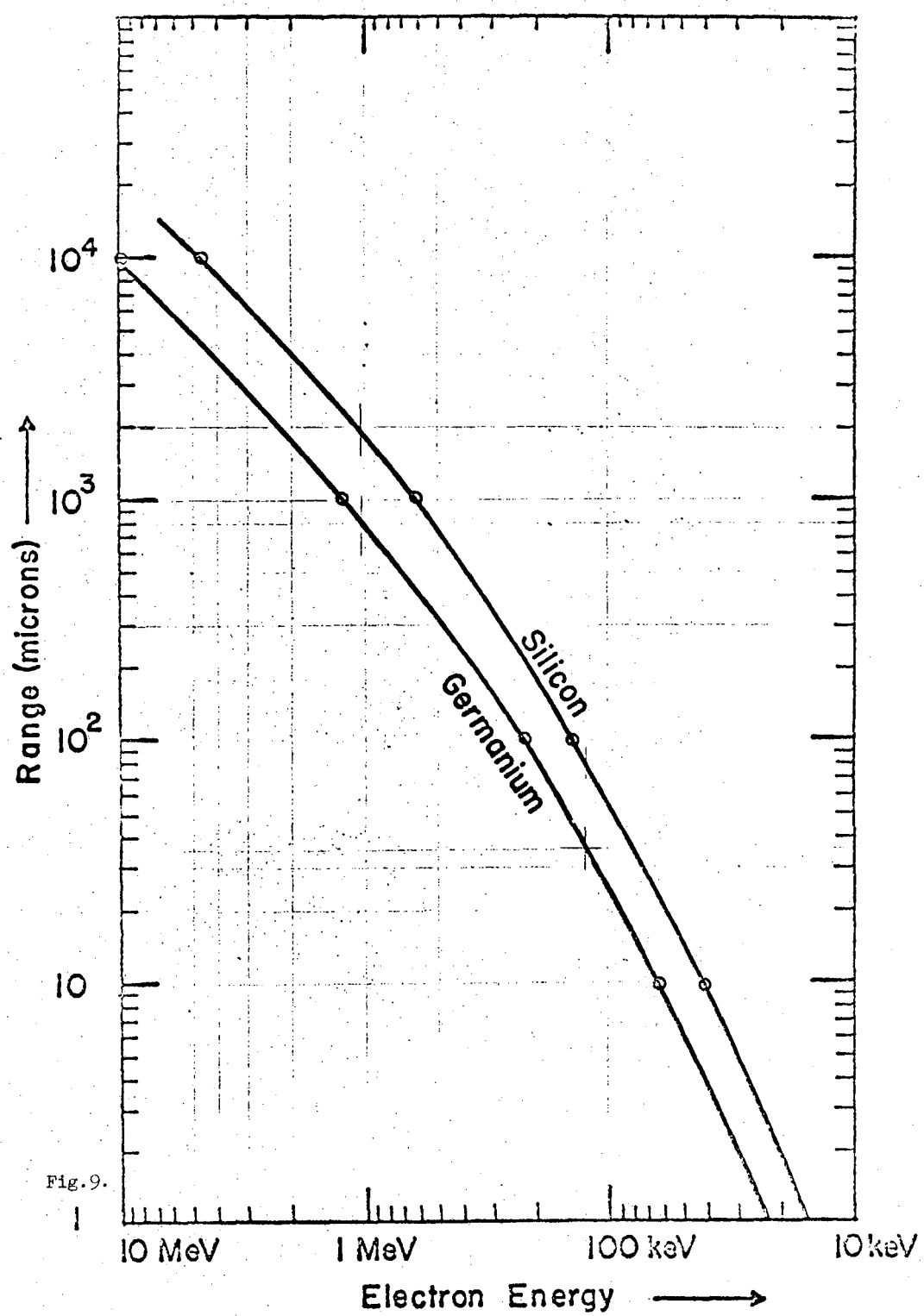

Fig.9.

XBL 728-1400

CHAPTER V

Fundamental Experimental Difficulties and their Solutions

It is probably instructive at this point to consider the problems encountered in the present work. The designs and experimental set-up are directed to overcome these difficulties.

The Gamma Response of the Detector

The decay scheme of ^{52}Mn is given in Fig. 6 . 33% of ^{52}Mn decays by positrons emission (end-point energy 580 kev) to the third excited state of ^{52}Cr , which in turns decays by the cascade emission of 744 , 935 , and 1434 kev gamma rays. The spin and parity sequence is $6+(\beta)6+(\gamma)4+(\gamma)2+(\gamma)0+$ [27]. The fact to be noted is that for every positron emitted there is a total of nine high energy gamma transitions plus two 511 kev annihilation photons. Because of the high gamma background, the detector should be as insensitive to gamma rays as possible. For this purpose, a high purity germanium detector with depletion depth of slightly in excess of 1/2 mm was used. The range-energy relationship of electrons in germanium and silicon is given in Figure 9 . According to the graph, electrons of up to 700 kev in energy should be stopped completely by the detector. Electrons in excess of 700 kev deposit only partial energy, and in general exhibit a skew and poorly resolved spectrum.

The gamma response of the thin detector used in this work is very small. Figure 10 shows the absorption cross-section of gamma rays in germanium due to various processes.[28] Appendix 3 contains a discussion on the theoretical aspects of the gamma reponse in germanium detectors. A ^{22}Na source of 50 mr/hr was placed one inch from the detector chamber window (maintained at LN temperature). The total count rate with the threshold cut-off level set at 100 kev was less than 50 counts/sec. , and the 511 kev line was hardly distinguishable.

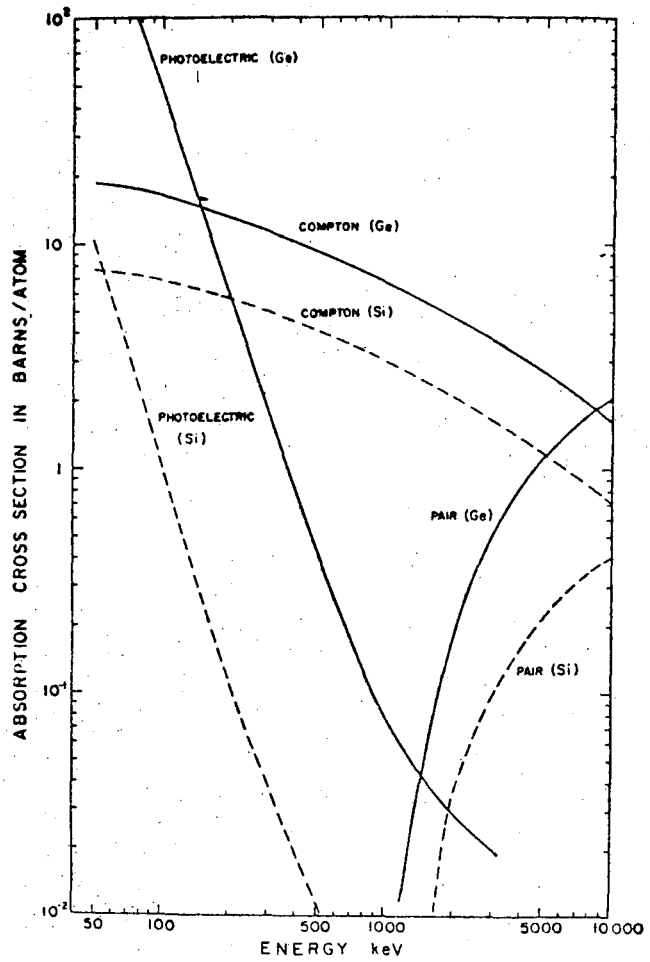

XBL 728-1403

Fig. 10. Cross-section in barns/atom for photoelectric absorption, Compton scattering and pair production of gamma rays in germanium. To obtain the mass absorption coefficient for germanium in cm^2/g multiply by 8.27×10^{-3} Multiply by 4.42×10^{-2} to obtain the linear absorption coefficient per cm.

To further reduce the gamma efficiency, the source is kept far away from the source(Figure 11). The detector has a surface area of 0.63 cm^2 , and the solid angle subtended is less than 0.1% *.

The Compton Electrons

The most serious problem in low temperature beta studies is the abundance of Compton electrons. Even though a thin detector is insensitive to the gamma rays, it has no means to distinguish the beta particles from the Compton electrons.

Compton electrons are produced from the interactions of the gamma rays with the cryostat walls, the detector housing, the copper fin and whatever object happens to be within the experimental chamber. Fig. 11 illustrates an arrangement in which a magnetic field can be used to guide the beta particles from the source to the detector.** Any Compton electrons produced from the cryostat walls will not be detected since they will miss the collimator of the detector as they spiral down the cryostat. Ultimately they will all be absorbed by the cryostat walls again.

By keeping the detector housing far away from the source, interactions between the gamma rays and the detector housing is minimized. Interactions between the gamma rays and the copper fin unfortunately cannot be reduced. It is believed that most of the Compton electrons detected in the present work originate from this process.

An earlier attempt without the long solenoid produced

---

* Collimator radius R = 8.75 cm ; the detector surface area is $A = .63\ cm^2$. The solid angle = $A/4\pi R^2 = 0.63/4\pi\ 8.75^2$ = 0.00065 = 0.065%

** The same field is used to polarize the iron foil.

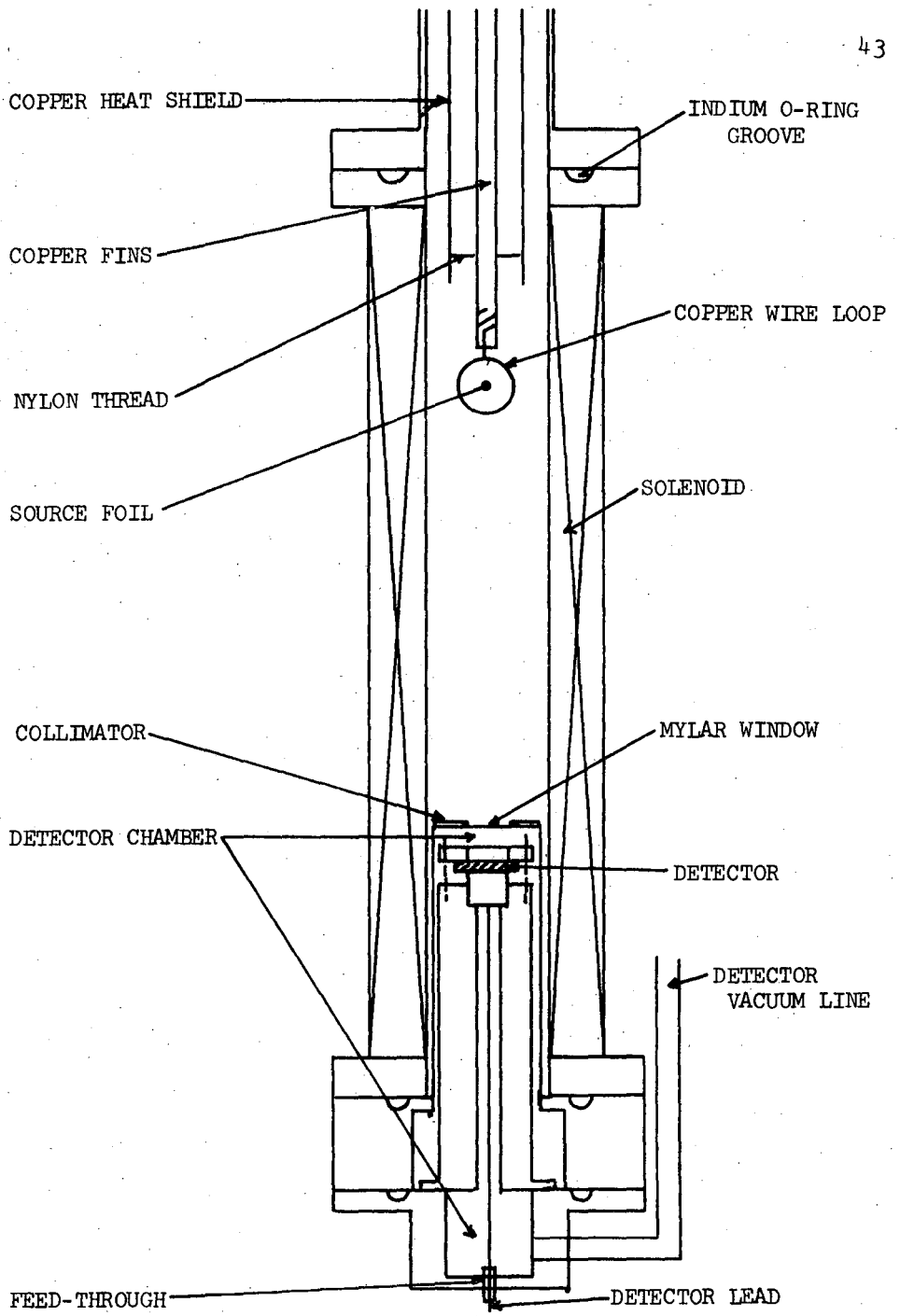

XBL 728-1402

Fig. 11. The experimental chamber.

a spectrum which indicated an overwhelming proportion of Compton electrons. The experimental set-up was basically the same as that of Ref. 24 (Figure 12). An 1/2 mm lithium drifted germanium detector maintained at $17^{\circ}K$ was used. The spectrum is shown in Figure 13; even though the statistics are poor, it does not resemble a positron spectrum.

Summary

In short, all the gamma ray related problems are solved by the use of a thin detector and a long focussing solenoid. The thin detector reduces the photon efficiency to a minimum, whereas the long solenoid optimizes the beta particles efficiency relative to the gamma rays and Compton electrons.

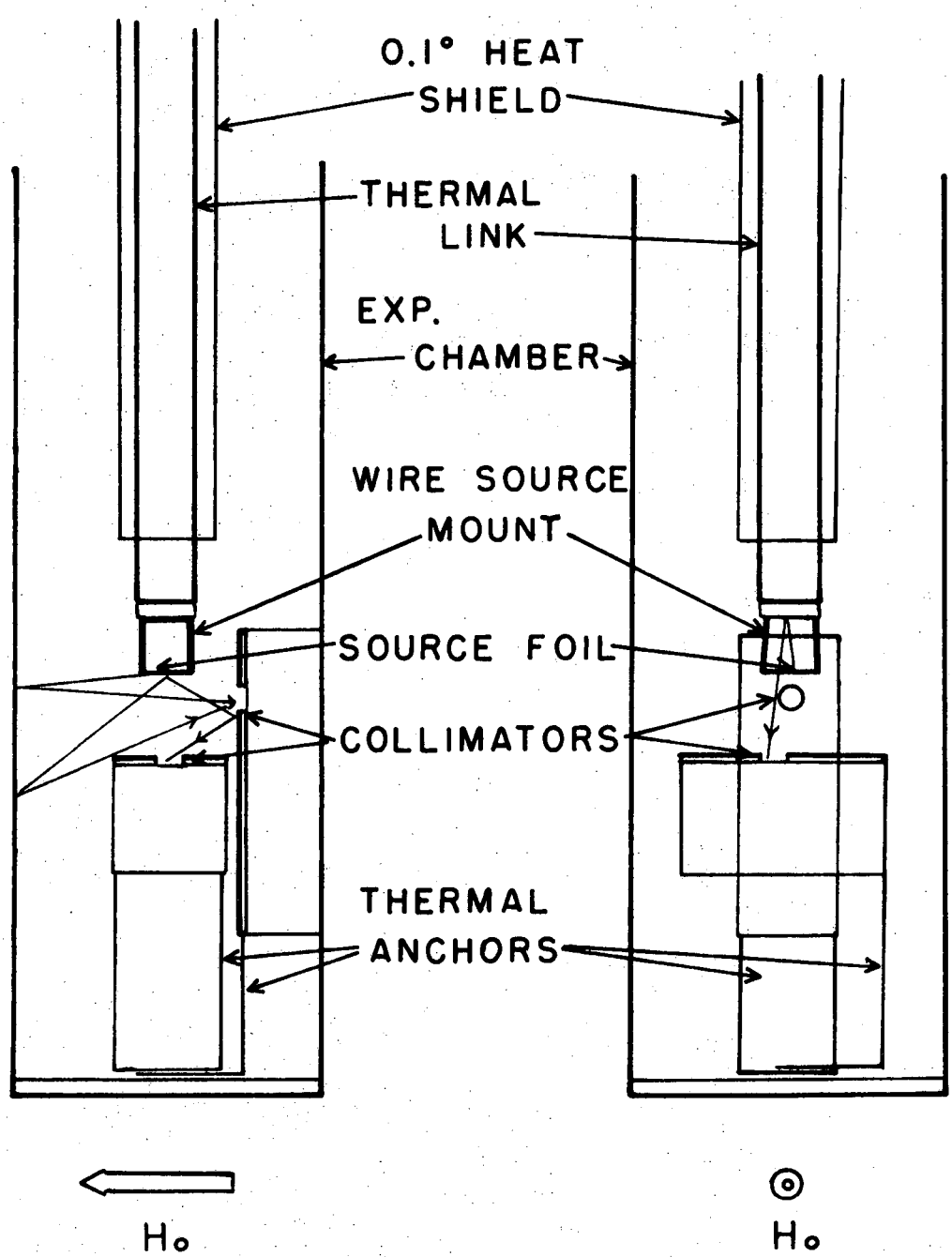

XBL 6912-6715

Fig. 12. The experimental arrangement which produced the spectrum shown in Figure 13.

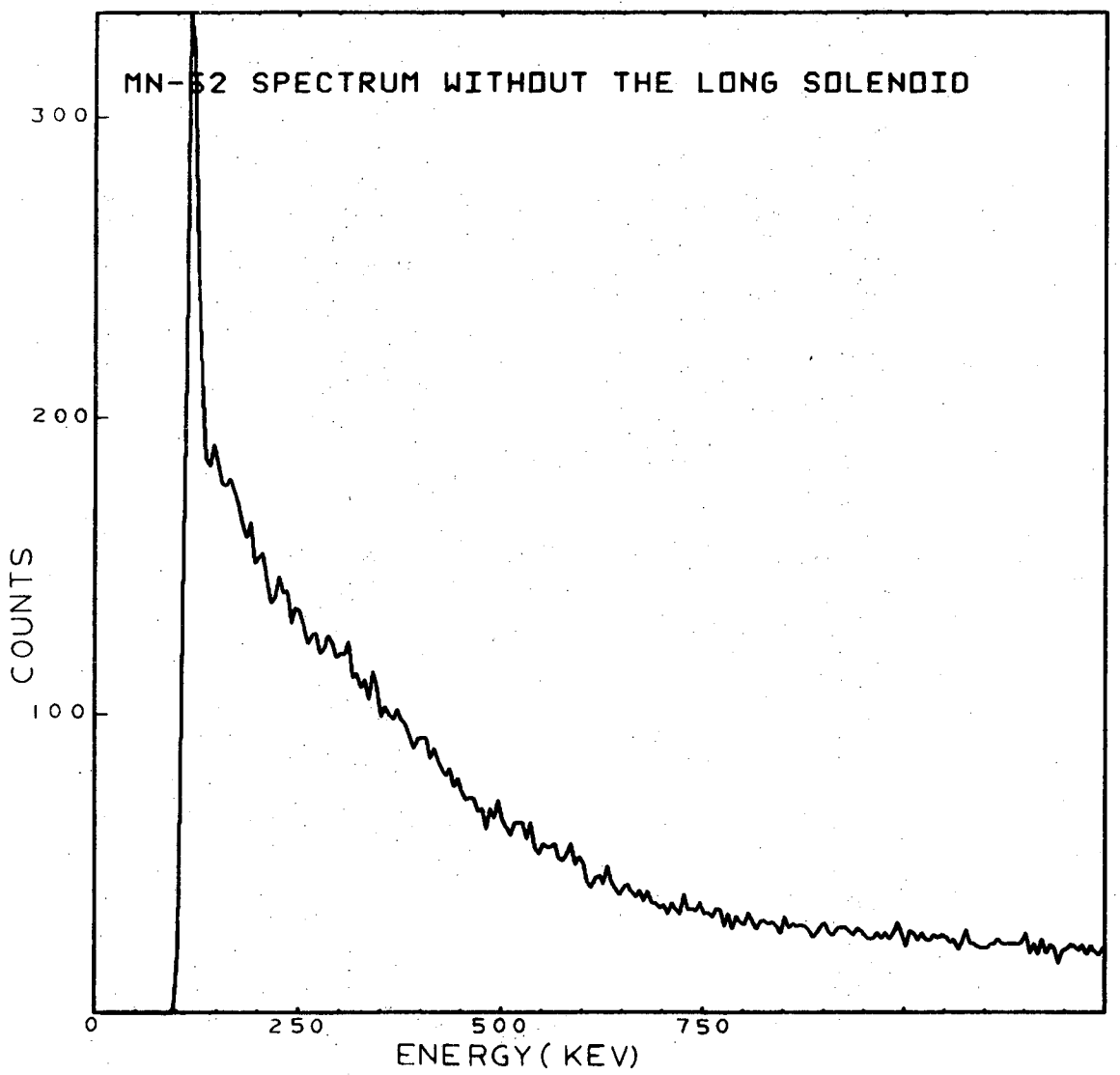

XBL 727-1279

Fig. 13. The beta spectrum obtained without the long solenoid.

CHAPTER VI

The Apparatus

The adiabatic demagnetization technique has been well described in the literature,[29] and the general aspects of the method will not be mentioned here. This chapter is dedicated primarily to the special features of the apparatus which are relevant to the present experiment.

The Liquid Helium Dewars System (Figure 14)

The set of dewars holding the liquid helium was originally designed for the definitive experiment on time reversal invariance. The following criteria were met:

1) Time reversal invariance experiment involves taking β-γ coincidences. The tail end of the system was made slender so that the gamma detectors may be placed as close to the source as possible to increase the solid angles.

2) The entire system was made long and slender so that the bath life of the liquid helium may be prolonged. It has been estimated that the duration of maintaining low temperature of the source is determined by the time it takes for the $1^{o}K$ bath to become empty [30]. Since the count rate is expected to be low for coincidence experiments, every effort was made to prolong the period in which the nuclei remain oriented.

3) Although the $4^{o}K$ bath may be refilled at any time during the entire experiment, it is a good practice not to disturb the entire system during the data gathering process. There is always the possibility that the vibrations induced during the refilling of the $4^{o}K$ bath may alter the position of the source. It is also possible to blow out the liquid helium already there accidentally, and cause the superconducting magnet to transition. Therefore, a liquid nitrogen (LN) heat shield was built to reduce

Fig. 14. Schematic diagram of the dewars system . Superinsulating aluminized mylar sheets were used in the OVJ to cut down radiation into the LN and LHe dewars.

Standard notations are:

OVJ- Outer Vacuum Jacket;

IVJ- Inner Vacuum Jacket;

4.2° Bath-Liquid helium bath at normal atmospheric pressure;

1° Bath- Liquid helium bath pumped to a pressure of about 60 microns;

77° Bath- Standard liquid nitrogen (LN) bath at atmospheric pressure.

The heat shield is made of copper.

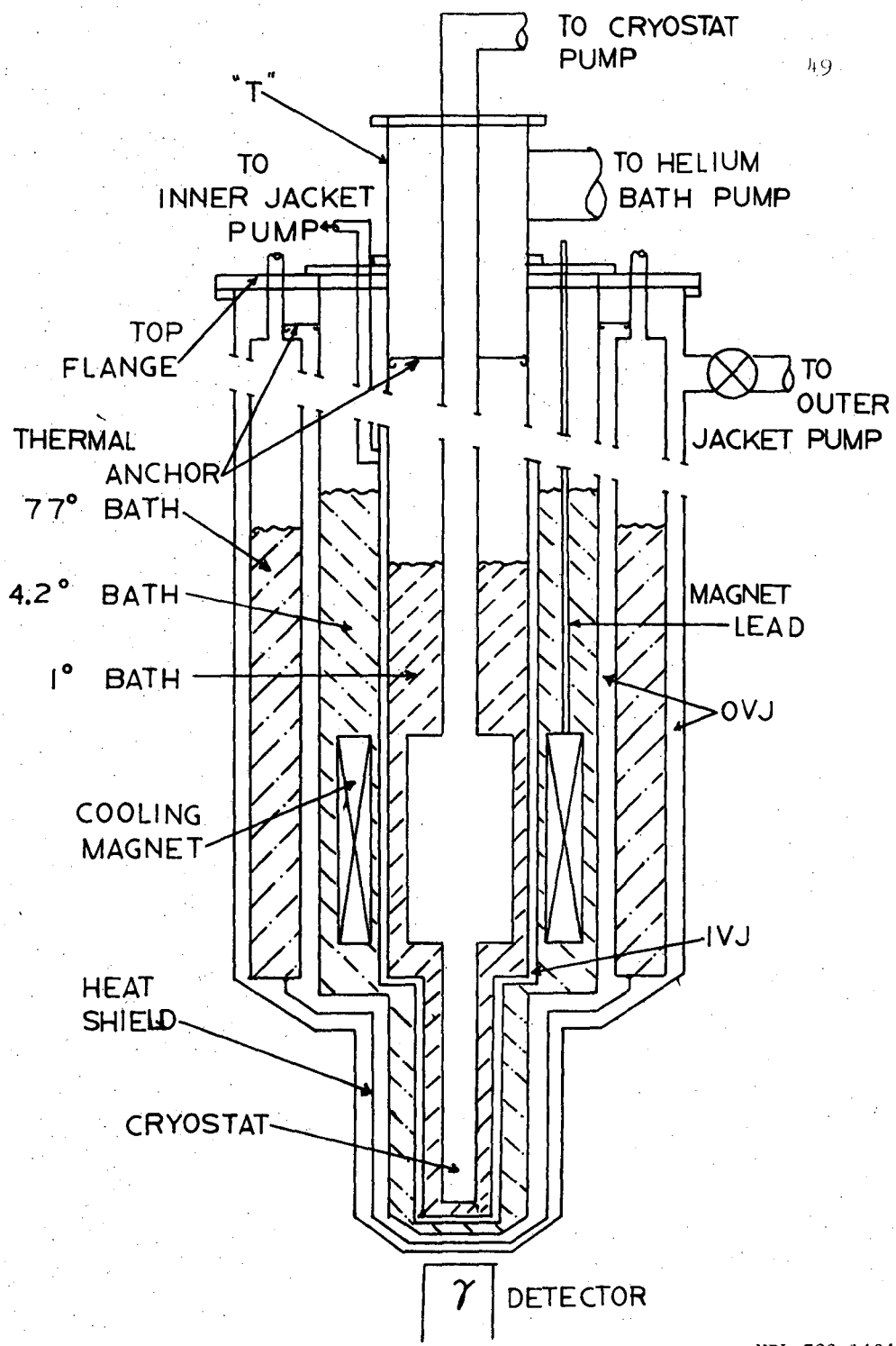

XBL 728-1404

Fig. 14.

the radiation heat influx from room temperature into the $4^{o}K$ bath.

A summary of the general performance of the dewars is given in Appendix 4 .

The Cryostat (Figure 15)

The cryostat is characterized by the use of the indium O-rings. Since the cryostat has to be opened up frequently to change the source and the cooling salt, joints which are trustworthy,* consistent and easy to operate are highly desirable. A well designed and well machined indium O-ring joint satisfies all the above requirements.

A typical indium O-ring seal is illustrated in Figure 16 . It consists basically of a groove semi-circular in cross-section. A flat flange is used to compress the indium O-ring which is situated in the groove. The indium O-ring is made out of an indium wire having the same radius as the radius of the cross-section of the groove. The joint of the O-ring is made carefully by overlapping the two ends of the wire(Fig. 16). When the flat flange is compressed against the indium O-ring by tightening the connecting bolts, indium is being squeezed out of the groove. It should be pointed out that the sealing edges are between the two surfaces of the flat flange and the flange containing the groove (Fig. 16). Therefore both flanges should be finely machined although the bottom of the groove need not be. Also, since the thermal contraction is larger for the indium than for the stainless steel down to liquid helium temperature. the layer of indium squeezed between the two surfaces should be as thin as possible.** For smaller flanges (1 - 2" in overall diameter)

---

* This means λ - leak tight.

** Approximately a couple of mils.

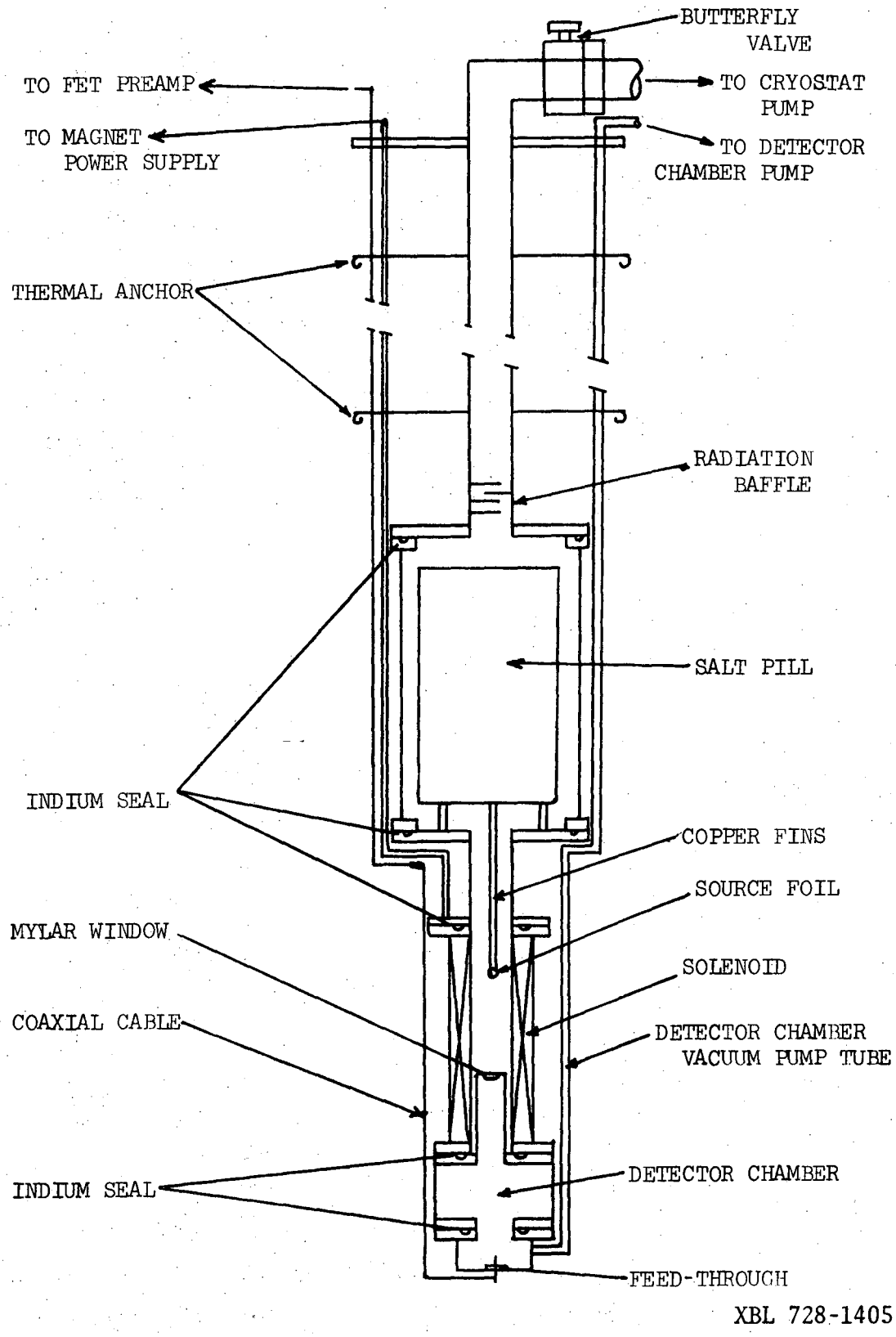

Fig. 15. The cryostat.

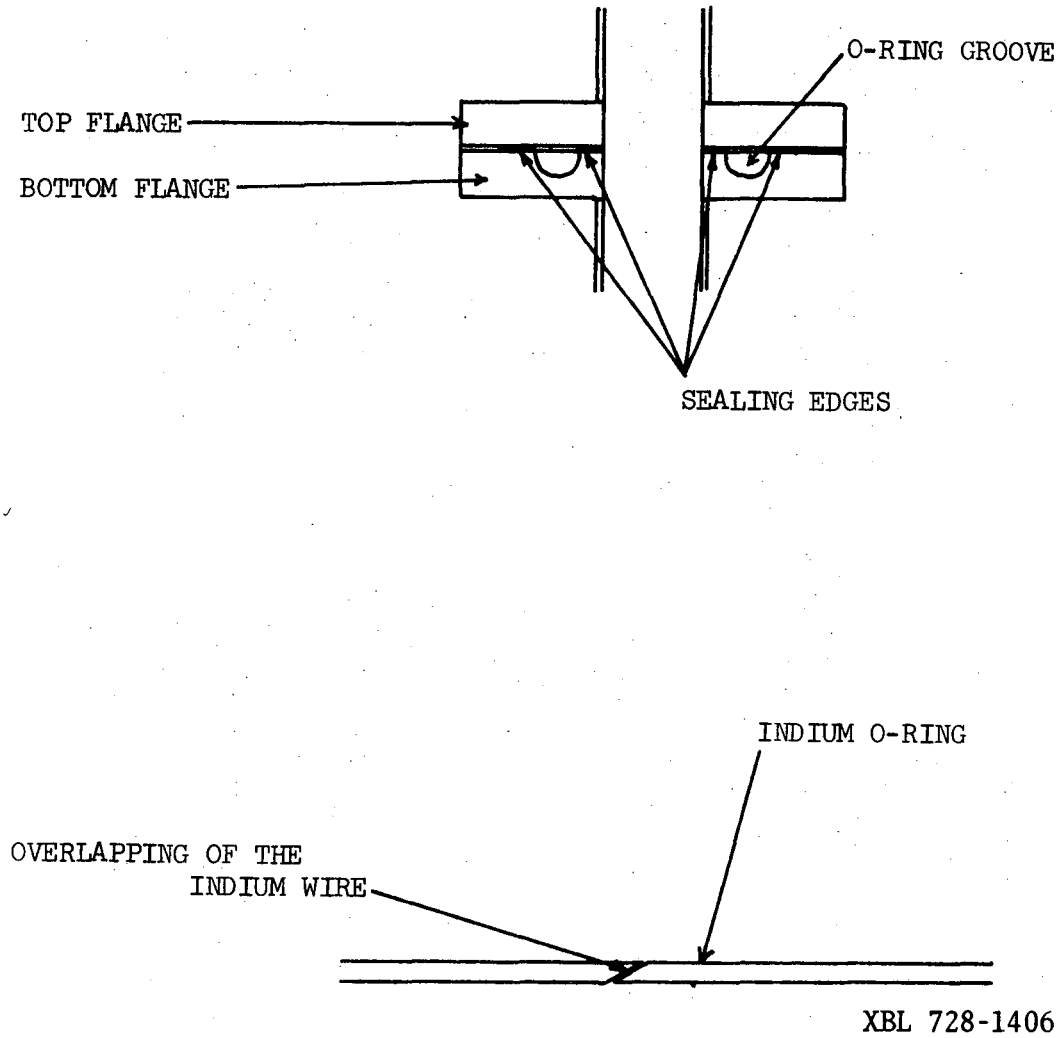

Fig. 16. Schematic diagrams of a typical Indium seal and an Indium O-ring. Note the sealing edges and the overlapping of the Indium wire.

with six or eight Number 8-32 tightening bolts, the two sealing surfaces can be tightened until they are practically flush against each other. But with larger flanges such as those sealing the salt pill can (about 4"), it is impossible to squeeze the indium layer to less than two mils. A torque of 60 in.-lbs. applied evenly over each bolt has been found to be sufficient to provide vacuum safe operations without a single incidence of failure.

One should be cautioned about the ways of connecting the tubes to the flanges. One would be well advised to weld all the tubes to the flanges rather than hard-soldering them. Intense heat has to be applied to the entire flange during silver-soldering, and the flange may wobble as a result.

The Long Focussing Solenoid(Figure 15)

The solenoid used to guide the beta particles from the the source to the detector has a coil constant of 300 gauss/amp. It is made out of ten layers of 10/16 Supercon T48 superconducting wires* wound on a stainless steel tube with a 1" O.D. Each layer consists of 343 turns of the wire, and the overall length of the solenoid is $5\frac{1}{2}$ inches. The detector and the source are arranged to be within the volume of the solenoid and each one inch away from the opposite ends of the magnet.This serves to prevent the beta particles from experiencing the non-uniformity of the fringe field. The critical current of the magnet is still unknown. It failed to transition at 110 Amps. (33 Kilogauss) - the limit of the D.C. power supply.**

---

* 10 mil diameter niobium-titanium superconducter coated to an overall diameter of 16 mil. The wire is insulated with CuO - made by Supercon Division of Norton Corp., Natick, Mass.

** The power supply is a Harrison 6260A, made by Hewlett-Packard

The Detector Chamber (Figure 17)

It should be kept in mind that the detector chamber is submerged within the $1^{o}K$ liquid helium bath. Therefore all the electrical feed-throughs and the thin beta window must be λ tight (leak tight to superfluid liquid helium).

The window for the beta particles was made out of a 1/4 mil aluminized mylar sheet. It was epoxied onto the brass surface with epoxy treated for low temperature vacuum operations. The epoxy was a mixture of 5 parts of EPON 826 and 1 part of DER 736 . The catalyst may be either VERSAMID 125 or 140 , mixed 1:1 with the epoxy, and softened by warming it with a heat gun. A very thin layer of the mixture was spread over the brass surface, and the mylar sheet was carefully laid on top and cured at $60^{o}C$ for 24 hours. The window was leak tight below LN temperature*, and it was capable of handling a pressure differential of one atmosphere.

Glass feed-throughs have been tried, but they were found to crack after a few thermal cycles. Ceramic feed-throughs were a lot more stable to thermal cycling, but care must be taken when the feed-throughs are soldered onto the chamber wall.

The detector contacts were made out of brass coated with indium. A top plate with a 5/16" hole, serving both as an additional collimator and a contact, was tightened down with three Number 0-80 screws onto the detector which was resting on the other contact. Indium coatings were necessary to remove some of the strain as well as to provide better electrical contacts.

---

* Mylar is permeable to Helium gas at room temperature, but not at LN temperature or below.

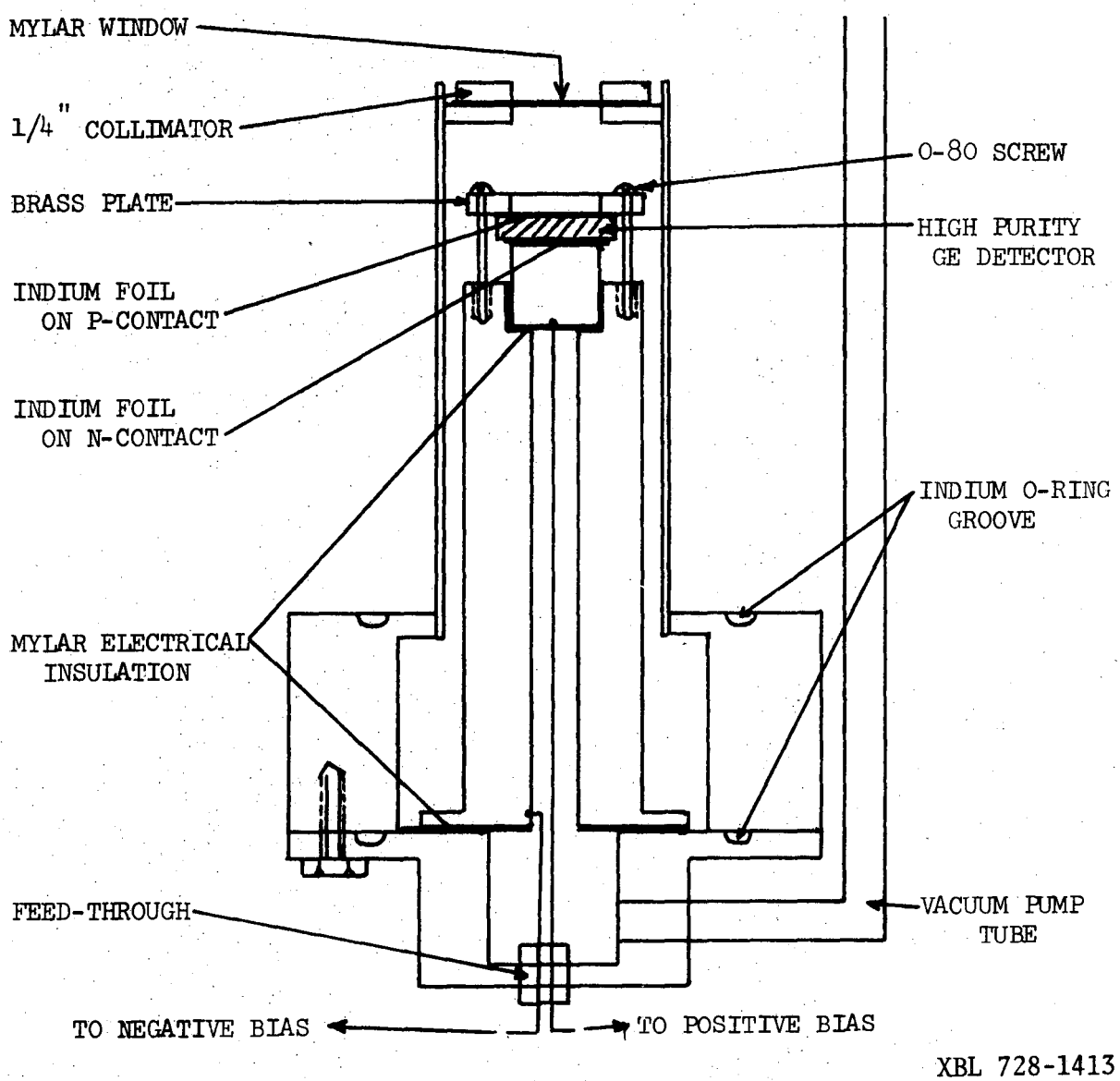

Fig. 17. Schematic diagram of the detector chamber showing also the mounting of the high purity germanium beta detector.

The Cooling Magnet (Figure 18)

The cooling magnet for the adiabetic demagnetization technique must be as large as possible. The present cooling magnet is made out of superconducting wire wound around a μ metal cylindrical coil form measuring 12" long, 5.8" I.D. and 7.375" O.D. The magnet windings consist of eight layers of Supercon 30/4-core* wire in the bottom layers, and twenty layers of Supercon 24/multi-core wire in the top layers.** In between each layer are two 3 mil sheets of glass cloth compressed to a thickness of about 4 mil. These layers of glass cloth are important not as layer-to-layer insulators, but as spacers in between which liquid Helium may be absorbed to cool each winding more effectively.

The magnet has a total of 13452 turns, and its coil constant is 499 Gauss/amp. It transitions at 142 amps. (71 Kilogauss) , and was normally run at about 100 amps(50000 Gauss) in this work.

The magnet leads are made out of two brass tubes 3/8" O.D. and 65 mil thick. Superconducting Pb/Sn have been soldered onto and along the brass tubings so that below the critical temperature*** the Pb/Sn solder would take over the carriage of the current. The leads are cooled by venting the evaporated liquid helium exhaust through their central ducts.

---

* Four strains of centrally located niobium/titanium superconductor embedded in copper to make an overall cross-section of 30 mil in diameter.

** A total of 54 strains twisted 1" per turn and coated with copper to an overall diameter of 24 mil. All the wires are insulated with CuO by simply oxidizing the copper.

*** About $10^{\circ}K$

0 0 0 0 3 8 0 7 6 3 6

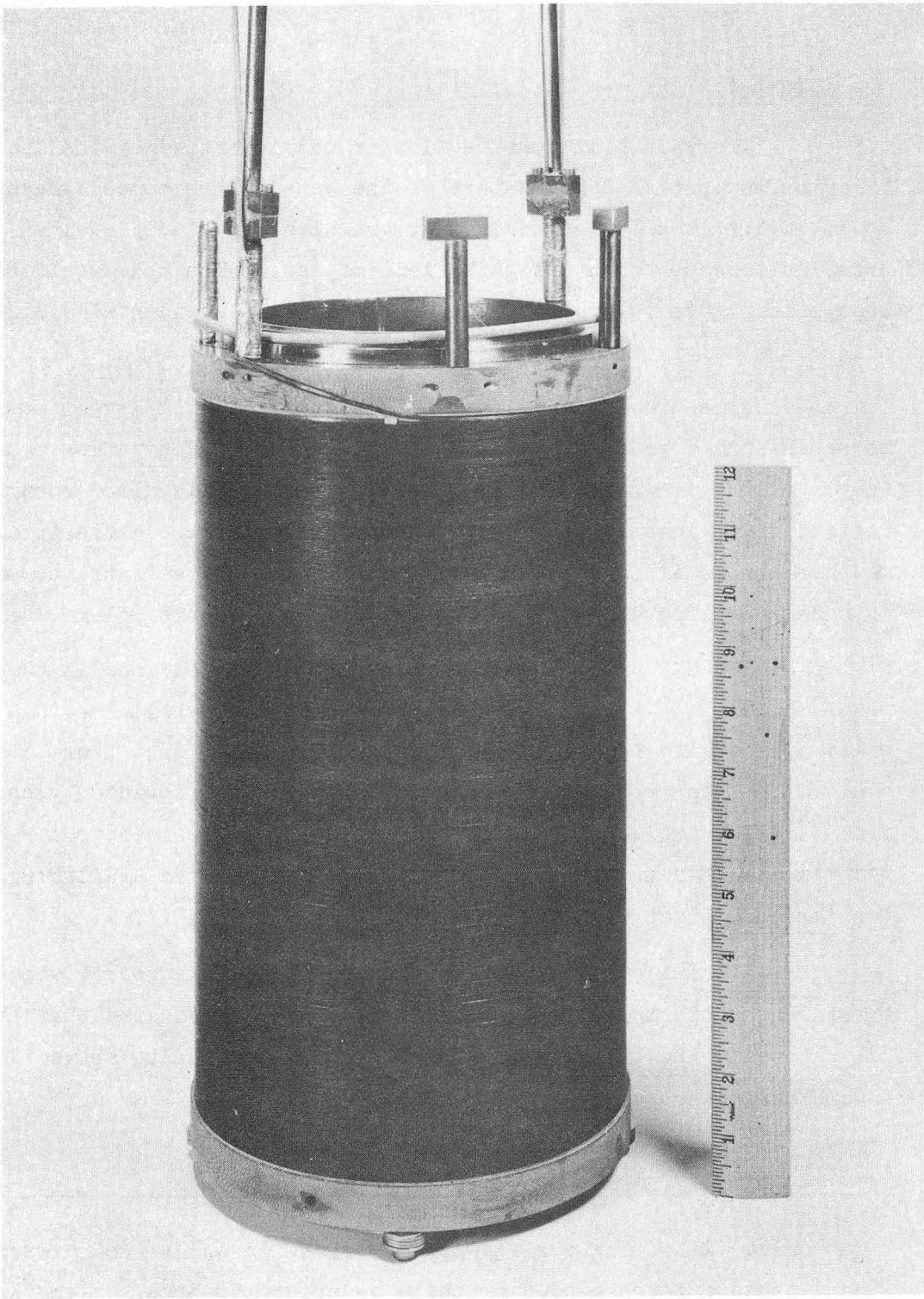

CBB 714-1587

Fig. 18. The 12" superconducting cooling magnet.

The Salt Pill (Figure 19)

The salt pill construction is characterized by the use of nylon supporting legs instead of the usual pitch-bonded graphite rods. Nylon is a lot stronger than graphite especially against shearing forces. With the high field magnet, nylon rods would be less susceptible to breakage should the pill be accidentally misaligned relative to the center of the magnet.

Nylon is a poorer thermal resistor below $1^{o}K$ when compared to pitch-bonded graphite.[31] * Therefore the heat conduction path length must be increased to maintain a comparable level of thermal resistivity. This is achieved by the addition of two extra intermediate chrome alum guard pills. The space for these extra components is made available due to the larger-than-usual magnet volume.

The CMN and chrome alum slurry have been made in the usual manner.[18,24] Care must be taken not to over-fill the CMN pill,** otherwise the salt may overflow after the first thermal cycle. The thermal contacts to the CMN salt are provided by copper fins*** silver-soldered together at one end and machined to a rod 1/8" in diameter and 12" long. The total surface area available for direct contact with the CMN slurry is 3600 cm^2 .

A trial run was made using ^{60}Co in a cobalt single crystal as a thermometer. The gamma anisotropy indicated that the pill stayed below 10 mK for 12 hours and warmed up to above 15 mK in another 6 hours.

---

* At below $1^{o}K$, the resistivity of nylon is about 260 ergs/sec-cm-^{o}K and that of pitch-bonded graphite is about 50 ergs/sec-cm-^{o}K .

** At most a 75% filling factor.

*** Made out of 5 mil thick 99.99% pure copper, annealed before assembly.

Fig. 19. Schematic diagram of the salt pill assembly.

KA stands for Chrome Alum, $CrK(SO_4)_2 \cdot 12H_2O$

CMN stands for Cerium Magnesium Nitrate, $Ce_2Mg_3(NO_3)_{12} \cdot 24H_2O$

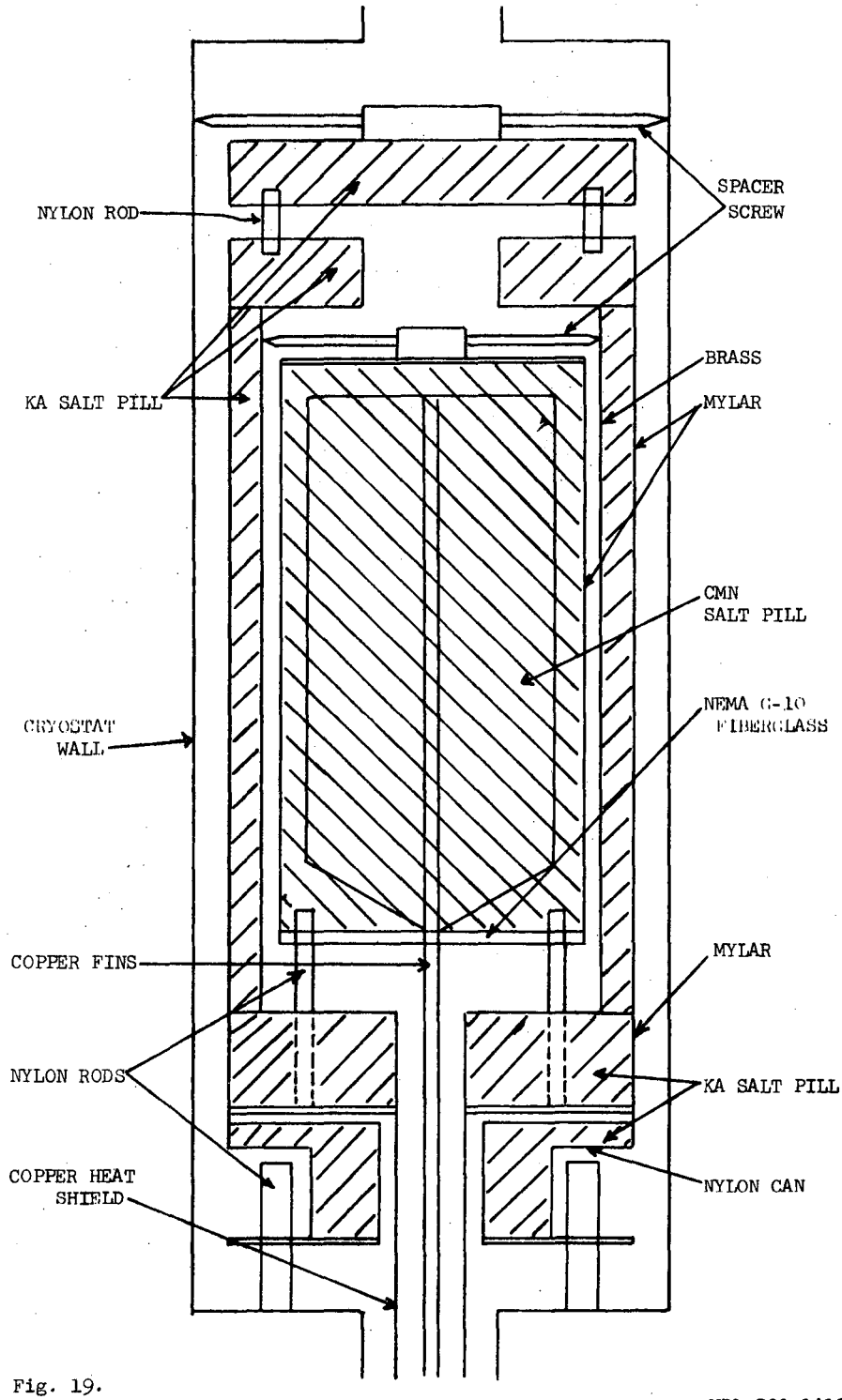

Fig. 19.

XBL 728-1412

The Beta Detector

The high purity germanium crystal (p type) is about 0.8 mm thick and has been cut into a hexagonal shape. Lithium has been diffused on one side to form the n- contact. The p- contact has been provided with the evaporation of a thin layer of chromium on the opposite side. Beta particles should enter through the p-contact.

Before installation, the detector was etched* with the chromium plated side well covered with a piece of tape. The detector was washed in pure methanol and dried immediately in dry nitrogen.

The depletion depth is about 0.5 mm , and it can be achieved with a voltage of just 5 volts. The total surface area is about 0.63 cm^2.

The Gamma Detector(Figure 20)

An axial gamma detector was placed at the end of the dewars system (Figure 14). The detector used was a lithium drifted coaxial germanium detector kept cool at the LN temperature by means of a LN chicken feeder. The energy resolution of the ^{52}Mn and ^{60}Co lines is about 1%.

The Electronics (Figure 21)

The electronics involved the usual amplifiers and pulse shapers. The time constant was set at 1 μsec. for both the integrator and differentiator. A FET pre-amplification stage has been provided for the β pulses. The leakage current was not detectable (less than 10^{-8} amp.) when a 10 volts bias was applied to the beta detector. The electronics noise came mainly from the rather high cable capacitance.

---

* The etching solution is 1 part HF, 1 part fuming HNO_3 and 7 parts conc. HNO_3 at room temperature.

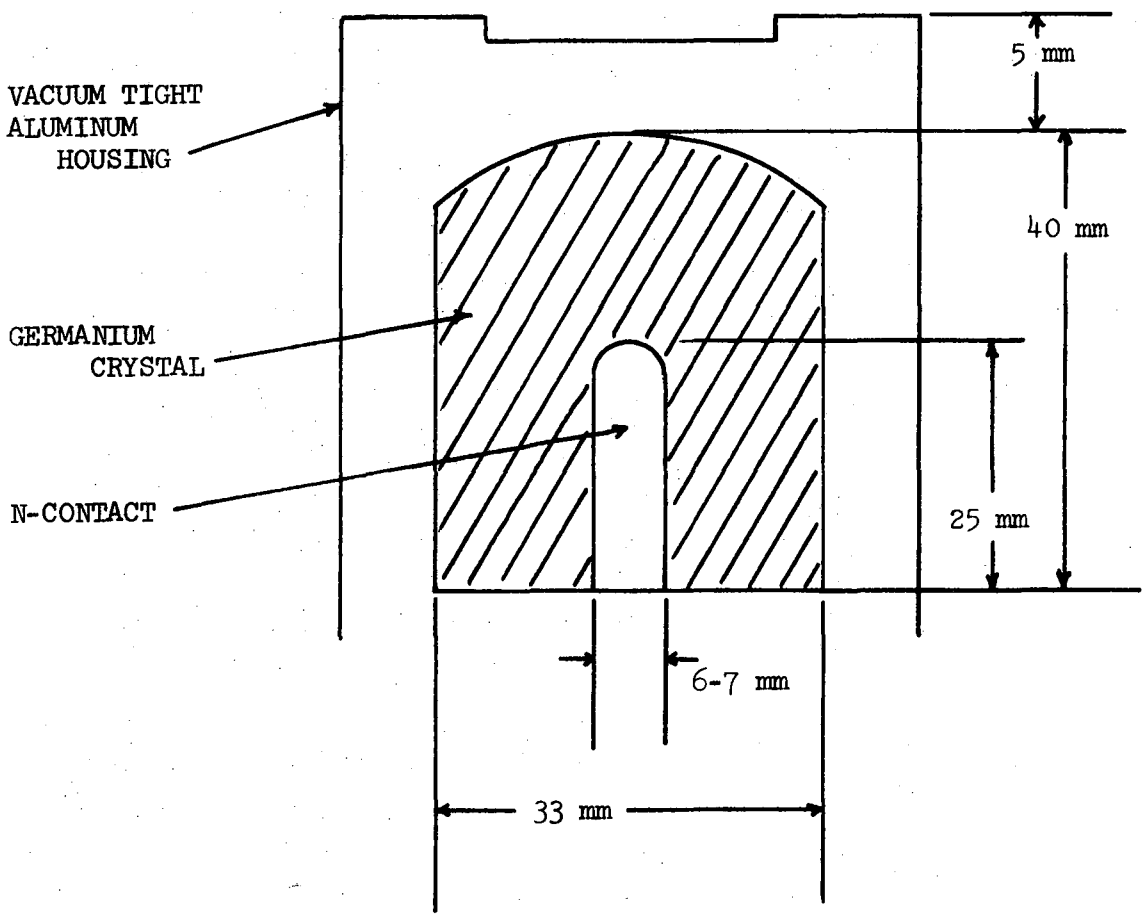

XBL 728-1411

Fig. 20. Schematic diagram of the gamma detector. The LN cooling system and the vacuum system are not shown.

The long cryostat necessitated the use of rather long coaxial cables (about 7 ft. long). The electronic noise worsens with increased cable capacitance. The cables used were two seven feet semi-rigid coaxial cables* with Teflon dielectric, copper central conductor and silver coated stainless steel wall. They had a characteristic impedance of 50 ohms, and a capacitance of 29.5 pf/ft. Being rigid, they were less susceptible to electronic noise induced by mechanical vibrations. It was found that the overall performance of the electronics improved and optimized with the setting of the lower discriminator level at 30 kev for the ^{52}Mn experiment, and 40 kev for the ^{60}Co experiment.

---

* Uniform Tubes No. 141 Semi-Rigid Cable.

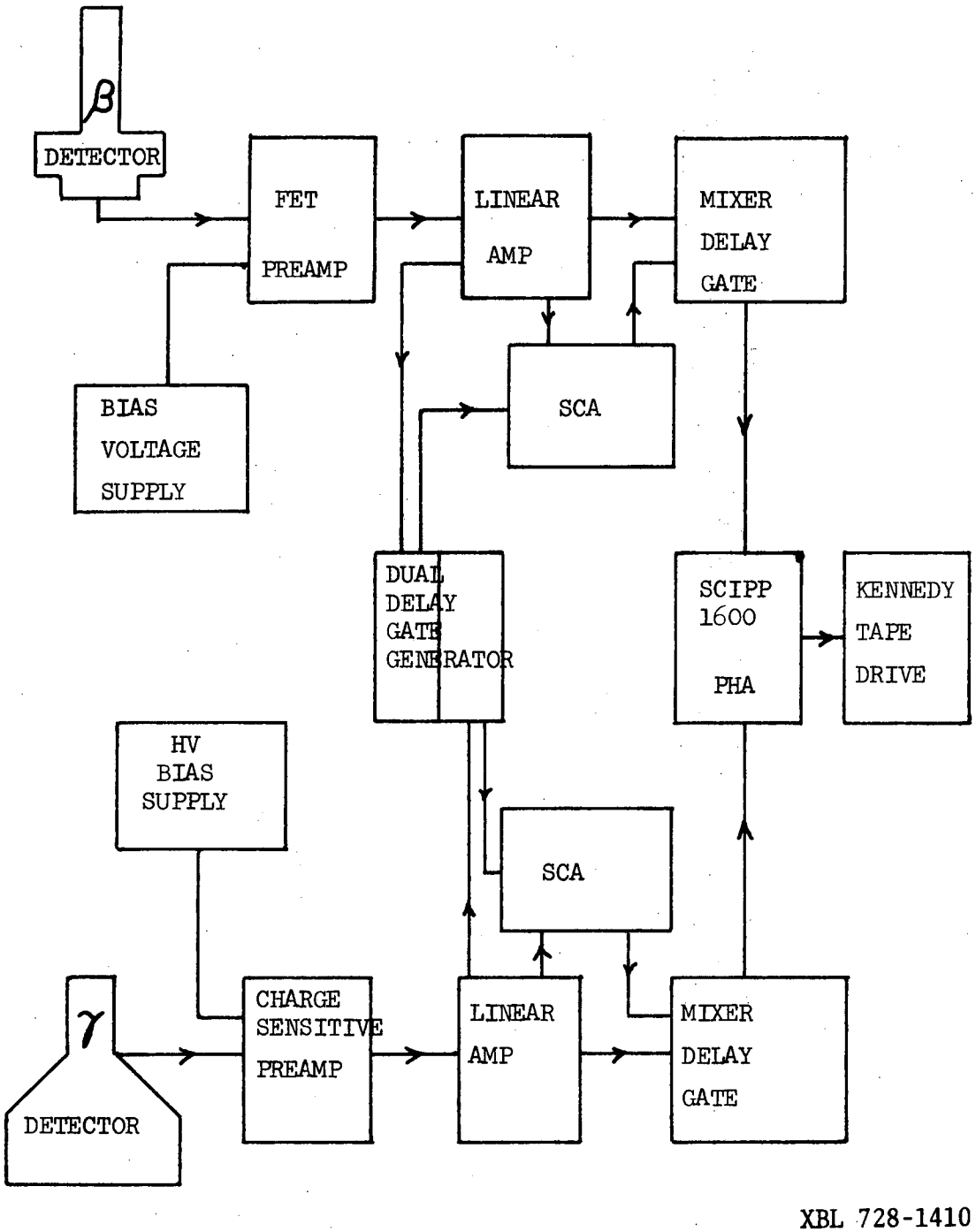

Fig. 21. The electronic blocks diagram. PHA stands for Pulse Height Analyzer; SCA stands for Single Channel Analyzer.

CHAPTER VII

The ^{52}Mn Beta Asymmetry Experiment

Source Preparation

^{52}Mn was produced by the reaction:

$$^{54}Fe\ (p,3n)\ ^{52}Co\ (\beta^+ \text{ short } t_{\frac{1}{2}})\ ^{52}Fe\ (\beta^+\ t_{\frac{1}{2}}=8.3h)\ ^{52}Mn$$

Commercially available 1/2 mil* natural iron foil (99.99% pure) was rolled down to about 6 mg/cm^2 . The foil thickness was a compromise between the thermal conductivity of the foil and the probability of multiple scattering of the beta particles within the source. A thin foil would reduce the amount of multiple scattering of the beta particles, but it is offset by the reduction of the thermal conductivity of the foil, which may make a high degree of polarization of the nuclei unattainable.

Using a 1/4" collimator, the iron foil was irradiated at the 88" cyclotron with 32 Mev p^+ for 3 hours at a rate of 5 μA/hr. The foil was then annealed in a quartz tube with a torch and then mounted onto the copper fins of the salt pill as shown in Figure 22. Bi/Cd solder was used for all the soldering of the source since superconducting solders (such as Pb/Sn solder) would be expected to be poor thermal conductors.[32]

^{55}Co and ^{56}Co were also produced in the process. ^{55}Co was produced by the reactions ^{56}Fe (p,2n) and ^{57}Fe (p,3n) , and its quantity was competitive with that of ^{52}Mn five hours after the irradiation. But its short half life (18 hours) rendered it harmless to the experiment after a period of two days. ^{56}Co was produced mostly by the reaction ^{58}Fe (p,3n), and its half-life is longer than that of ^{52}Mn (77 days). But since ^{58}Fe

---

* 1/2 mil corresponds to 9.8 mg/cm^2 of Fe.

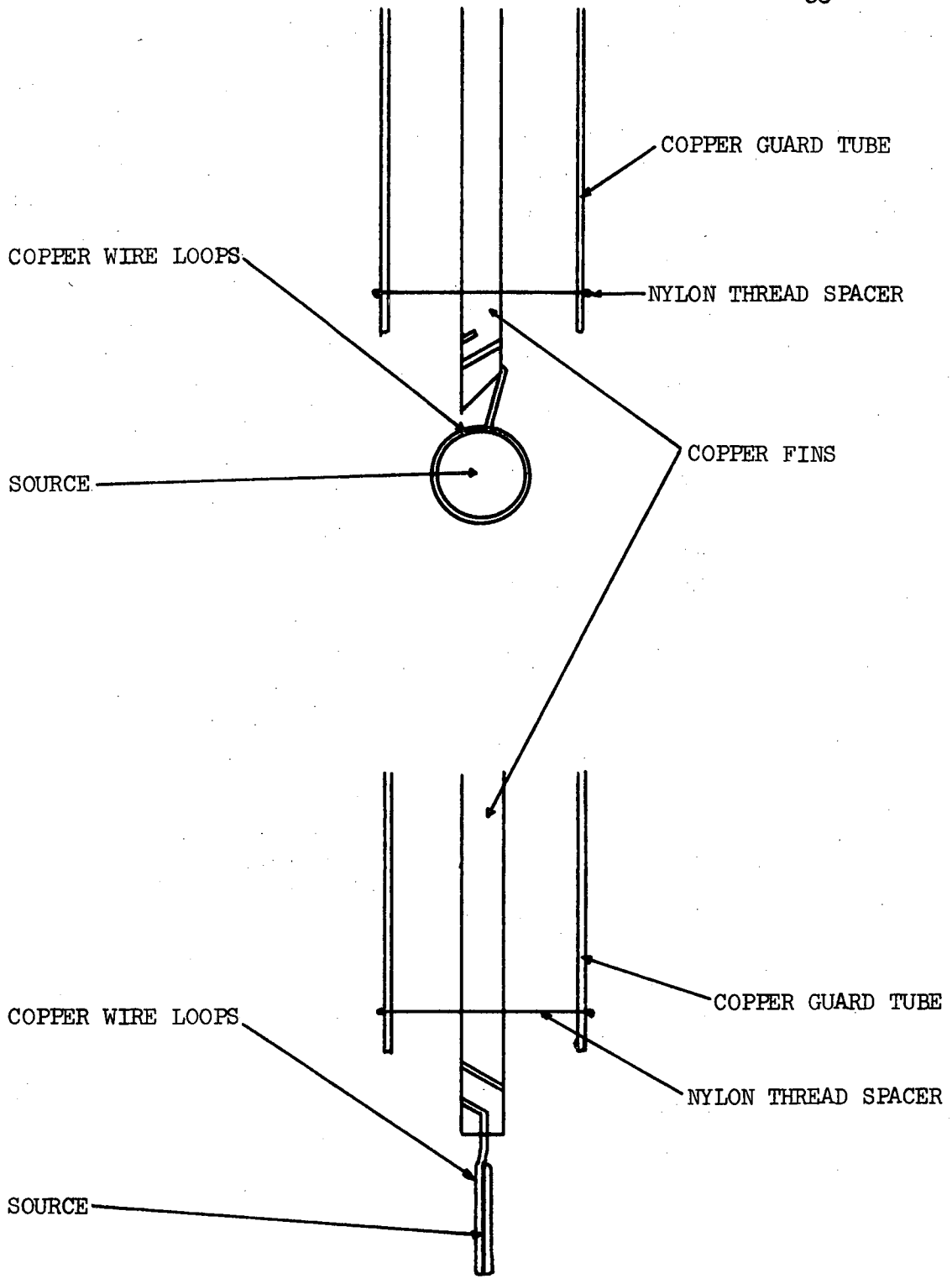

XBL 728-1409

Fig. 22. The mounting of the source. The copper wire used is of No. 24 gauge. The source foil is circular, 3/8" in diameter.

is much less abundant compared to ^{54}Fe in nature*, the total positrons impurity due to ^{56}Co as determined by the intensity of the 850 kev line was found to be less than 4%.

Experimental Procedure

The nuclei were cooled following the usual adiabetic demagnetization procedure. After the source has become cold, a polarizing field of -10.5 KG** was applied. The current through the long focussing solenoid was read directly off a digital voltmeter which measured the voltage drop across a 50 mv/100 A shunt. The power supply was set at the current regulated mode with remote sensing to minimize current fluctuation due to the inconsistency of the power cables.

Six consecutive ten minute runs were taken, and the data from the beta and gamma spectra were recorded onto a magnetic tape. Between each run, the beta detector bias voltage was dropped from +10 v. to -2 v. to avoid polarization of the detector. The beta spectra were checked carefully for any evidence of gain shift or anomalous behaviors of the detector. There were none.

After six runs, the polarizing field was gradually decreased to zero. The polarity of the magnet leads was then reversed, and the field was brought back to +10.5 KG. Six more runs were taken. The gamma spectra indicated no significant warm-up due to eddy current heating.

The pill was now allowed to warm up by stopping the pumping of the $1^{o}K$ liquid helium bath as well as introducing about 300 micron of helium exchange gas. The polarizing field was allowed

---

* 0.33% of ^{58}Fe in comparison with 5.82% of ^{54}Fe.

** The positive direction is the direction downwards towards the beta detector.

to remain at +10.5 KG throughout the entire warming up procedure.

After half an hour, the exchange gas was pumped out and three warm counts were taken. The polarity of the field was then reversed to -10.5 KG and three more warm counts were taken. The two sets of warm counts (three runs each) were compared carefully for any evidence of effects introduced by the difference in field polarity. There was again none.

Results

The counts of the six cold runs with H = -10.5 KG were combined, as were the six cold runs with H = +10.5 KG, and the six warm runs with H = ±10.5 KG. Combination of the data was done to simplify data analysis as well as to improve the statistics. Each separate run was compared carefully with other runs to check for any inconsistency. The beta spectra are plotted in Figure 23.

Energy calibration of the beta detector was done after the experiment . A ^{137}Cs source * was used and the detector maintained at $4^{o}K$. The local maxima of the spectra in Figure 23 agree well with the energy calibration scale.

The temperature reached was determined from the 744 kev line anisotropy of the gamma spectra. Since the gamma detector has excellent energy resolution, background corrections should be routine. The final temperature is 8 mK , which corresponds to a polarization of 76% (B_1 = 1.22).

---

* Gamma energy = 662 kev;
K conversion electron energy = 626 kev;
L conversion electron energy = 635 kev.

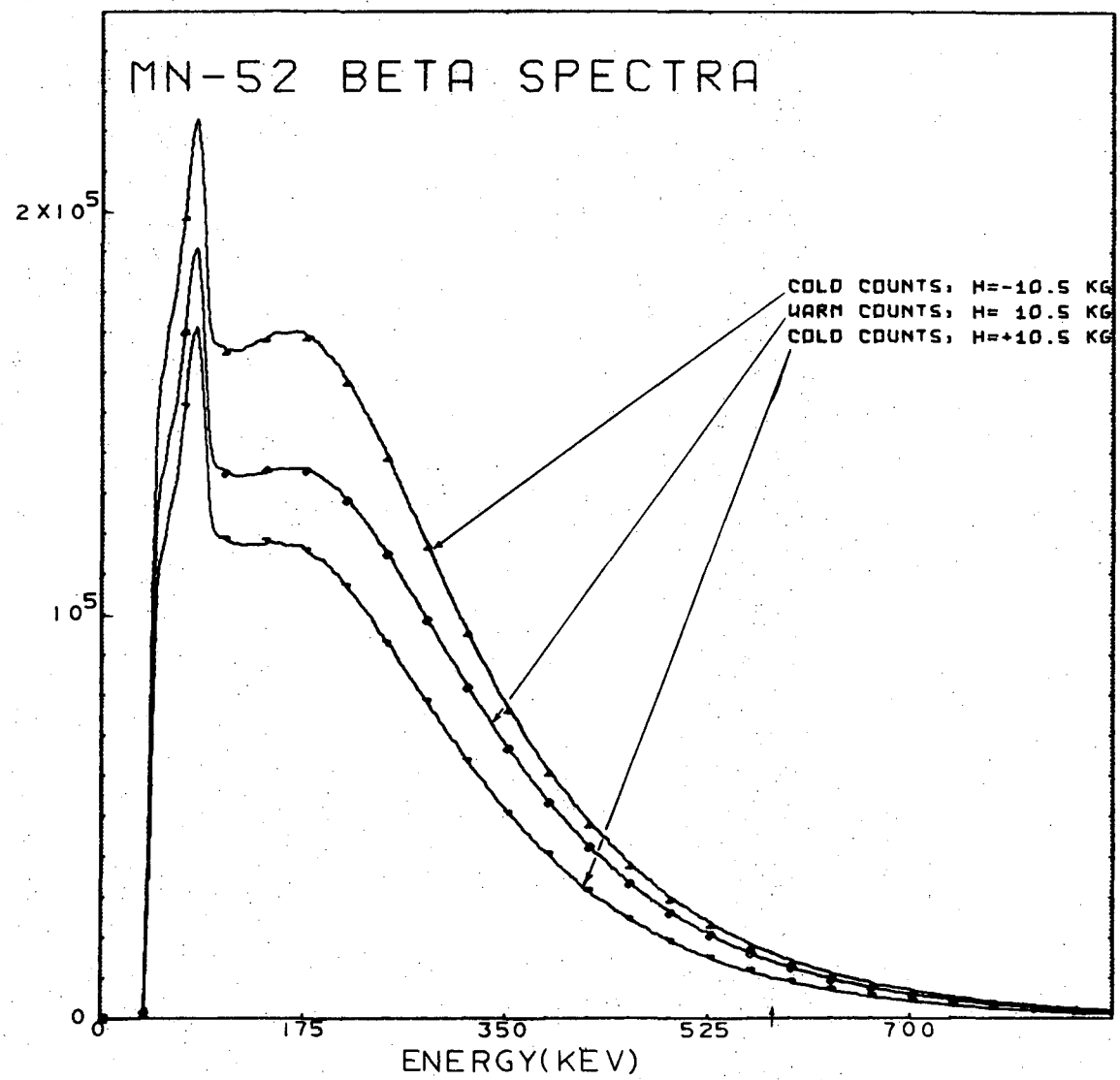

XBL 727-1276

Fig. 23. The observed beta spectra of ^{52}Mn. The energy per channel has been calibrated separately with ^{137}Cs.

Data Analysis

Compton Electrons

Starting with the Eq.3-2 , one can write:

Eq.7-1 $$W(0) = 1 + \frac{v}{c} A \frac{\langle m_z \rangle}{I} Q_1(0)$$

where $Q_1(0)$ is the solid angle correction factor.

Since Compton electrons from scattered γ rays would also be detected, Eq.7-1 should contain one more term:

Eq.7-2 $$\Delta_c W_\gamma(0)$$

where Δ_c is an arbitrary constant, and

$W_\gamma(0)$ is the angular distribution of the gamma rays in the 0° direction:

Eq.7-3 $$W_\gamma(0) = 1 + U_2F_2B_2Q_2(0) + U_4F_4B_4Q_4(0)$$

where $Q_2(0)$ and $Q_4(0)$ are the solid angle corrections.

Eq.7-2 is a consequence of the interactions of the gamma rays with the copper fins (see Chpt. 5). There is no way to determine $Q_2(0)$ and $Q_4(0)$ exactly, but they can be estimated to be about 0.9 * or larger. The solid angle correction factors $Q_2(0)$ and $Q_4(0)$ are therefore taken to be 1 in the data analysis. The intensity of Compton electrons is estimated to be about 10% of the beta spectrum;

---

* The angle subtended by the source to the copper fins is about 5° . $\cos^2(5^\circ) = .992$; $\cos^4(5^\circ) = .984$. Therefore the solid angle correction factors should be larger than .9 .

an uncertainty of 10% in Eq.7-2 produces only an uncertainty of 1% in Eq.7-1. With $Q_2(0) = Q_4(0) = 1$, $W_\gamma(0)$ can be read directly off the gamma spectra. Thus $W_\gamma(0)$ can be written as:

$$W_\gamma(0) = 1 - \delta$$

where δ is the decrease in count rate of the gamma spectra when the nuclei are oriented.

Eq.7-1 is re-written as:

$$\text{Eq.7-4} \qquad W(\beta,0) = 1 + \frac{v}{c} A\, B_1 \sqrt{(I+1)/3I}\; Q_1(0) + \Delta_c(1-\delta)$$

where the inclusion of the term β , $\beta = v/c$, is to emphasize the energy dependency of the correlation function.

The Δ_c is a function of the energy, but the whole term $\Delta_c(1-\delta)$ is independent of the direction of the field (only postive or negative direction).

The hyperfine field of ^{52}Mn in Fe is negative, therefore Eq.7-4 may be written as:

$$\text{Eq.7-5} \qquad W_+(\beta,0) = 1 - \beta\, A \sqrt{(I+1)/3I}\;\; B_1\, Q_1(0) + \Delta_c(1-\delta)$$

$$\text{Eq.7-6} \qquad W_-(\beta,0) = 1 + \beta\, A \sqrt{(I+1)/3I}\;\; B_1\, Q_1(0) + \Delta_c(1-\delta)$$

where W_+ (W_-) is the correlation function when the polarizing field is in the positive (negative) direction.

Subtraction of Eq.7-5 from Eq.7-6 yields:

$$\text{Eq.7-7} \qquad \frac{W_+(\beta,0) - W_-(\beta,0)}{2\, W_o(\beta,0)} = -\beta\, \frac{A\sqrt{(I+1)/3I}}{1 + \Delta_c}\, B_1\, Q_1(0)$$

where the warm count $W_o(\beta,0)$ is simply:

Eq.7-8 $$W_o(\beta,0) = 1 + \Delta_c$$

Δ_c can be determined from the sum of Eqs.7-5 and 7-6 :

Eq.7-9 $$(W_+ + W_-) / 2 W_o = \frac{1 + \Delta_c(1-\delta)}{1 + \Delta_c}$$

The asymmetry parameter A can be determined from the combination of Eqs.7-7 and 7-9 .

Pile-Up

The introduction of the long solenoid allows one to collect beta particles with a large solid angle, since the purpose is to increase the beta efficiency. A field of 10.5 KG corresponds to a solid angle of about π (25%) for the beta particles between the energy of 100 kev and 580 kev. Assuming isotropic emission, one of the positrons would be detected for every four positrons emitted. Since only 1/3 of all decaying ^{52}Mn emit positrons, therefore about 1/12 of all decaying ^{52}Mn would result in a count in the beta detector. It follows that about one out of every twelve Compton electrons detected would be detected simultaneously with a positron. The pile-up intensity from this mechanism is expected to be about 10% of the Compton electron background.

Another serious source of pile-up stems from the fact that annihilation photons are emitted after a positron is stopped within the detector. Most of these annihilation photons originating from within the detector see only a depletion depth of about 1/2 mm, the thickness of the detector. However, about 3% of these photons would be emitted perpendicular to the detector thickness, and the depletion depth they see would be of the order of 8 mm . About 5% of the 511 kev photons in 8 mm thick germanium produce photoelectric effect

(see Figure 10). Compton interactions between the 511 kev photons and the germanium atoms also contribute to the pile-up intensity. Therefore pile-up would occur to more than 5% of all the positrons detected.

The first mechanism provides about 1% pile-up in the observed beta spectra* whereas the second mechanism provides about 5%. It should be pointed out that the second mechanism occurs to all positron emitters, and the introduction of a focussing solenoid does not affect the probability of pile-up. The present view is supported by a comparison between the ^{52}Mn and the ^{60}Co spectra. From Figure 23 and Figure 30, it is obvious that there is a lot less pile-up in the ^{60}Co beta spectra (negatron emitter) than in the ^{52}Mn spectra (positron emitter).

Pile-up pulses are usually large, and are basically responsible for the high energy end of the beta spectra beyond the end-point energy of the beta particles. While there are numerous high energy Compton electrons, they can only deposit part of their kinetic energy when their energy exceeds their range within the detector(which is about 700 kev). Therefore only pile-up can explain the existence of counts beyond the energy of 700 kev in the spectra.

Three observations may be made about the pile-up phenomenon. First of all, the percentage of pile-up as mentioned above is independent of the source strength. This is quite unlike the usual γ-γ pile-up in gamma spectroscopy when the count rate is too high. Secondly, because the pileup pulses also involve positrons (or negatrons), they should exhibit beta asymmetry just like normal pulses (except for the v/c term). Thirdly, they tend to reduce the count rate at the low energy protion and increase the count rate at the high energy portion of the beta spectra.

---

* We assume a 10% contribution of Compton electrons in the beta spectra.

The pile-up due to the coincidence between the Compton electrons and the positrons adds a term to Eq.7-4 :

Eq.7-10 $\Delta_{pc}(1 + \beta' A\sqrt{(I+1)/3I}\ B_1 Q_1) W_\gamma(0)$

where Δ_{pc} is an unknown constant;

β' is a certain average of the velocity of all the positrons;* the probability of the Compton electrons detected is proportional to $W_\gamma(0)$.

The pile-up due to the coincidence between the positrons and their own annihilation photons add the following term to Eq.7-4 :

Eq.7-11 $\Delta_{pa} (1 + \beta'' A\sqrt{(I+1)/3I}\ B_1 Q_1(0))$

where Δ_{pa} is an arbitrary constant;

β'' is another average velocity of the positrons.

Both β' and β'' should not deviate more than 0.05 from the most probable velocity , which is about 0.7 . It is not terribly important to know the values of the average velocity. For positrons energy between 150 kev and 500 kev, the velocity ranges from 0.60 to 0.85 , which is only a 25% change.

Eq.7-4 can now be re-written as:

Eq.7-12
$$W(\beta,0) = 1 + \beta A\sqrt{(I+1)/3I}\ B_1 Q_1(0) + \Delta_c(1-\delta)$$
$$+ \Delta_{pa} (1 + \beta'' A\sqrt{(I+1)/3I}\ B_1 Q_1)$$
$$+ \Delta_{pc} (1 + \beta' A\sqrt{(I+1)/3I}\ B_1 Q_1) (1-\delta)$$

---

* This should be very close to the most probable velocity of 0.7

Scattering

A good discussion on electron scattering may be found in Ref.33 . The following rules may be used qualitatively:

1) Single scattering predominates in a thin scatterer such as the iron source foil.

2) Single scattering cross-section is roughly proportional to the Rutherford scattering cross-section. The probability for electrons to be scattered into an angle θ with respect to the incident direction is $\sim 1 / \sin^4 \theta/2$. The back-scattering probability is very small in a thin foil.

3) Multiple scattering is significant in thick scatterers. This is the major cause of back scattering.

One of the major shortcoming of the present experimental arrangement is the relatively large probability of source scattering. However, since the source foil is thin, a positron with a positive velocity component would continue to spiral towards the detector after single scattering. Source scattering affects only the final energy of the particle but not its general direction. Since some of these positrons with relatively large v/c end up in the low energy end of the beta spectra, the asymmetry parameter A calculated from the lower energy portion of the spectra is expected to be too high(Eq.7-1).

A potentially more dangerous scattering mechanism is due to the backscattering from the copper fins. This mechanism admixes the particles going in opposite directions. A systematic asymmetry may exist even when the emission is supposed to be isotropic. However, when the difference $W_+ - W_-$ is taken , the admixture of directionally opposite beta particles causes a reduction in the observed asymmetry. It is indeed unfortunate that a theoretical calculation on all the scattering mechanisms is an impossibility. But it is safe to assert that most of these mechanisms lead to a net decrease in the observed asymmetry.

Back scattering from the detector has been discussed before. It is basically reponsible for the large count rate at the very low energy end of the spectra.

Scattered beta particles exhibit asymmetry also, and they add another term to Eq.7-12 of the order :

Eq.7-13 $$\Delta_s \left(1 + \beta''' A \sqrt{(I+1)/3I} \; B_1 Q_1 \right)$$

where β''' is expected to be close to the value of 0.7 .

Eq.7-12 becomes:

Eq.7-14 $$W(\beta,0) = 1 + \beta_a A \sqrt{(I+1)/3I} \; B_1 Q_1 - \delta \left(\Delta_c + \Delta_{pc}\right) / \left(1 + \Delta_c + \Delta_{pc} + \Delta_{pa} + \Delta_s \right)$$

where β_a is the velocity of the positrons detected as indicated by the energy scale of the beta spectra, but it contains the admixture of positrons which energy has been altered due to either scattering or pile-up.

β_a is given by:

Eq.7-15 $$\beta_a = \beta \; \frac{\left(1 + (\beta'/\beta)(1-\delta)\Delta_{pc} + (\beta''/\beta)\Delta_{pa} + (\beta'''/\beta)\Delta_s \right)}{1 + \Delta_{pc} + \Delta_{pa} + \Delta_s + \Delta_c}$$

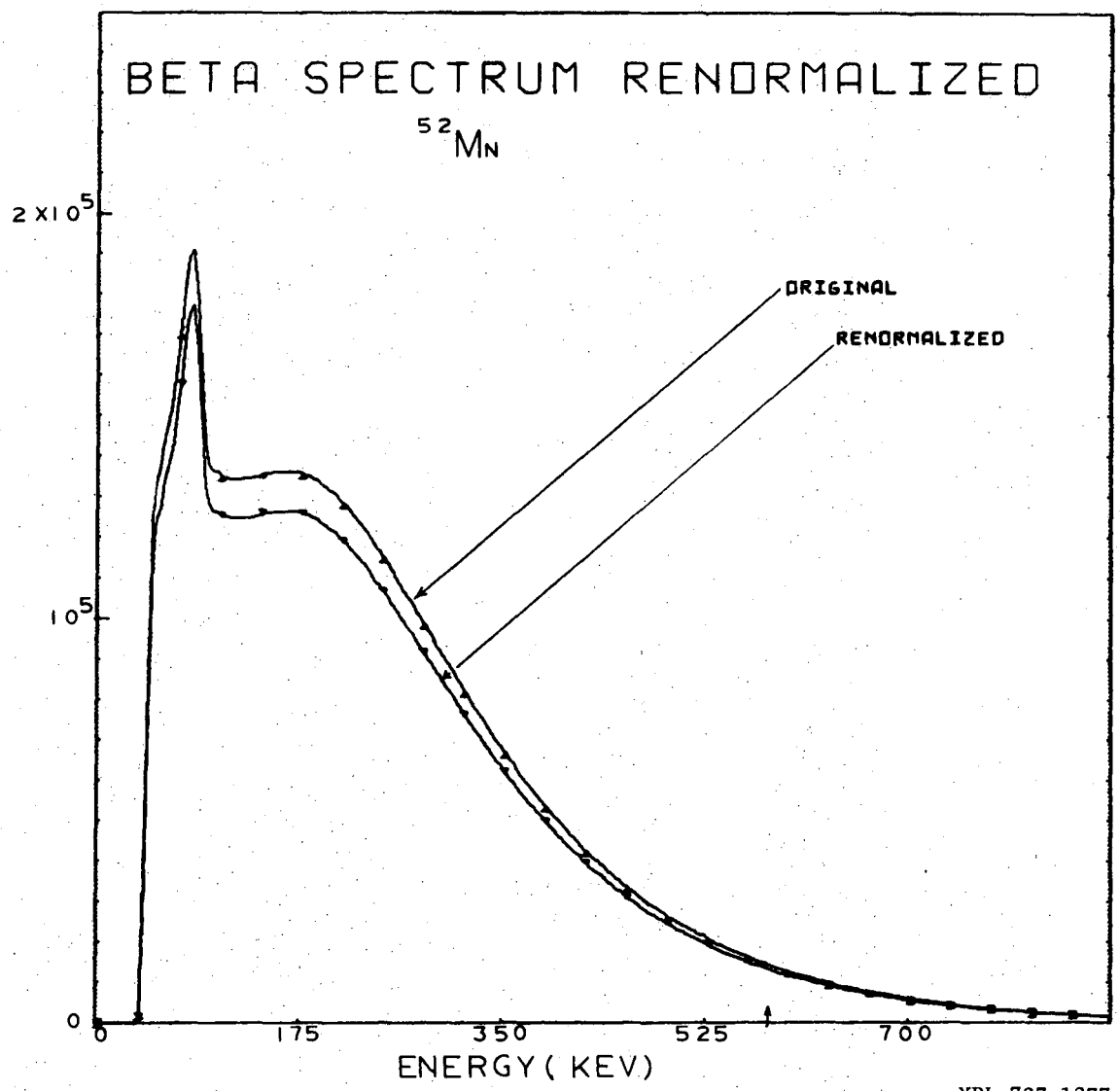

XBL 727-1277

Fig. 24. The renormalized beta spectrum of ^{52}Mn after the Compton electrons and some of the pile-up effects have been accounted for.

The following observations may be made:

1) The term $\delta\,(\Delta_c + \Delta_{pc})/(1 + \Delta_c + \Delta_{pc} + \Delta_{pa} + \Delta_s)$ disappears when we take the difference $W_+ - W_-$. In fact,

$$\text{Eq.7-16} \quad W_+(\beta,0) - W_-(\beta,0) = -\beta_a 2A\sqrt{(I+1)/3I}\; B_1 Q_1$$

and the asymmetry A can be calculated.

2) The order of magnitude of all the spurious effects due to scattering, pile-up and Compton electrons may be known by taking the sum $W_+ + W_-$. In fact,

$$\text{Eq.7-17} \quad (W_+ + W_-)/2 = 1 + \delta(\Delta_c + \Delta_{pc})/(1 + \Delta_c + \Delta_{pc} + \Delta_{pa} + \Delta_s)$$

where δ, the decrease in gamma rays in the 0° direction, can be determined from the gamma anisotropy. If we ignore the terms Δ_{pa} and Δ_s, then we can calculate the factor $(\Delta_c + \Delta_{pc})$. We can use the knowledge of $(\Delta_c + \Delta_{pc})$ to renormalize the beta spectra, i.e., to subtract the contributions due to the Compton electrons and some of the pile-up. Figure 24 indicates that the renormalized spectrum is just about 10% less in intensity than the warm beta spectrum.

3) The terms Δ_{pa} and Δ_s tend to be opposite in sign. At high energy end of the spectrum, scattering tends to reduce the count rate whereas pile-up tends to increase it. At the low energy end, pile-up tends to promote more positrons into the higher energy channels of the spectrum, whereas scattering causes more higher energy particles to lose part of their kinetic energy.

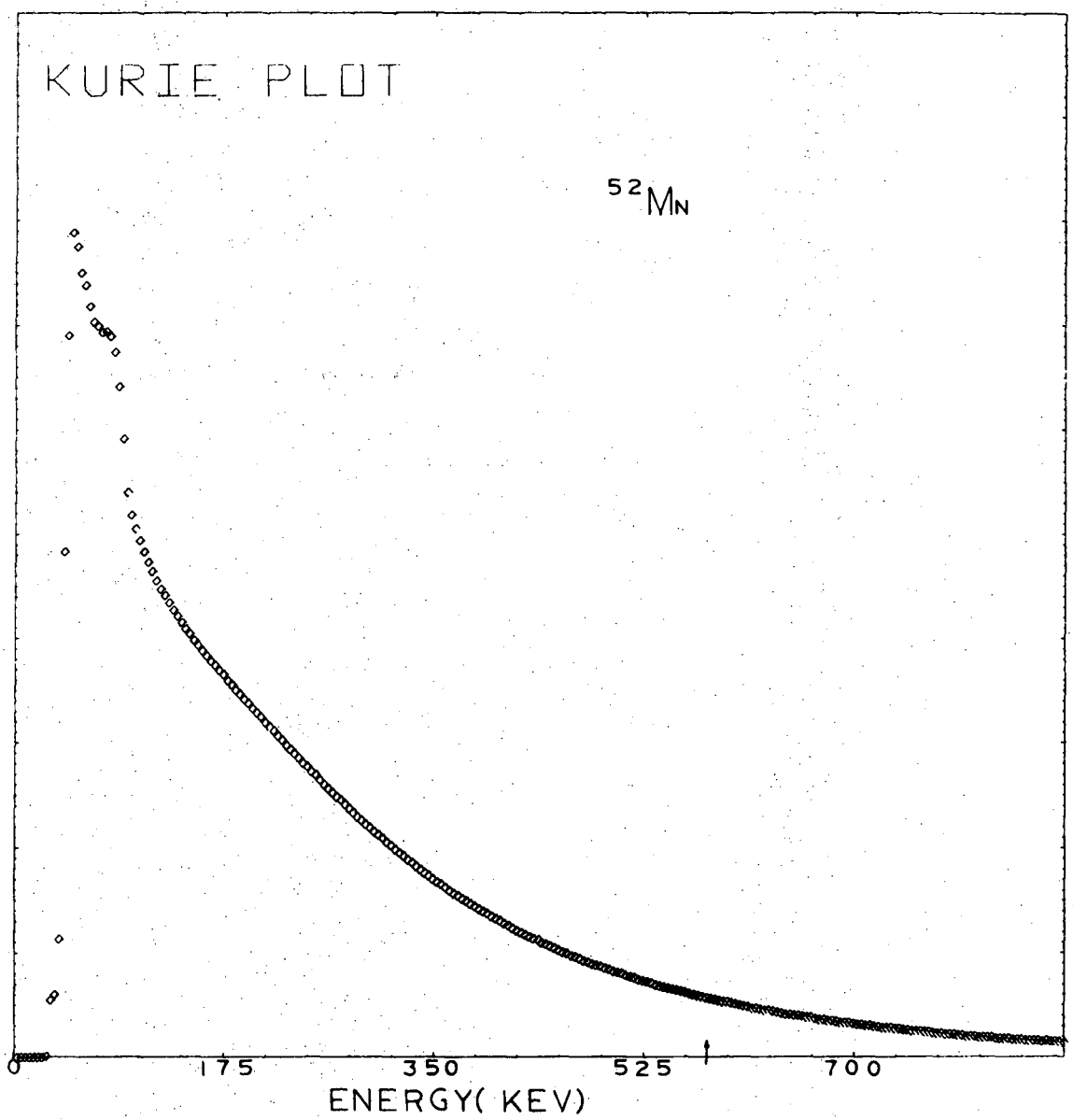

XBL 727-1281

Fig. 25. The Kurie plot of the observed beta spectrum of ^{52}Mn.

4) Eq.7-15 can best be viewed as v/c mixing. The beta asymmetry is proportional to the true v/c of the beta particles. Scattering and pile-up mix up the true beta asymmetry of the positrons, and tend to cause the beta asymmetry to approach a value corresponding to the most probable v/c of 0.7 .

The Kurie Plot

The Kurie plot of the ^{52}Mn spectrum supports the arguments in the preceding paragraphs (Figure 25). Scattering causes an increase in the count rate in the lower energy portion, whereas the Compton electrons and pile-up increase the count rate in the higher energy portion of the allowed beta spectrum.

The Solid Angle Correction

The solid angle correction factor $Q_1(0)$ is a function of the field strength, the collimator size, the source foil size as well as the velocity of the positrons v/c . The value of $Q_1(0)$ is therefore energy dependent. A computer calculation (see Appendix 5) indicates that the maximum angle subtended θ ranges from $\theta = 65^{\circ}$ for $\beta = 0.6$ (E = 128 kev) to $\theta = 52.5^{\circ}$ for $\beta = 0.88$ (E = 565 kev). The same calculation also indicates that about 25% of the positrons would be bent by the field and collide with the thin source foil. When this happens, some of the energy is lost either due to single scattering or due to penetration . Although this adds to the complexity of the analysis, it affects mostly the asymmetry derived from the lower energy portion of the beta spectrum.

The solid angle correction factor $Q_1(0)$ calculation as described in Appendix 5 is depicted in Figure 26 as a function of the positrons' kinetic energy. A complete listing is also presented in Figure 27 .

0 0 0 0 3 8 0 7 5 4 8

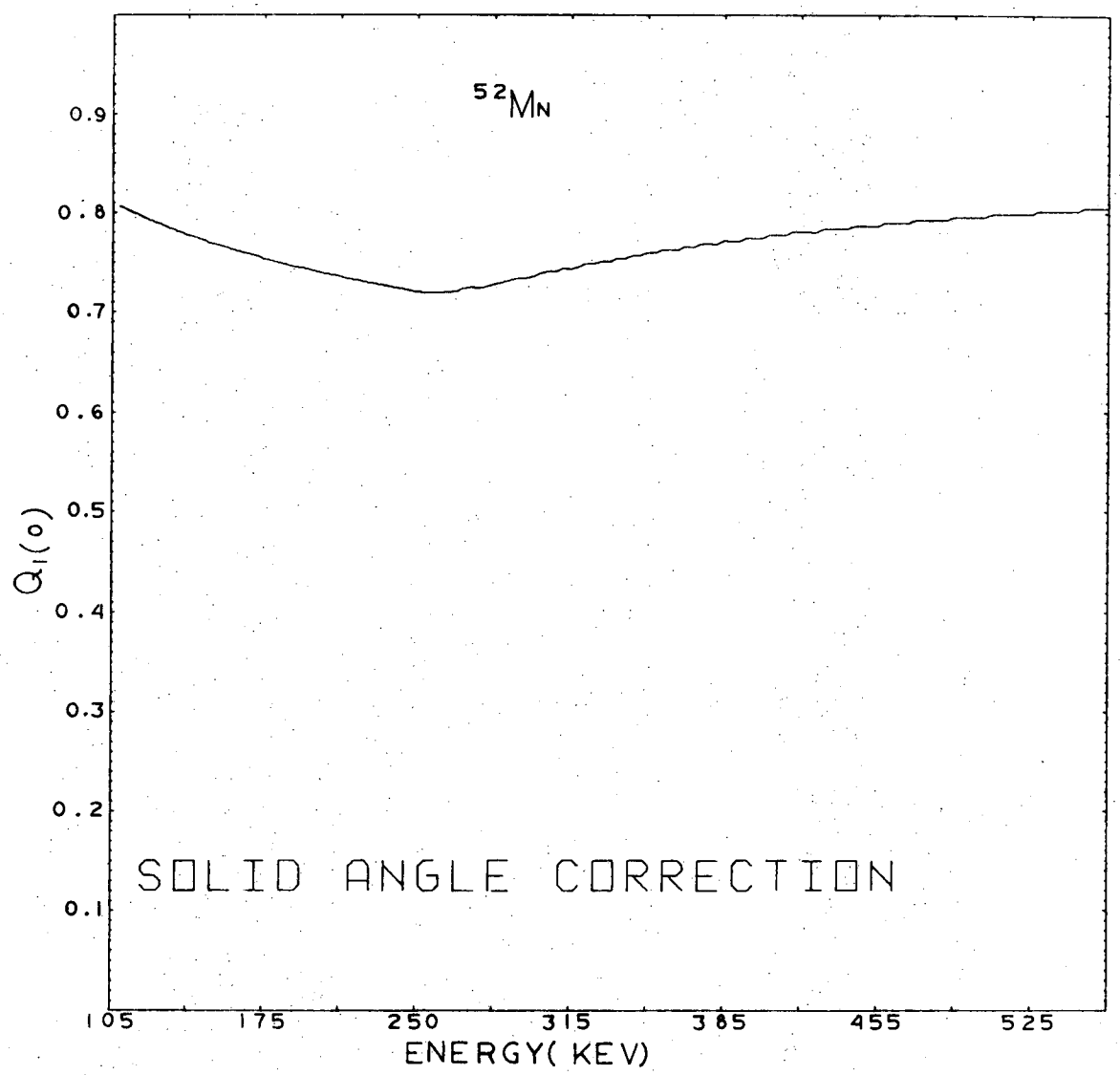

XBL 727-1280

Fig. 26. The values of the solid angle correction factor as a function of the energy of the positrons from oriented ^{52}Mn.

The Asymmetry Parameter

Eq.7-16 is used for the calculation of the asymmetry parameter A . The actual $\beta = v/c$ is used instead of the β_a in the calculation. To calculate β_a exactly, all the factors Δ_c , Δ_s , Δ_{pa} , and Δ_{pc} would have to be known. Unfortunately only the combined $\Delta_c + \Delta_{pc}$ is known. It should be pointed out, however, that v/c ranges only from 0.64 to 0.88 for all the positrons in question. Furthermore, β_a represents a value somewhere between β and 0.7 , the most probable v/c . Therefore, the asymmetry parameter A determined from any channel of the spectrum is not expected to pose an error in excess of 10% . The value of A from the lower energy channels forms the upper limit of the true asymmetry parameter, whereas the value of A determined from the higher energy channels forms the lower limit.

The result is $A = 0.402 \pm 0.011$

The aymmetry parameter reported here represents a least square fit of all the values of A as a function of the energy taken between E = 105 kev and E = 560 kev (see Figure 28). The error is three times the standard deviation in the same least square fit.

Assuming time-reversal invariance, the Fermi/Gamow-Teller mixing ratio is

$$\frac{|C_V||M_F|}{|C_A||M_{GT}|} = -14.5 \begin{matrix} +0.6 \\ -0.7 \end{matrix} \%$$

A plot of the mixing ratio as a function of the relative phase between the Fermi and Gamow-Teller matrix elements is given in Figure 29. A complete tabulation of the experimental results is given in Figure 27.

Fig. 27. A complete tabulation of the ^{52}Mn beta asymmetry results.
SAC stands for the Solid Angle Correction factor.
A(Fl) stands for the asymmetry after the degree of nuclear polarization has been accounted for.
A(SAC) is calculated by dividing A(Fl) by the solid angle correction factor.
A(V/C) is calculated by dividing A(SAC) by the term V/C . A(V/C) gives the values of the asymmetry parameter A as a function of the positron energy. Comparison between the A(SAC) values and the A(V/C) values indicates that the true values of V/C have been altered by the scattering and pile-up effects.

CH NO	KEV	V/C	SAC	A(F1)	A(SAC)	A(V/C)	PLUS C	WARM C	MINUS C
10	35.15	.3530	.955	.2005	.2099	.5948	186	443	337
11	38.67	.3684	.940	.1762	.1874	.5086	799	1793	1336
12	42.18	.3830	.927	.2121	.2288	.5974	29214	37225	42639
13	45.70	.3968	.915	.2155	.2354	.5933	71376	85874	102831
14	49.21	.4098	.905	.1929	.2132	.5202	106316	125092	147517
15	52.73	.4223	.895	.1910	.2134	.5054	115204	133992	158715
16	56.24	.4341	.886	.1866	.2106	.4851	118982	137247	162549
17	59.76	.4455	.878	.1878	.2139	.4803	125466	144696	171660
18	63.27	.4563	.870	.1826	.2098	.4599	129506	148636	175564
19	66.79	.4667	.863	.1923	.2112	.4525	133768	153150	181225
20	70.30	.4767	.856	.1740	.2032	.4262	143152	161920	191046
21	73.82	.4863	.850	.1637	.1925	.3958	151492	169925	198770
22	77.33	.4956	.844	.1561	.1848	.3730	162536	181170	210604
23	80.85	.5045	.839	.1575	.1877	.3721	164216	188995	219607
24	84.36	.5131	.834	.1587	.1904	.3711	171417	191207	223018
25	87.88	.5215	.829	.1676	.2023	.3879	162131	181854	213452
26	91.39	.5295	.824	.1795	.2179	.4115	143955	162578	193577
27	94.91	.5373	.819	.1963	.2371	.4412	125515	142457	172567
28	98.42	.5449	.815	.2010	.2466	.4526	120301	137223	167200
29	101.94	.5522	.811	.2050	.2528	.4577	119038	135841	166382
30	105.45	.5593	.807	.2050	.2540	.4541	118918	135918	166282
31	108.97	.5662	.803	.2055	.2558	.4517	118361	134929	165445
32	112.48	.5730	.800	.2095	.2619	.4572	117820	134714	165795
33	116.00	.5795	.796	.2092	.2627	.4534	117418	134163	165131
34	119.52	.5858	.793	.2109	.2659	.4539	117475	134232	165590
35	123.03	.5920	.790	.2135	.2703	.4567	116944	134199	165647
36	126.55	.5980	.787	.2142	.2723	.4553	117560	134877	166663
37	130.06	.6038	.784	.2146	.2739	.4536	117649	134933	166931
38	133.58	.6095	.781	.2174	.2785	.4569	117510	134949	167309
39	137.09	.6151	.778	.2197	.2824	.4592	117544	135211	168043
40	140.61	.6205	.775	.2218	.2862	.4612	117327	135231	168317
41	144.12	.6258	.772	.2204	.2853	.4559	117923	135586	168719
42	147.64	.6309	.770	.2227	.2893	.4585	117665	136091	169393
43	151.15	.6360	.767	.2285	.2977	.4681	117334	136011	170157
44	154.67	.6409	.765	.2236	.2922	.4560	118017	136133	169834
45	158.18	.6457	.763	.2277	.2985	.4623	117095	136011	169737
46	161.70	.6504	.760	.2287	.3008	.4625	116975	135956	169830
47	165.21	.6549	.758	.2274	.2999	.4579	117387	136311	170077
48	168.73	.6594	.756	.2309	.3055	.4632	116846	136247	170337
49	172.24	.6638	.754	.2282	.3027	.4561	117040	136130	169857
50	175.76	.6681	.752	.2311	.3074	.4602	116341	136093	169818
51	179.27	.6723	.750	.2331	.3109	.4624	115370	135274	168977
52	182.79	.6764	.748	.2362	.3158	.4669	114720	135772	169034
53	186.30	.6804	.746	.2344	.3142	.4618	113966	134551	167564
54	189.82	.6844	.744	.2347	.3155	.4610	113432	134233	167001
55	193.33	.6882	.742	.2311	.3113	.4523	113115	133376	165507
56	196.85	.6920	.741	.2306	.3115	.4501	112132	132548	164104
57	200.36	.6957	.739	.2342	.3171	.4558	111012	131946	163555
58	203.88	.6993	.737	.2348	.3186	.4556	109889	131152	162250
59	207.39	.7029	.735	.2345	.3188	.4536	109256	130602	161312
60	210.91	.7064	.734	.2349	.3200	.4530	107928	129199	159496
61	214.42	.7098	.732	.2347	.3206	.4517	106694	128185	157848
62	217.94	.7131	.731	.2370	.3244	.4549	105488	127278	156764
63	221.45	.7164	.729	.2328	.3193	.4457	104486	125776	154258
64	224.97	.7197	.728	.2362	.3247	.4512	102894	124638	152950
65	228.48	.7228	.726	.2337	.3218	.4453	101713	123266	150679
66	232.00	.7259	.725	.2346	.3238	.4460	103444	122119	149153
67	235.52	.7290	.723	.2324	.3214	.4409	99597	120935	147184
68	239.03	.7320	.722	.2340	.3243	.4430	97608	119276	145064
69	242.55	.7349	.720	.2397	.3327	.4527	95339	117292	143133
70	246.06	.7378	.720	.2376	.3301	.4473	94561	116617	141671
71	249.58	.7407	.720	.2380	.3307	.4465	92747	114900	139243
72	253.09	.7435	.720	.2331	.3237	.4354	92030	113588	137034
73	256.61	.7462	.720	.2330	.3234	.4334	90260	111679	134489
74	260.12	.7489	.721	.2369	.3285	.4386	88233	110097	132569
75	263.64	.7516	.724	.2337	.3227	.4294	86059	108289	129875
76	267.15	.7542	.726	.2345	.3232	.4286	85388	106690	127917
77	270.67	.7567	.725	.2318	.3198	.4226	83936	105045	125336
78	274.18	.7592	.727	.2338	.3218	.4239	82703	103898	124006
79	277.70	.7617	.728	.2338	.3210	.4214	80985	101849	121472
80	281.21	.7642	.730	.2311	.3164	.4141	79698	100294	119101
81	284.73	.7666	.732	.2325	.3174	.4140	78103	98619	117078
82	288.24	.7689	.735	.2349	.3197	.4158	76224	96793	114871
83	291.76	.7712	.734	.2300	.3132	.4061	75389	95545	112748
84	295.27	.7735	.737	.2336	.3171	.4100	73458	93499	110591
85	298.79	.7758	.739	.2320	.3139	.4046	72061	91884	108300
86	302.30	.7780	.742	.2311	.3116	.4005	70403	90183	105832
87	305.82	.7801	.741	.2326	.3137	.4021	68974	88570	103991
88	309.33	.7823	.744	.2266	.3045	.3892	68258	87291	101879
89	312.85	.7844	.744	.2304	.3097	.3948	66487	85904	99694
90	316.36	.7865	.747	.2343	.3139	.3991	64829	83884	98242
91	319.88	.7885	.749	.2333	.3113	.3948	63265	81969	95768
92	323.39	.7905	.749	.2324	.3103	.3925	61943	80287	93668
93	326.91	.7925	.752	.2300	.3058	.3859	60629	78736	91412
94	330.42	.7945	.752	.2300	.3060	.3851	59318	77103	89467
95	333.94	.7964	.755	.2281	.3022	.3795	58465	75798	87856
96	337.45	.7983	.755	.2341	.3102	.3886	56712	74262	86265
97	340.97	.8002	.758	.2321	.3065	.3830	55589	72553	84222
98	344.48	.8020	.757	.2300	.3037	.3787	54213	70913	81945
99	348.00	.8038	.760	.2281	.3000	.3732	52964	69458	79899
100	351.52	.8056	.760	.2322	.3055	.3792	51825	68182	78763
101	355.03	.8074	.763	.2339	.3065	.3796	50268	66557	76715
102	358.55	.8091	.763	.2324	.3046	.3764	49406	65128	75135
103	362.06	.8108	.763	.2328	.3068	.3799	46629	64091	73770
104	365.58	.8125	.766	.2329	.3060	.3751	47114	62135	71793
105	369.09	.8142	.766	.2331	.3063	.3718	45401	60912	69960
106	372.61	.8158	.769	.2284	.2970	.3660	45177	59651	68339
107	376.12	.8174	.769	.2328	.3078	.3704	43911	58101	66791
108	379.64	.8190	.769	.2361	.3071	.3750	42779	57186	65736
109	383.15	.8206	.772	.2341	.3035	.3698	41742	55404	63969
110	386.67	.8222	.772	.2320	.3006	.3656	41064	54720	62690
111	390.18	.8237	.772	.2309	.2986	.3625	40277	53467	61225
112	393.70	.8252	.778	.2340	.3026	.3667	39076	52201	59892
113	397.21	.8267	.779	.2361	.3047	.3686	37988	50951	58453
114	400.73	.8282	.775	.2360	.3045	.3677	37036	49157	56994
115	404.24	.8296	.778	.2378	.3054	.3681	36247	48832	56012
116	407.76	.8311	.778	.2403	.3088	.3716	35462	47674	54814
117	411.27	.8325	.778	.2323	.2986	.3586	34604	46443	52942
118	414.79	.8339	.781	.2387	.3055	.3664	33655	45506	52118
119	418.30	.8352	.781	.2364	.3026	.3623	32820	44457	50686
120	421.82	.8366	.781	.2444	.3129	.3740	31722	43220	49676
121	425.33	.8380	.781	.2366	.3030	.3616	31424	42435	48495
122	428.85	.8393	.784	.2404	.3065	.3652	30604	41197	47237
123	432.36	.8406	.784	.2427	.3095	.3682	29662	40400	46330
124	435.88	.8419	.784	.2391	.3050	.3622	29108	39637	45220
125	439.39	.8432	.784	.2416	.3082	.3655	28439	38669	44323
126	442.91	.8444	.787	.2348	.2982	.3531	27805	37667	42837
127	446.42	.8457	.787	.2409	.3060	.3618	27043	36830	42123
128	449.94	.8469	.787	.2424	.3079	.3636	26462	35810	41018
129	453.45	.8481	.787	.2402	.3051	.3598	25771	35036	40075
130	456.97	.8493	.790	.2386	.3019	.3555	25108	34213	38988
131	460.48	.8505	.790	.2429	.3073	.3613	24340	33362	38164
132	464.00	.8517	.790	.2394	.3029	.3557	23867	32580	37126
133	467.52	.8528	.790	.2403	.3041	.3565	23427	31948	36477
134	471.03	.8540	.794	.2482	.3128	.3663	22528	31054	35633
135	474.55	.8551	.793	.2366	.2981	.3487	22341	30358	34550
136	478.06	.8562	.793	.2494	.3143	.3671	21504	29991	34050
137	481.58	.8573	.793	.2488	.3136	.3658	20980	28909	33204
138	485.09	.8584	.793	.2380	.2999	.3494	20779	28268	32214
139	488.61	.8595	.797	.2449	.3074	.3577	20065	27561	31539
140	492.12	.8605	.797	.2348	.2947	.3425	19842	27053	30640
141	495.64	.8616	.797	.2444	.3069	.3562	18988	26194	29874
142	499.15	.8626	.797	.2485	.3120	.3617	18518	25614	29338
143	502.67	.8636	.796	.2469	.3100	.3590	18031	25005	28528
144	506.18	.8647	.800	.2458	.3073	.3554	17769	24423	27973
145	509.70	.8657	.800	.2544	.3181	.3674	17205	23977	27573
146	513.21	.8666	.800	.2421	.3028	.3494	16965	23336	26570
147	516.73	.8676	.800	.2492	.3116	.3591	16443	22760	26084
148	520.24	.8686	.800	.2504	.3132	.3606	15924	22153	25355
149	523.76	.8696	.800	.2512	.3141	.3613	15597	21571	24808
150	527.27	.8705	.803	.2484	.3094	.3555	15449	21276	24435
151	530.79	.8714	.803	.2503	.3118	.3578	14822	20832	23602
152	534.30	.8724	.803	.2478	.3087	.3539	14471	20110	22944
153	537.82	.8733	.803	.2513	.3130	.3584	14036	19461	22319
154	541.33	.8742	.803	.2542	.3167	.3623	13646	19058	21863
155	544.85	.8751	.803	.2534	.3157	.3607	13176	18502	21146
156	548.36	.8760	.806	.2568	.3186	.3637	12926	18197	20869
157	551.88	.8768	.806	.2562	.3178	.3625	12644	17703	20353
158	555.39	.8777	.806	.2591	.3215	.3663	12343	17280	19954
159	558.91	.8786	.806	.2565	.3183	.3623	11956	16958	19307
160	562.42	.8794	.806	.2476	.3072	.3494	11972	16507	18920
161	565.94	.8803	.806	.2526	.3134	.3560	11512	16108	18428
162	569.45	.8811	.806	.2565	.3184	.3613	11154	15624	17968
163	572.97	.8819	.809	.2505	.3096	.3511	10854	15239	17344
164	576.48	.8827	.809	.2611	.3227	.3656	10595	14888	17203
165	580.00	.8835	.809	.2509	.3107	.3510	10495	14597	16720
166	583.52	.8843	.809	.2657	.3284	.3713	9938	14089	16301
167	587.03	.8851	.809	.2598	.3211	.3628	9870	13829	15978
168	590.55	.8859	.809	.2452	.3031	.3421	9693	13460	15304
169	594.06	.8867	.809	.2468	.3026	.3412	9497	13197	14988

Fig. 27.

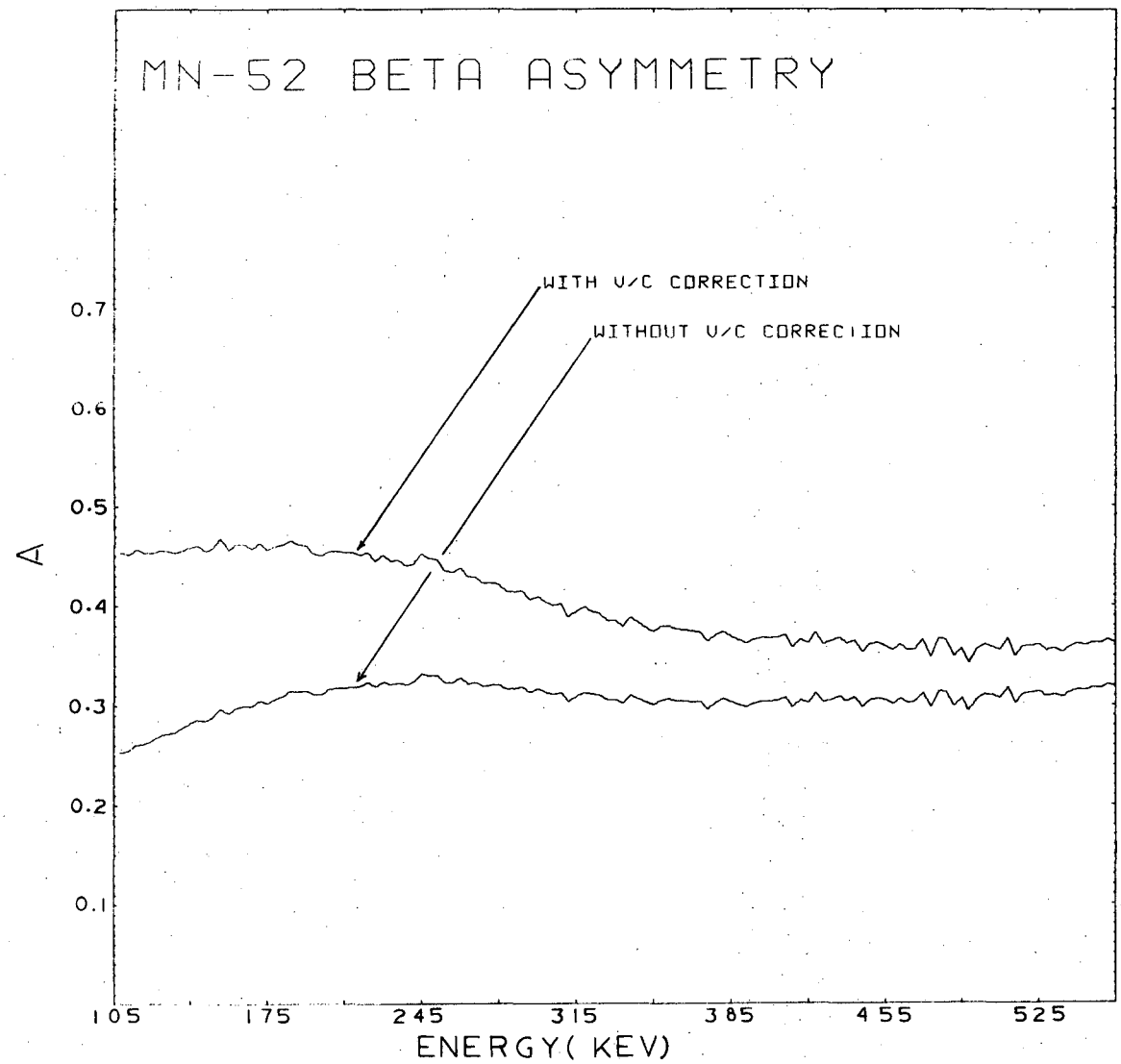

XBL 727-1282

Fig. 28. The ^{52}Mn beta asymmetry parameter A as a function of the energy scale of the electronics.

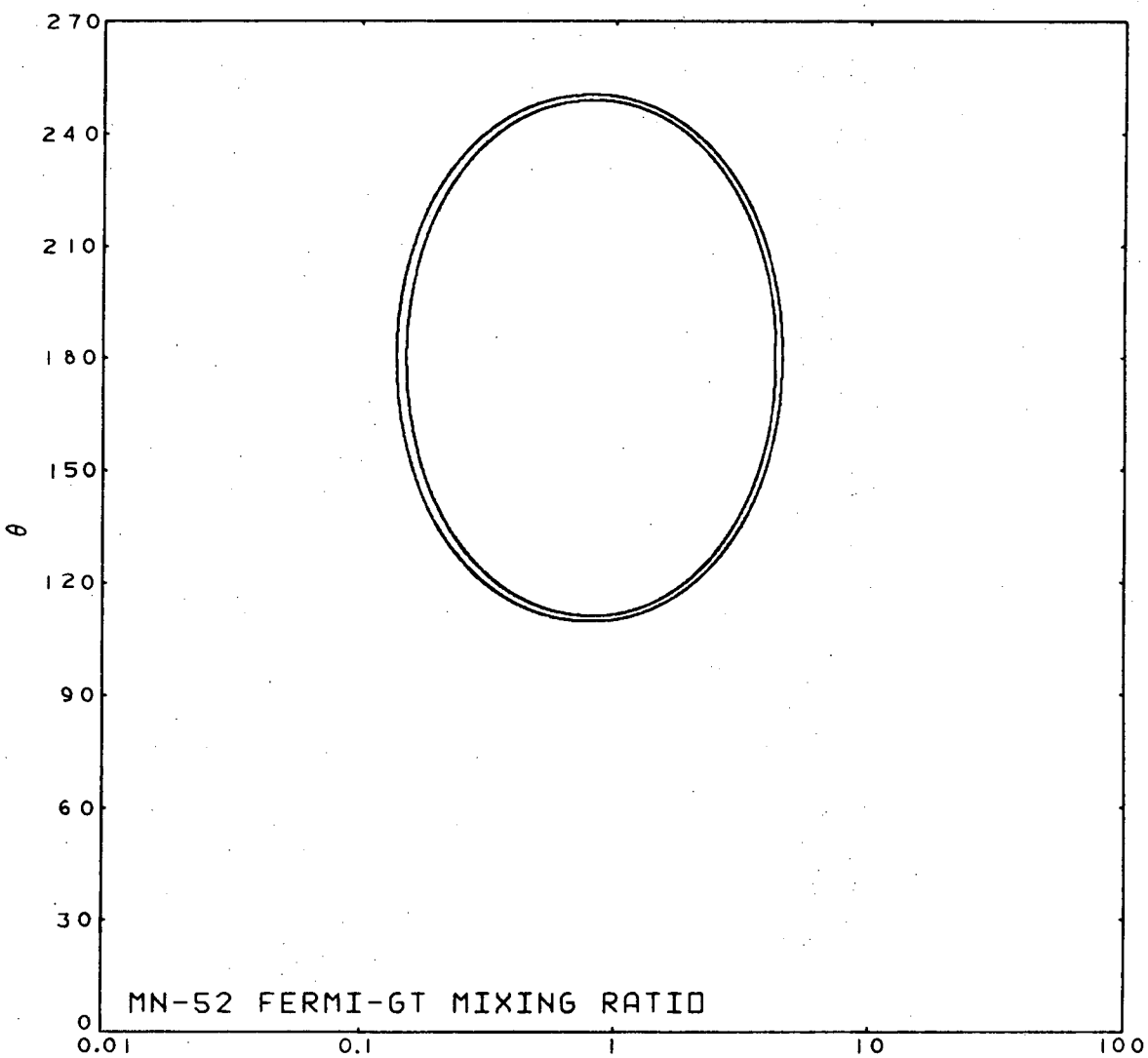

XBL 727-1270

Fig. 29. The measured Fermi/Gamow-Teller mixing ratio as a function of the phase angle. The two separate curves form the upper and lower limits when the reported errors are included.

CHAPTER VIII

The ^{60}Co Beta Asymmetry Experiment

The ^{60}Co experiment has been designed to be performed under conditions as similar to the ^{52}Mn experiment as possible. A polarizing field of ± 6.9 KG was used instead, which would provide a similar solid angle correction factor.

The decay scheme is given in Figure 5 . ^{60}Co udergoes a pure Gamow-Teller transition to an excited state of ^{60}Ni . Its spin sequence is $5+(\beta)4+(\gamma E2)2+(\gamma E2)0+$. Since the two gamma transitions are "stretched", either one of them may be used to determine the temperature reached. Being a negatron emitter, ^{60}Co is expected to have a negative asymmetry of -1 .

The spectra are given in Figure 30.

The Kurie plot(Figure 31) indicates that it is a lot cleaner experiment than the ^{52}Mn experiment. This is not surprising since it doesn't have as many gamma rays associated with each beta transition. The pile-up effect diminished since it doesn't have the problems associated with positron emitters.

The solid angle correction factor $Q_1(0)$ as a function of energy between 140 kev and 280 kev is plotted in Figure 32 , and a complete tabulation of the experimental results is given in Fig. 33.

Figure 34 depicts the value of A as a function of beta energy between 140 kev and 280 kev , with the true value lying somewhere in between the two extremes of -0.95 and - 1.03 . A least square fit has been done with these values, and the result is

$$A = -0.971 \pm 0.034$$

where the error is three times the standard deviation of the same least square fit. This result agrees very well with the expected theoretical result of A = - 1 .

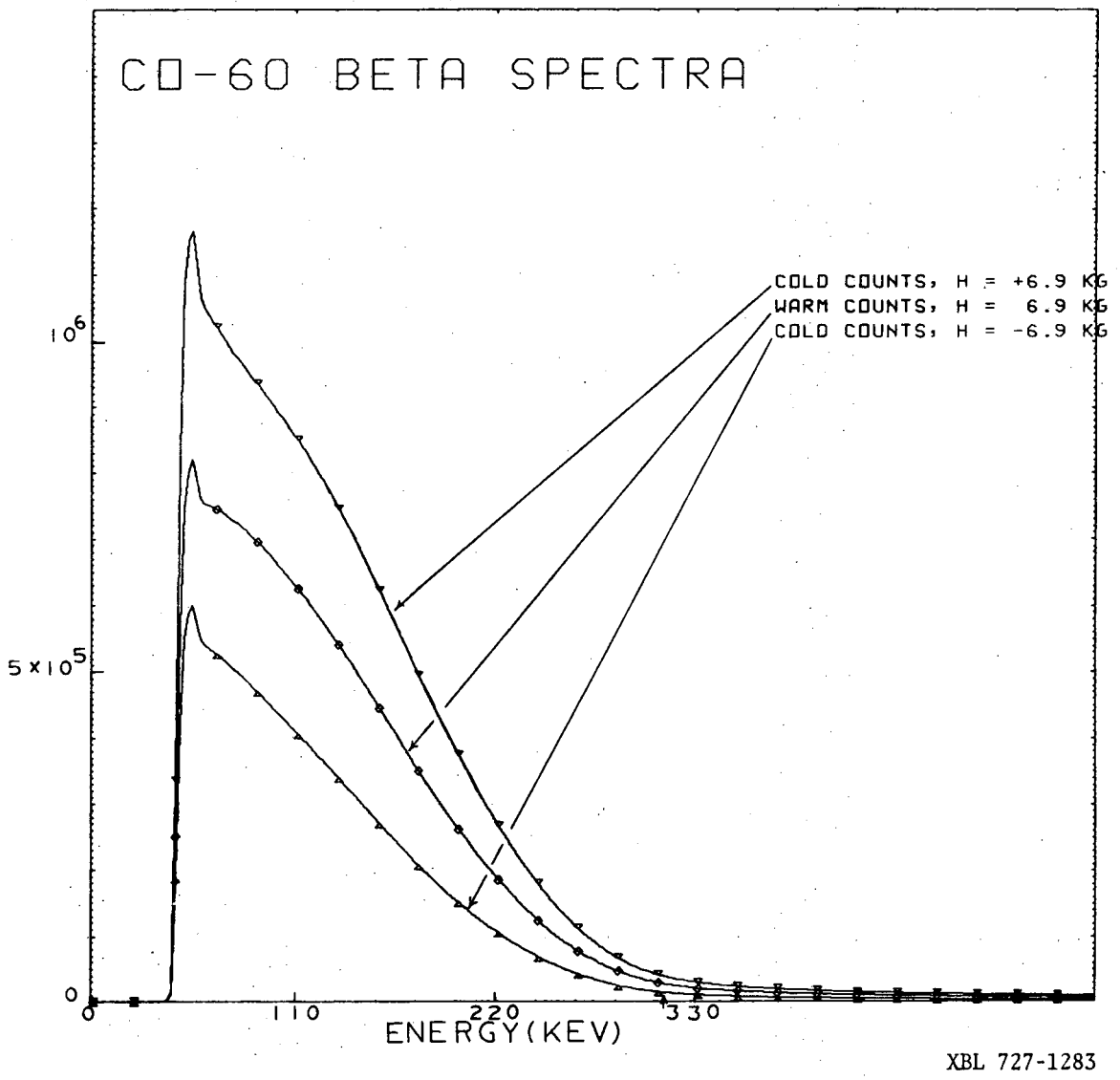

Fig. 30. The observed beta spectra of ^{60}Co.

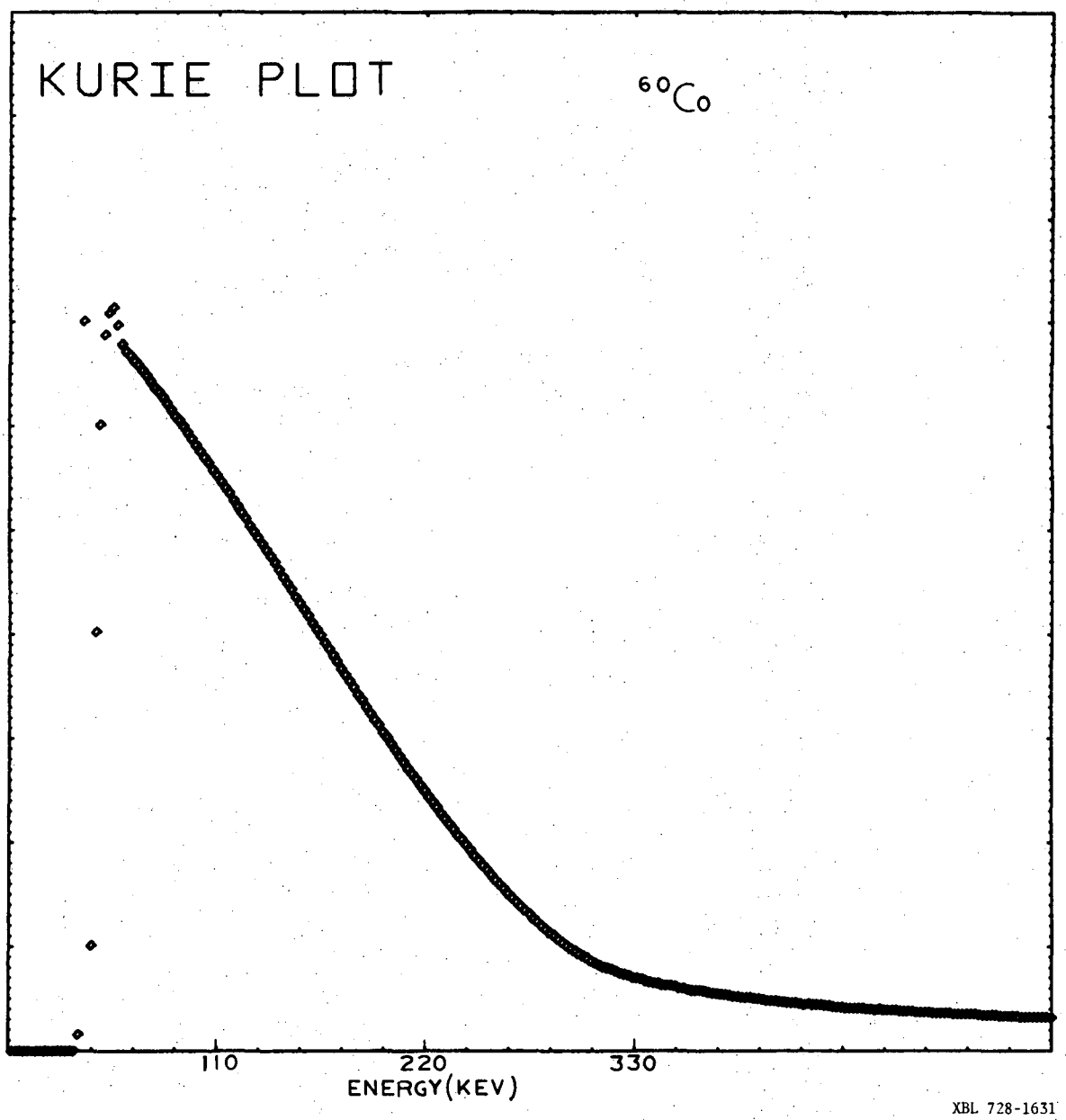

Fig. 31. The Kurie plot of the observed beta spectrum of ^{60}Co.

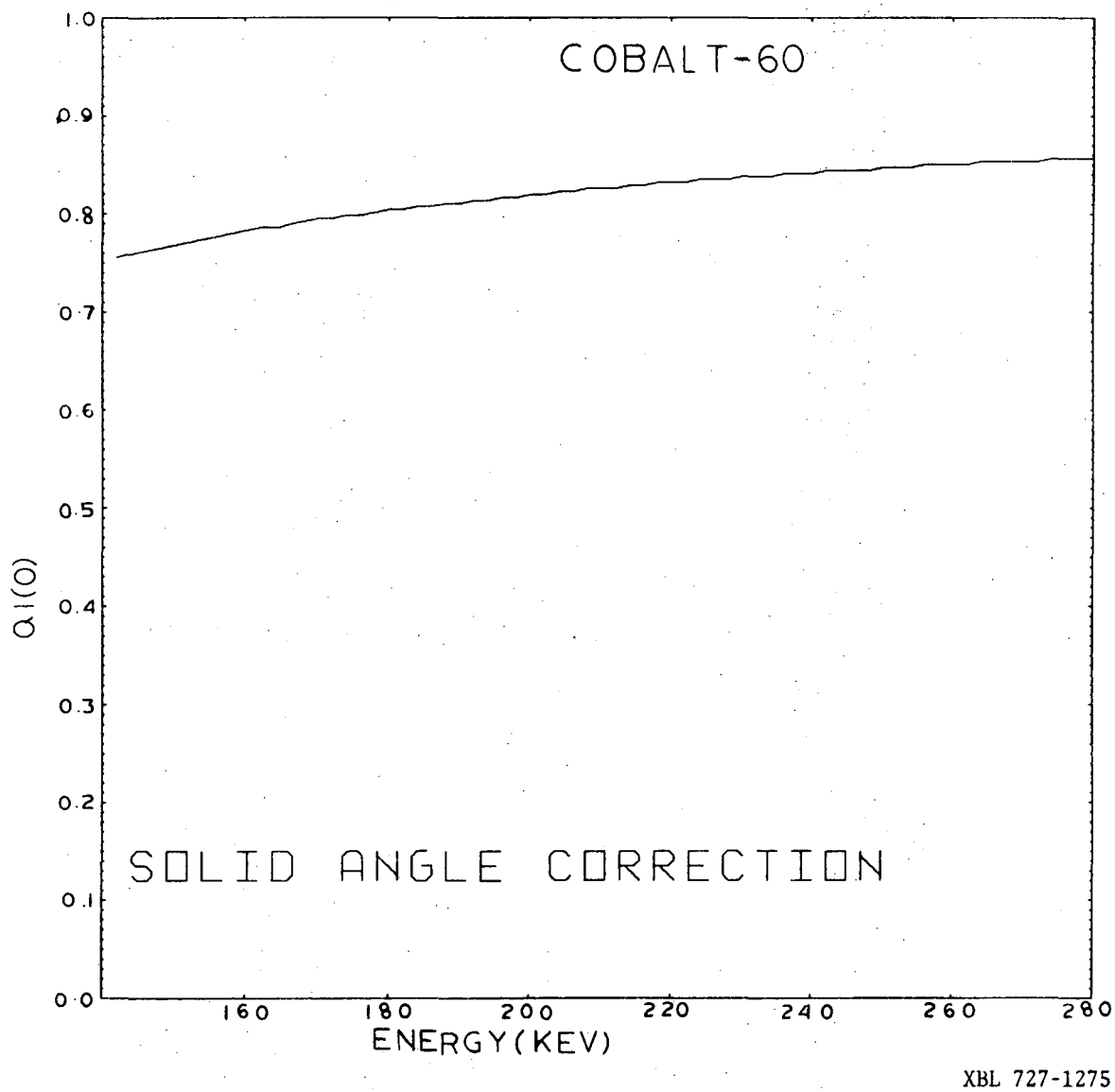

Fig. 32. The calculated solid angle correction factor for ^{60}Co.

Fig. 33. A complete tabulation of the ^{60}Co beta asymmetry results. SAC stands for the Solid Angle Correction factor.
A(Fl) stands for the asymmetry after the degree of nuclear polarization has been accounted for.
A(SAC) is calculated by dividing A(Fl) by the solid angle correction factor.
A(V/C) is calculated by dividing A(SAC) by the term V/C. A(V/C) gives the values of the asymmetry parameter A as a function of the negatron energy. Comparison between the A(SAC) values and the A(V/C) values indicates that the true values of V/C have been altered by the scattering and pile-up effects.

CH NO	KEV	V/C	SAC	A(F1)	A(SAC)	A(V/C)	PLUS C	WARM C	MINUS C
20	43.97	.3901	.811	-.2611	-.3219	-.8251	17964	15596	11774
21	46.17	.3986	.806	-.3850	-.4778	-1.1987	335024	250903	188183
22	48.37	.4068	.801	-.4755	-.5937	-1.4596	829468	564995	421084
23	50.57	.4147	.796	-.4719	-.5927	-1.4292	1088211	746383	552848
24	52.77	.4224	.792	-.4631	-.5850	-1.3848	1153046	800608	589452
25	54.96	.4299	.788	-.4533	-.5756	-1.3389	1166810	821164	601041
26	57.16	.4371	.784	-.4502	-.5746	-1.3163	1117174	791197	575788
27	59.36	.4442	.780	-.4475	-.5739	-1.2920	1066135	759449	549586
28	61.56	.4511	.776	-.4434	-.5714	-1.2667	1047613	751684	540983
29	63.76	.4578	.773	-.4402	-.5698	-1.2448	1038862	750103	536946
30	65.96	.4643	.769	-.4370	-.5681	-1.2236	1028329	747154	532021
31	68.16	.4707	.766	-.4351	-.5679	-1.2067	1020284	744900	527680
32	70.35	.4769	.763	-.4337	-.5685	-1.1922	1010862	741046	522295
33	72.55	.4829	.760	-.4319	-.5683	-1.1769	1001192	737331	517098
34	74.75	.4888	.757	-.4310	-.5692	-1.1644	990340	731963	510834
35	76.95	.4946	.754	-.4312	-.5716	-1.1557	980737	726440	504596
36	79.15	.5002	.752	-.4313	-.5737	-1.1469	974897	723786	500352
37	81.35	.5058	.749	-.4324	-.5771	-1.1410	966561	718443	494366
38	83.55	.5112	.747	-.4338	-.5808	-1.1362	957922	712568	488100
39	85.74	.5165	.744	-.4357	-.5852	-1.1331	949248	706212	481590
40	87.94	.5216	.742	-.4370	-.5889	-1.1289	940339	700046	475292
41	90.14	.5267	.740	-.4395	-.5940	-1.1277	935359	695933	470462
42	92.34	.5317	.738	-.4416	-.5986	-1.1259	926142	688866	463708
43	94.54	.5365	.736	-.4445	-.6042	-1.1261	917068	681326	456717
44	96.74	.5413	.734	-.4471	-.6094	-1.1257	909469	675113	450692
45	98.94	.5460	.732	-.4499	-.6149	-1.1263	900657	667747	443970
46	101.13	.5506	.730	-.4525	-.6200	-1.1261	890512	659638	436829
47	103.33	.5551	.728	-.4557	-.6260	-1.1277	883888	653658	431169
48	105.53	.5595	.726	-.4583	-.6312	-1.1281	874828	646250	424633
49	107.73	.5638	.724	-.4610	-.6365	-1.1289	864343	637728	417635
50	109.93	.5681	.723	-.4640	-.6421	-1.1302	856360	630919	411426
51	112.13	.5723	.723	-.4669	-.6460	-1.1289	849142	624687	405853
52	114.33	.5766	.724	-.4697	-.6491	-1.1261	837416	615143	398192
53	116.52	.5804	.726	-.4726	-.6512	-1.1219	831163	609697	393219
54	118.72	.5844	.729	-.4751	-.6520	-1.1157	818764	599914	385560
55	120.92	.5883	.732	-.4781	-.6530	-1.1101	808901	591670	378929
56	123.12	.5921	.736	-.4810	-.6534	-1.1034	797127	582144	371538
57	125.32	.5959	.738	-.4835	-.6551	-1.0993	789335	575772	366218
58	127.52	.5996	.743	-.4864	-.6548	-1.0921	778354	566614	359306
59	129.72	.6033	.745	-.4889	-.6563	-1.0879	767235	557989	352536
60	131.91	.6068	.750	-.4916	-.6553	-1.0799	755919	548964	345696
61	134.11	.6104	.753	-.4941	-.6565	-1.0755	745278	540548	339294
62	136.31	.6139	.755	-.4966	-.6575	-1.0710	733192	531114	332306
63	138.51	.6173	.758	-.4992	-.6586	-1.0669	721195	521678	325371
64	140.71	.6206	.761	-.5018	-.6596	-1.0628	711359	513824	319473
65	142.91	.6240	.763	-.5044	-.6606	-1.0588	698572	503845	312303
66	145.11	.6272	.766	-.5067	-.6613	-1.0543	684265	492918	304601
67	147.30	.6304	.769	-.5091	-.6618	-1.0498	671755	483318	297770
68	149.50	.6336	.772	-.5115	-.6625	-1.0455	661021	474965	291755
69	151.70	.6367	.775	-.5137	-.6629	-1.0410	644651	463953	284154
70	153.90	.6398	.778	-.5163	-.6636	-1.0371	635041	455096	277921
71	156.10	.6428	.781	-.5184	-.6638	-1.0326	621289	444741	270819
72	158.30	.6458	.784	-.5207	-.6641	-1.0283	609899	435920	264696
73	160.50	.6488	.787	-.5230	-.6645	-1.0243	596366	425815	257836
74	162.70	.6517	.787	-.5251	-.6672	-1.0238	583489	416207	251321
75	164.89	.6545	.790	-.5273	-.6675	-1.0198	570758	406596	244845
76	167.09	.6574	.793	-.5294	-.6674	-1.0154	557436	396698	238239
77	169.29	.6601	.796	-.5315	-.6676	-1.0113	544130	386764	231651
78	171.49	.6629	.796	-.5336	-.6702	-1.0111	531900	377661	225601
79	173.69	.6656	.799	-.5356	-.6702	-1.0069	519316	368317	219443
80	175.89	.6683	.799	-.5375	-.6726	-1.0065	505796	358406	212986
81	178.09	.6709	.802	-.5395	-.6725	-1.0024	493949	349629	207238
82	180.28	.6735	.805	-.5415	-.6723	-.9983	480738	339919	200973
83	182.48	.6760	.805	-.5434	-.6748	-.9982	468755	331100	195268
84	184.68	.6786	.808	-.5452	-.6745	-.9939	456056	321832	189332
85	186.88	.6811	.808	-.5471	-.6768	-.9937	444182	313155	183776
86	189.08	.6835	.811	-.5492	-.6767	-.9901	431545	303873	177897
87	191.28	.6860	.811	-.5509	-.6790	-.9898	419181	294893	172225
88	193.48	.6884	.815	-.5526	-.6784	-.9856	406503	285746	166487
89	195.67	.6907	.814	-.5544	-.6807	-.9854	396729	278615	161951
90	197.87	.6931	.818	-.5561	-.6802	-.9814	384122	269921	156300
91	200.07	.6954	.818	-.5577	-.6821	-.9809	373545	261904	151533
92	202.27	.6977	.821	-.5593	-.6815	-.9768	362535	253994	146622
93	204.47	.6999	.821	-.5611	-.6837	-.9768	351525	246031	141705
94	206.67	.7021	.824	-.5624	-.6827	-.9723	339351	237397	136427
95	208.87	.7043	.824	-.5640	-.6847	-.9721	327576	228960	131288
96	211.06	.7065	.827	-.5656	-.6841	-.9682	316602	221111	126510
97	213.26	.7087	.827	-.5671	-.6859	-.9679	307127	214334	122367
98	215.46	.7108	.827	-.5685	-.6877	-.9675	296395	206712	117762
99	217.66	.7129	.830	-.5699	-.6867	-.9633	287056	200085	113745
100	219.86	.7149	.830	-.5710	-.6881	-.9624	277066	193055	109517
101	222.06	.7170	.833	-.5724	-.6872	-.9585	266839	185805	105185
102	224.26	.7190	.833	-.5736	-.6887	-.9578	257243	179039	101146
103	226.45	.7210	.833	-.5752	-.6906	-.9579	248186	172568	97291
104	228.65	.7230	.836	-.5760	-.6890	-.9530	237647	165252	92976
105	230.85	.7249	.836	-.5773	-.6907	-.9527	228992	159128	89353
106	233.05	.7269	.836	-.5783	-.6918	-.9518	219971	152824	85643
107	235.25	.7288	.839	-.5798	-.6911	-.9483	211465	146788	82099
108	237.45	.7307	.839	-.5803	-.6917	-.9467	202721	140755	78571
109	239.65	.7325	.839	-.5818	-.6935	-.9468	194915	135220	75336
110	241.84	.7344	.842	-.5824	-.6918	-.9420	186696	129529	72028
111	244.04	.7362	.842	-.5836	-.6932	-.9416	179033	124146	68904
112	246.24	.7380	.842	-.5845	-.6943	-.9408	170402	118136	65449
113	248.44	.7398	.845	-.5856	-.6931	-.9369	163652	113401	62705
114	250.64	.7415	.845	-.5863	-.6939	-.9358	155462	107725	59457
115	252.84	.7433	.845	-.5870	-.6948	-.9348	149338	103477	57008
116	255.04	.7450	.845	-.5882	-.6962	-.9345	141831	98224	54016
117	257.23	.7467	.848	-.5887	-.6943	-.9298	135144	93607	51385
118	259.43	.7484	.848	-.5893	-.6950	-.9287	129324	89575	49085
119	261.63	.7501	.848	-.5903	-.6962	-.9282	123524	85528	46785
120	263.83	.7517	.851	-.5898	-.6932	-.9221	116487	80750	44094
121	266.03	.7533	.851	-.5910	-.6946	-.9220	111307	77114	42036
122	268.23	.7550	.851	-.5911	-.6948	-.9203	105760	73306	39892
123	270.43	.7566	.851	-.5917	-.6954	-.9192	100740	69831	37936
124	272.62	.7581	.854	-.5927	-.6942	-.9157	96205	66656	36150
125	274.82	.7597	.854	-.5926	-.6941	-.9137	91457	63412	34334
126	277.02	.7612	.854	-.5928	-.6943	-.9121	86437	59959	32410
127	279.22	.7628	.854	-.5936	-.6953	-.9115	82652	57320	30933
128	281.42	.7643	.854	-.5932	-.6948	-.9090	77215	53606	28882
129	283.62	.7658	.857	-.5932	-.6923	-.9041	74228	51564	27737
130	285.82	.7673	.857	-.5933	-.6925	-.9026	69650	48404	25996
131	288.01	.7688	.857	-.5933	-.6925	-.9009	67282	46787	25087
132	290.21	.7702	.857	-.5934	-.6926	-.8993	63460	44151	23637
133	292.41	.7717	.860	-.5929	-.6897	-.8938	60637	42232	22574
134	294.61	.7731	.860	-.5928	-.6895	-.8919	56875	39642	21157
135	296.81	.7745	.860	-.5930	-.6898	-.8907	54342	37888	20190
136	299.01	.7759	.860	-.5925	-.6892	-.8882	52390	36566	19457
137	301.21	.7773	.860	-.5927	-.6889	-.8863	49491	34575	18369
138	303.40	.7787	.863	-.5919	-.6862	-.8812	47098	32905	17496
139	305.60	.7800	.863	-.5921	-.6864	-.8800	45464	31801	16849
140	307.80	.7814	.863	-.5911	-.6853	-.8771	42984	30113	15928
141	310.00	.7827	.863	-.5901	-.6841	-.8741	41340	29008	15321
142	312.20	.7840	.863	-.5906	-.6847	-.8733	39583	27776	14649
143	314.40	.7853	.863	-.5893	-.6832	-.8700	37799	26574	13995
144	316.60	.7866	.865	-.5899	-.6817	-.8666	36952	25975	13660
145	318.79	.7879	.865	-.5891	-.6807	-.8639	35722	25147	13208
146	320.99	.7892	.865	-.5892	-.6808	-.8627	34341	24184	12683
147	323.19	.7904	.865	-.5882	-.6797	-.8600	33159	23387	12248
148	325.39	.7917	.865	-.5878	-.6792	-.8579	32012	22601	11820
149	327.59	.7929	.868	-.5873	-.6766	-.8531	31458	22232	11611
150	329.79	.7941	.868	-.5869	-.6759	-.8511	30127	21312	11115
151	331.99	.7953	.868	-.5873	-.6744	-.8504	29665	20986	10931

Fig. 33.

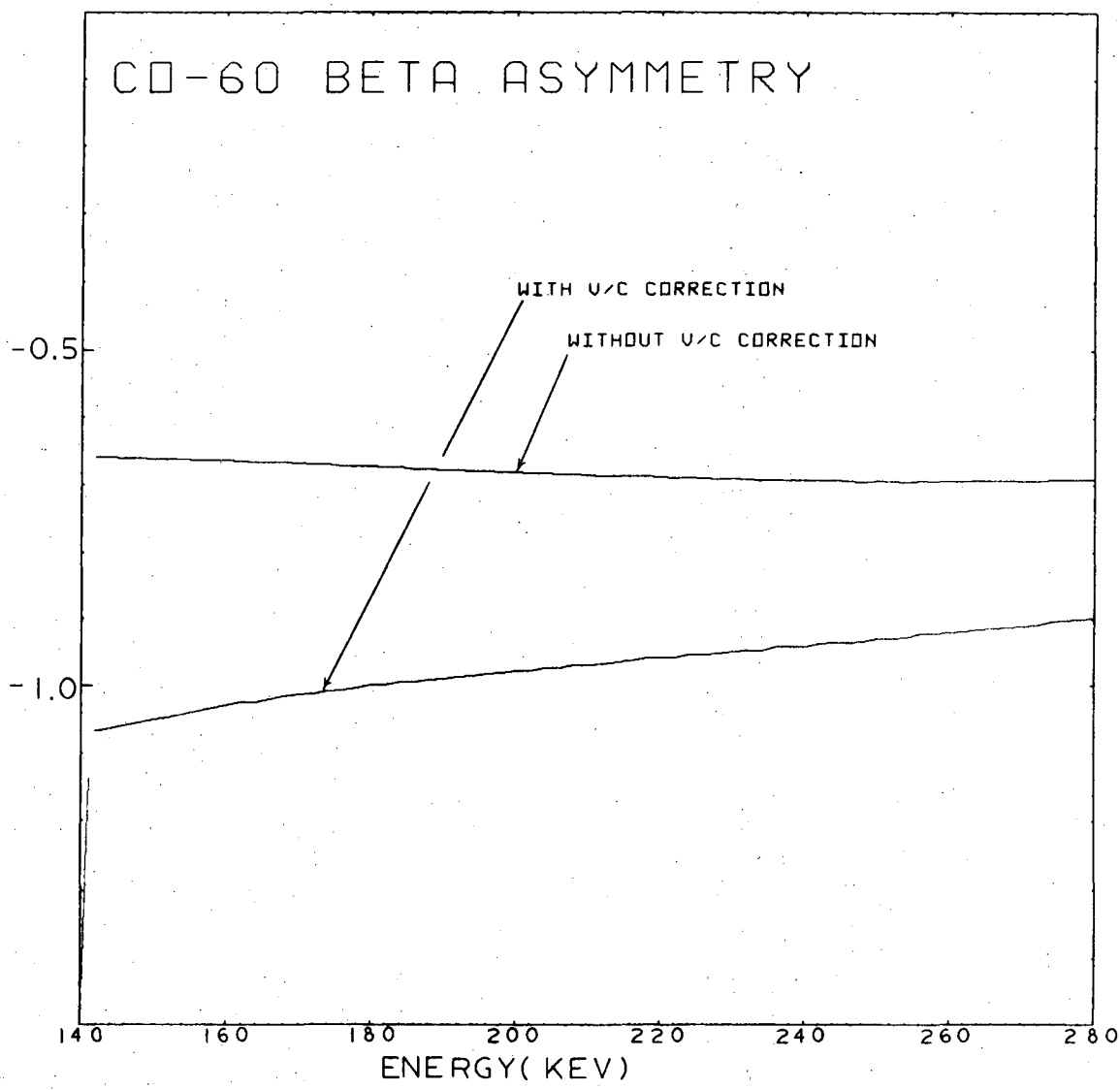

XBL 727-1274

Fig. 34. The values of the ^{60}Co asymmetry parameter A .

CHAPTER IX

Critique of the Experiment

The problems related to electron scattering are most susceptible to criticism in a typical beta experiment. For accurate beta studies, the experimental chamber should be spacious so that the electrons may be free to move about. Due to the backscattering property, solid states detectors are relatively inferior to the beta spectrometers utilizing focussing magnets for the energy determination.[34] Nevertheless, the requirements for cryogenic designs are such that roominess is a luxury, and the adoption of a beta spectrometer within a cryostat is virtually impossible. The magnitude of the error lessens a great deal when the beta counts are displayed as an energy spectrum, as this enables one to pick the particles at the high energy end of the spectrum where scattering is the least.

As mentioned in Chapter V , the inherent difficulty with the ^{52}Mn experiment lies in the abundance of the gamma rays background relative to the positron signals. To improve the signal-to-noise ratio, a long guiding solenoid was used. Despite the obvious advantage manifested by the improved spectral shapes, there are three potentially dangerous shortcomings. The most serious of all is the increase in source scattering. But as argued in Chapter VII, single scattering events predominate in a thin film, and the backscattering cross-section should be minimal. A less serious problem associates itself with the increase in the pile-up probability. This is undesirable only because of the v/c dependency of the beta asymmetry. Nevertheless, the fact that these two spurious effects cannot be determined precisely leaves one with some uncertainty about the result. Thirdly, the solid angle correction calculation demands a thorough knowledge of the geometric arrangements of the system. Obviously there is a limitation to an experimentalist's ability to accurately place and measure all the relevant geometric objects.

To alleviate any doubt concerning the accuracy of the ^{52}Mn result, the following observations may become helpful:

1) The experimental values of the asymmetry parameter A as a function of energy set the limits within which the true value of A exists. The relative independence of A on the positron energy indicates that all the unwanted effects have not contributed detrimentally to the experimental finding.

2) The asymmetry measured with ^{60}Co has a value very close to the expected theoretical value.

It is natural to ponder over the possibility that systematic errors may still exist in the ^{52}Mn experiment. β-polarized γ coincidence experiments may provide an alternative approach to the problem, although they have their own handful of difficulties. As mentioned in Chapter II, an "in-plane" nuclear orientation β-γ coincidence experiment provides the same information as the present work, and it also may be helpful in double-checking the result published in this report.

Comparison with other Experiments

Numerous experiments have been done on ^{52}Mn in the past with disappointingly conflicting results. Figure 35 tabulates a few of them to demonstrate the degree of discrepancy. According to the "isospin selection rule ",*5 the Fermi matrix element should vanish since $\Delta T = 1$ for the transition $^{52}Mn\ (T = 1) \xrightarrow[\beta]{} {}^{52}Cr\ (T = 2)$.

But obviously the isospin "symmetry" T is highly distorted by the charge-dependent electromagnetic interactions. It is doubtful whether T itself is a good quantum number for a medium-weight nucleus like ^{52}Mn.

---

* $1 = M_F = 0$ except when $\Delta T = 0$

Fig. 35. A vs X in the case of ^{52}Mn. X is the absolute magnitude of the Fermi/Gamow-Teller mixing ratio if time-reversal invariance is assumed.

The contributors are:

F. Boehm (Ref. 37, 1958)

E. Ambler et al (Ref. 2, 1958)

H. Postma et al (Ref. 38, 1958)

S.D. Bloom et al (Ref. 39, 1962)

F. Boehm (Quoted in Ref. 39)

H. Daniel et al (Ref. 40, 1962)

H.F. Schopper (Ref. 41, 1966)

L.G. Mann et al (Ref. 42, 1965)

J.A. Sawyer (Ref. 43, 1968)

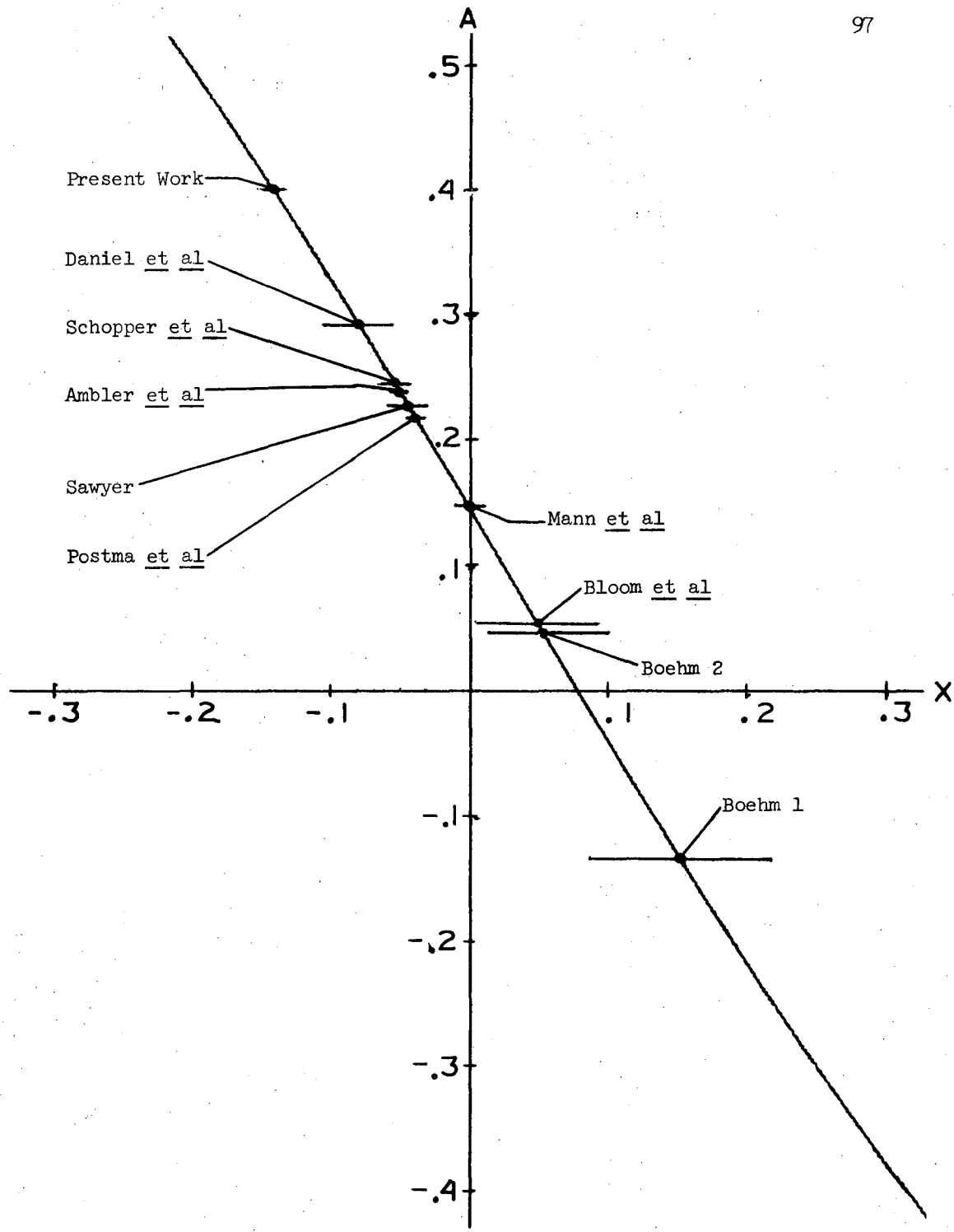

Fig. 35.

XBL 728-1399

Nevertheless, a non-vanishing Fermi matrix element for many other similar nuclei very often is explained by the contribution of isospin impurities which arises from the Coulomb interactions between the protons.

Using j-j coupling shell model, theoretical calculations have been made, and the value of $|C_V||M_F|/|C_A||M_{GT}|$ ranges from -0.04 to -0.07 [35,36] for ^{52}Mn.

It should be pointed out that the shell-model is rather inadequate for the description of the Coulomb effects and the mesonic effects within the nuclei. A large discrepancy still exists between the shell-model calculations and the experimental results.

The Fermi/Gamow-Teller mixing ratio reported here represents the largest negative value in comparison with other works. The asymmetry parameter A is about 70% larger than that measured by Ambler et al, [*2] but the F/GT mixing ratio is still within the experimental error reported for the "in-plane" β-γ correlation measurement in the same report. Unfortunately, this experiment can only add to the already existing confusion about the true F/GT ratio value. Perhaps it should be suggested here that due to the unfavorable decay scheme of ^{52}Mn, systematic errors may be very large for all the experiments performed to date. However, even if this report is not taken seriously for its accuracy, it can still be inferred that a negative and non-vanishing interference term does exist, and ^{52}Mn is still a possible candidate for a future time-reversal experiment.

---

* Ambler et al reported $A = 0.232 \pm 0.010$

Time-Reversal Invariance

Final words should be said on the prospects of the nuclear orientation β-γ correlation experiment. The lesson learned in this work is that systematic errors are worse foes than statistical errors. It is true that good statistics is always being fought for by the experimentalists doing coincidence experiments, but systematic errors are more dangerous in the sense that they may lead one into completely different conclusions.

The nuclear orientation β-γ correlation technique relies on placing the gamma detectors such that the plane defined by the H field and the gamma detectors in exactly perpendicular to the plane defined by the H field and the beta detector(Fig. 3) . But the magnetic rigidity of the electrons complicates the whole situation tremendously. The introduction of a polarizing field tends to cause the beta particles to follow a circular path. As depicted in Figure 36, a large field can easily cause a low energy positron originally emitted "in-plane" to be detected by a " out-of-plane" beta detector. A simple calculation indicates that a field of 1 KG (normally used to polarize the source foil) would be sufficient to bend a positron 200 kev in energy by an angle of 18° when the beta detector is placed 1 cm from the source. Although this 18° can be readily compensated by placing the gamma detector accordingly, the magnetic rigidity is energy dependent, and other positrons of different energy would yield an "in-plane" component for an "out-of-plane" arrangement. The source size and the solid angle correction may complicate significantly the data analysis. Furthermore, scattering makes the mixing of "in-plane" and "out-of-plane" particles unavoidable.

The low energy end point of the ^{52}Mn beta spectrum does not

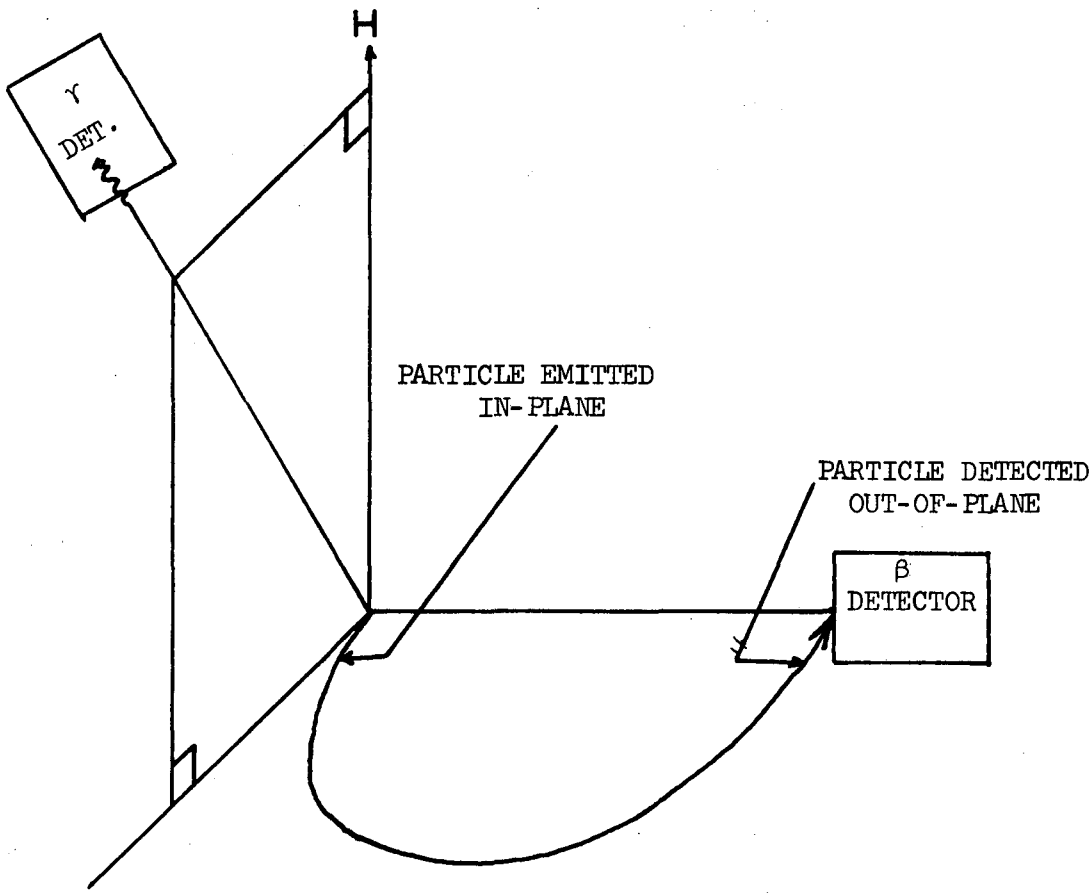

XBL 728-1408

Fig. 36. A schematic diagram to demonstrate the effect of a magnetic field on the "in-plane" and "out-of-plane" measurements.

help the situation favorably. Even though ^{52}Mn may have a large Fermi/Gamow-Teller mixing ratio, perhaps it would be wiser to find other nuclei with more favorable decay schemes (higher beta energy and lower gamma energy and intensity, such as ^{55}Co and ^{56}Co). After all, the F/GT mixing ratio is just one of many factors responsible for the accuracy of a time-reversal invariance experiment.

REFERENCES

1) T.D. Lee and C.N. Yang, Phys.Rev. 105, 1671 (1957)

2) E. Ambler, R.W. Hayward, D.D. Hoppes and R.P. Hudson, Phys.Rev.Letters 110,3,787 (1958)

3) J.H. Christenson, J.W. Cronin, V.L. Fitch and R.Turlay, Phys.Rev.Letters 13,138 (1964)

4) F.P. Calaprice, E.D. Commins, H.M. Gibbs, G.L. Wick and D.A. Dobson, Phys.Rev.Letters 18,21,918 (1967)

5) E.J. Konopinski, The Theory of Beta Radioactivity (Oxford; 1966)

6) E. Fermi, Zeits.Phys. 88,161 (1934)

7) R.P. Feynman and M. Gell-Mann, Phys.Rev. 109,193(1958)

8) E.C.G. Sudarshan and R.E. Marshak, Phys.Rev. 109,1960 (1958)

9) J.J. Sakurai, Nuovo Cimento 7,649 (1958)

10) R.B. Curtis and R.R. lewis, Phys.Rev. 107,5,1381 (1957)

11) U. Fano, Phys.Rev. 90,577 (1953)

12) M. Morita, Prog.Th.Phy. 14,1,27 (1955)

13) M. Morita and R.S. Morita, Phys.Rev. 107,5,1316 (1957)

14) M. Ferentz and N. Rosenzweig, ANL-5324 (1954)

15) R.J. Blin-Stoyle and M.A. Grace, Handbuch der Physik 42,555 (1957)

16) E. Matthias and D.A. Shirley, Hyperfine Structure and Nuclear Radiation, (N. Holland-Amsterdam; 1968)

17) G.A. Westengarger, Ph.D. Thesis, UCRL-11143 (1963)

18) J.A. Barclay, Ph.D. Thesis, UCRL-18986 (1969)

19) C.S. Wu, E. Ambler, R.W. Hayward, D.D. Hoppes and R.P. Hudson, Phys.Rev.Letters 105,4,1413 (1957)

20) J.E. Templeton, Ph.D. Thesis, Oxford (1967)

21) D.R. Brundrit and S.K. Sen, Nucl.Instr. Meth. 34,225 (1965)

22) F.S. Goulding, UCRL-16231 (1965)

23) E.M. Pell, Nat.Acad.Sci.Report NAS-NSS 32 Pub. 871, 139 (1961)

24) W.D. Brewer, Ph.D. Thesis, UCRL-19533 (1969)

25) E.M. Pell, private communication.

26) T.F. Knott, H.R. Andrews, E.J. Cohen, F.M. Pipkin and D.C. Santry, Phys.Rev.Letters 25,8,543 (1970)

27) C.M. Lederer, J.M. Hollander and I. Perlman, Table of Isotopes, (John Wiley and Sons-New York; 1967)

28) G.T. Ewan and A.J. Tavendale, AECL-2079 (1964)

29) See for example, J.A. Barclay, UCRL-18986 (1969)

30) W.D. Brewer, private communication.

31) A.C. Anderson, W. Reese and J.C. Wheatley, Rev.Sci.Instr. 34,12,1386 (1963)

32) See for example, C. Kittel, Introduction to Solid States Physics, (John Wiley and Sons,New York; 1970)

33) K. Siegbahn, Alpha-,Beta- and Gamma-Ray Spectroscopy, Chpt. 1, (N. Holland-Amsterdam; 1965)

34) K. Siegbahn, Alpha-,Beta- and Gamma-Ray Spectroscopy, Chpt. 3, (N. Holland-Amsterdam; 1965)

35) P.S. Kelly and S.A. Moszkowski, Z. Physik 158,304 (1960)

36) C.C. Bouchiat, Phys. Rev. 118,540 (1960)

37) F. Boehm, Phys.Rev. 109, 1018 (1958)

38) H. Postma, W.J. Huiskamp, A.R. Miedema, M.J. Steenland, H.A. Tolhoek and G.J. Gorter, Physica 23, 259 (1957); 24,157 (1958)

39) S.D. Bloom, L.G. Mann and J.A. Miskel, Phys.Rev. 125,2021 (1962)

40) H. Daniel, O. Mehling, O. Muller and K.S. Subudhi, Phy.Rev. 128,261 (1962)

41) H.F. Schopper, Weak Interactions and Nuclear Beta Decay, (N. Holland-Amsterdam; 1966)

42) L.G. Mann, D.C. Camp, J.A. Miskel and R.J. Nagle, Phys.Rev. 137,B1 (1965)

43) J.A. Sawyer, UCRL-50440 (1968)

APPENDIX 1

Formulae for B_k , U_k and F_k

B_k is defined as

$$B_k = (2I+1)^{\frac{1}{2}} \sum_m (-1)^{I-m} \; C(IIk;m\,-m)\; W(m)$$

$$= (2I+1)^{\frac{1}{2}} (2k+1)^{\frac{1}{2}} \sum_m (-1)^{I-m} \left(\frac{I\;I\;k}{m\text{-}m\;0}\right) W(m)$$

where $C(IIk;m\,-m)$ is the usual Clebsch-Gordon coefficients and the $\left(\frac{I\;I\;k}{m\text{-}m\;0}\right)$ the 3-j symbols.

The more commonly used B_k are: (After simplification)

$$B_1 = \sqrt{3I/(I+1)} \sum_m m\, W(m)$$

$$B_2 = \sqrt{5/I(I+1)(2I+3)(2I-1)} \sum_m \left[3\, m^2\, W(m) - I(I+1)\right]$$

$$B_3 = \sqrt{7\,/(I+2)(I+1)I(I-1)(2I+3)(2I-1)} \quad X$$

$$\sum_m \left[5\, m^3 - (3I^2 + 3I - 1)\, m\right] W(m)$$

$$B_4 = 3/2\sqrt{1/(I+2)(I+1)I(I-1)(2I+5)(2I+3)(2I-1)(2I-3)} \quad X$$

$$\sum_m \left[35\, m^4 - (30I(I+1) - 25)\, m^2 + 3I(I+2)(I+1)I(I-1)\right] W(m)$$

where m is the eigenvalue of I_z , and $W(m)$ is the relative population of these m magnetic substates. For Zeeman splitting, $W(m)$ can be given by:

$$W(m) = \frac{\exp(-m\ g\ \mu_N\ H\ /\ k\ T\ )}{\sum_m \exp(-m\ g\ \mu_N\ H\ /\ k\ T\ )}$$

where H is the magnetic field applied or the hyperfine field; μ_N is the nuclear magneton; g is the nuclear g-factor.

For the transition $I_i\ (\ L\ )\ I_f$, U_k are given as:

$$U_k(I_i I_f L) = (2I_i+1)^{\frac{1}{2}}(2I_f+1)^{\frac{1}{2}}\ (-1)^{I_i+I_f-L}\ W(I_i I_i I_f I_f;kL)$$

The F_k are given as:

$$F_k(LL'I_i I) = (-1)^{I_i+I-1}\sqrt{(2L+1)(2L'+1)(2I+1)(2k+1)}\quad X$$

$$\left(\frac{L\ L'k}{1-1\ 0}\right)\left\{\frac{L\ L'k}{I\ I\ I_i}\right\}$$

And:

$$(-1)^{j_1+j_2+L_1+L_2}\ W(j_1 j_2 L_2 L_1;j_3 L_3) = \left\{\frac{j_1\ j_2\ j_3}{L_1\ L_2\ L_3}\right\}$$

The $\left\{\frac{j_1\ j_2\ j_3}{L_1\ L_2\ L_3}\right\}$ are the usual 6-j symbols.

APPENDIX 2

Pertinent Data Concerning ^{52}Mn

Spin: 6 +

Magnetic Moment: 3.075 μ_N

Hyperfine Field in Fe: - 226.97 KG

$U_2(661)$: 13/14

$U_4(661)$: 16/21

$F_2(2246)$: $-5/(154)^{\frac{1}{2}}$

$F_4(2246)$: $-4/9 \times (17/77)^{\frac{1}{2}}$

U_2F_2 : - 0.3741

U_4F_4 : - 0.1591

APPENDIX 3

Gamma Response in Germanium Detectors

The efficiency of a germanium detector depends on the photoelectric cross-section of the gamma rays in the material. Figure 10 indicates that the cross-section drops off extremely fast as the energy of the photons is increased.

An electron is ejected when a photon is absorbed via the photoelectric effect. This electron has an kinetic energy equal to the photon energy minus the binding energy of the electron. The electron in turns causes secondary ionization within the bulk material, and these ionizations are swept away by the intense electric field if they are within the depletion region.

It is obvious that a thin detector has very low efficiency for gamma rays. Not only that the probability for the interactions with the photons decreases due to the lack of thickness, the photoelectrons produced when the photons are absorbed very often have energy higher than their range in germanium. Consequently most of the photoelectrons escape the bulk material depositing only a small fraction of their energy. Those produced at the center of the detector and ejected perpendicular to the detector thickness have a larger chance of producing significant ionization, whereas those produced at the periphery of the detector ultimately escape the detector if the detector is thin enough. Obviously there are many different combinations of the various mechanisms, but the point to keep in mind is that most of the energy transferred to the detector happen only at the end of the range of the electrons in the material. By keeping the detector thin, the electric signals produced by relative high energy gamma rays(such as the 511 kev annihilation photons)can be made small in their pulse heights so that they won't interfere with the signals produced by particles.

APPENDIX 4

Some Useful Data Concerning the Dewars System

The LN Tank:

Dimension: $51\frac{1}{8}$" long, 11" O.D., 9" I.D.

LN Volume: 25 litres.

Boil-off Rate: $1\frac{1}{2}$ "/hr. when full (more than 12" from top flange; 1 "/hr. when half full.

The 4°K Liquid Helium Tank:

Dimension: $79\frac{3}{4}$" overall length, $70\frac{1}{2}$" from the top flange to the beginning of the taper.

LHe Volume: 18 litres when filled to 15" from the top flange.

Boil-off Rate: 1/3 litre/hr. when the 1°K bath is pumped on; about 1 litre/hr. without pumping on the 1°K bath, and the magnet current set at 100 A.

Location of the Cooling Magnet:

$56\frac{1}{4}$" from the top flange to the top of the first magnet winding.

The 1°K Liquid Helium Tank:

Dimension: 75" overall length from the top of the T . $9\frac{1}{2}$" from the top of the T to the beginning of the taper.

LHe volume: 55 litres when filled to 15" from the top flange(23" from the top of the T); this should be subtracted by the volume of of the cryostat which is typically 30 litres.

Typical Bath Life: About 30 hours.

APPENDIX 5

The Solid Angle Correction

The magnetic rigidity of electrons have the relationship:

$$(B r)^2 \lambda^2 = \beta^2/(1-\beta^2)$$

where $\lambda = e/mc = 1.75890\text{x}10^7/2.997930\text{x}10^{10}$ $\text{gauss}^{-1}\text{cm}^{-1}$;

B is the magnetic field in gauss;

r is the radius of the electron path perpendicular to B ;

$\beta = v/c$ of the electron.

Consider Figure 37. At a given emission angle θ , certain electrons emitted in an angle φ will be bent by the magnetic field B and interact with the source foil again. It is obvious that the amount of electrons free of interactions with the source is dependent on the angle θ , the angle φ , the energy of the electron β and the source foil size (radius R) .

It can be shown that for a given angle θ , φ assumes values governed by the equation:

$$\pi - \frac{R}{2\,r\,(1-\beta^2)^{\frac{1}{2}}} \frac{(1 - \beta^2 \sin^2\theta\,)^{\frac{1}{2}}}{\cos\,\theta} \geqslant \varphi \geqslant 0$$

Now , all possible φ are integrated:

$$\int d\varphi = 2\pi - \varphi_o(\,\theta)$$

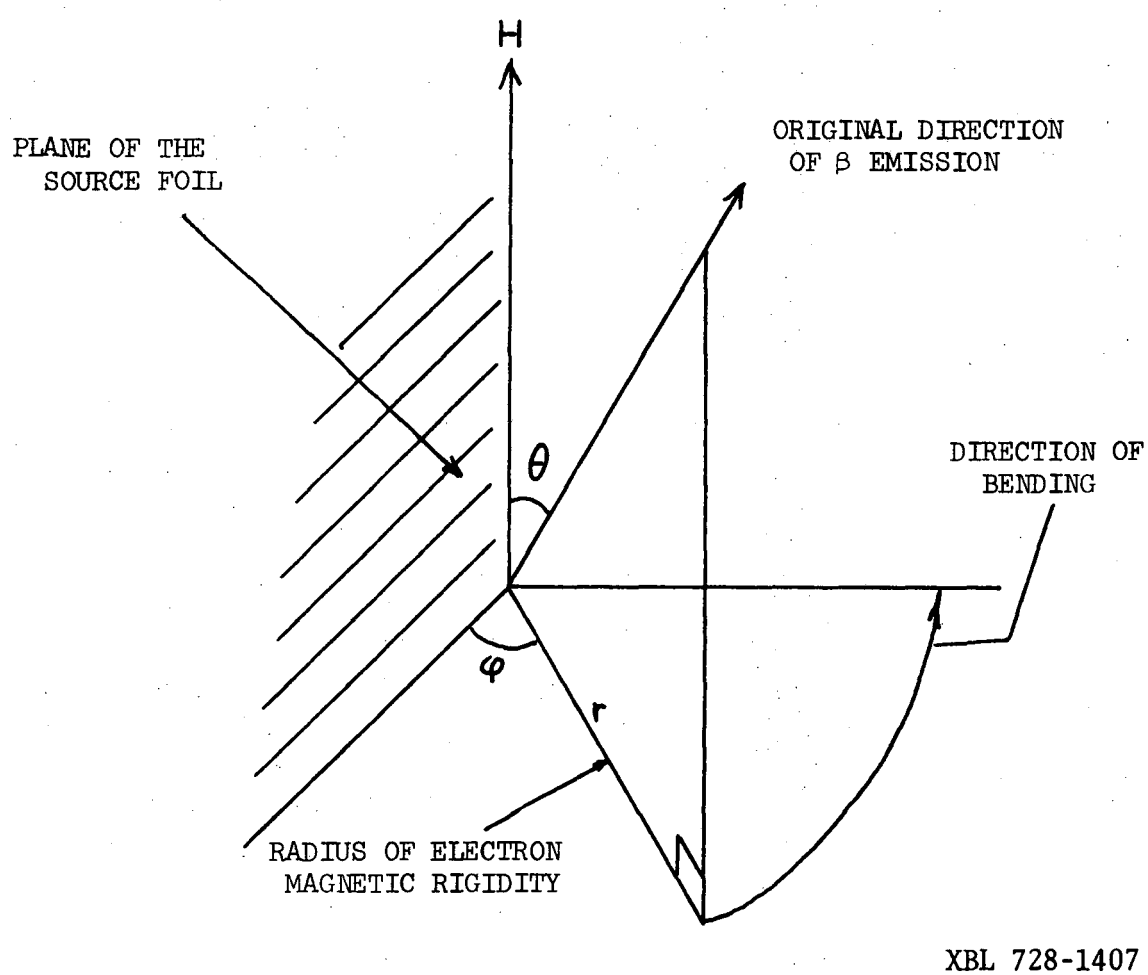

Fig. 37. Schematic diagram of the geometry for the solid angle correction.

$$\varphi_o(\theta) = \frac{R}{r\,(1-\beta^2)^{\frac{1}{2}}} \quad \frac{(1-\beta^2\sin^2\theta)^{\frac{1}{2}}}{\cos\theta}$$

Now, all possible θ are integrated to obtain the solid angle correction factor :

$$Q_1(0) = \int d\theta \cos\theta \sin\theta \int d\varphi \Big/ \int d\theta \sin\theta \int d\varphi$$

The values of θ range from 0 to an angle determined by the energy of the electron β and the collimator size of the beta detector. The integration can be done with a computer.

ACKNOWLEDGEMENTS

It gives me pleasure to acknowledge the sources of many contributions which made this work possible.

My first thank goes to Prof. David A. Shirley who introduced me into the field of nuclear orientation. Despite of his extremely heavy schedule in the past few years, we have managed to maintain enough communication to keep the present project going smoothly. His finacial and moral support have been more than generous.

Dr. Gunter Kaindl should be given thank for his help and ideas at the premordial stage of the project. His advanced technical knowledge has upgraded the technical performance of the entire laboratory, and I have benefitted enormously from his contributions.

Thanks should also be given to Mr. Ed Voronin for his expertise in vacuum design, Mr. Vic Walton for winding reliable superconducting magnets, and Ms. Winnie Heppler for her kindness, which always managed to turn a day of disappointment into a day of less disappointment.

Although my acquaintance with Dr. Bill Brewer has been brief, his patience and clear explanations have helped me in understanding low temperature techniques at a time when I had enough problems with room temperature techniques.

My warmest thank goes to my wife, Patricia. Without her warmth and encouragement, I would have quitted many times before. There were many periods in the course of this project during which science seemed to be so irrelevant to life. In very subtle and indirect ways she inspired me to see science not as subject matters but as disciplines through which human dignity and the quality of life can be improved.

Obviously the list of people cannot stop here. My final thanks go to all those whom I have associated with during my entire graduate career. The financial support of the United States Atomic Energy Commission should also be acknowledged.

LEGAL NOTICE

This report was prepared as an account of work sponsored by the United States Government. Neither the United States nor the United States Atomic Energy Commission, nor any of their employees, nor any of their contractors, subcontractors, or their employees, makes any warranty, express or implied, or assumes any legal liability or responsibility for the accuracy, completeness or usefulness of any information, apparatus, product or process disclosed, or represents that its use would not infringe privately owned rights.

TECHNICAL INFORMATION DIVISION
LAWRENCE BERKELEY LABORATORY
UNIVERSITY OF CALIFORNIA
BERKELEY, CALIFORNIA 94720